

University of Potsdam
Faculty of Science
Institute of Geosciences
Remote Sensing, geoInformation and Visualization (RSIV)

Master's Thesis

In Partial Fulfilment of the Requirements for the Degree of Master of Science (M.Sc.)

**Land-cover Classification and Time Series Analysis of
Sentinel-1 and Sentinel-2 Images at Two Contrasting Sites
(Northern Treeline vs. Taiga) with Integration of Additional
Ground and Satellite Validation Data**

Adeola Olanrewaju Obidiya

Supervisors

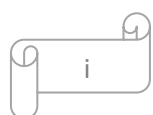
Dr. Birgit Heim
Alfred Wegener Institute
Helmholtz Center for Polar & Marine Research, Potsdam
Geosciences/Polar Terrestrial Environmental Systems Research Group

Dr. Taylor Smith
University of Potsdam
Institute of Geosciences
Geological Remote Sensing

15 July 2022

Dedication

This work is dedicated to my Mum of blessed memory



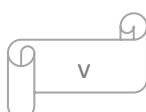
ABSTRACT

The desire to assess the performance of different methods of supervised classification on Sentinel-1 and Sentinel-2 datasets independently and synergically in the arctic region birthed this experiment. Two (2) study areas were examined namely, Lake Illirney region of Bilibinsky district, Chukotka Autonomous Okrug, Russia and Lake Khamra region, Lensky district in the south-western part of Yakutia, Russia. Both study areas have different forest types. The data applied were taken from the Copernicus Open Access Hub. These data were Sentinel-1 and Sentinel-2 products representing the month of July over a 5-year period (2017-2021). The geographic locations of twenty-nine (29) vegetation plots were collected from both study areas in-situ during Russian-German expedition in 2018. Reference data for both study areas were downloaded from ESRI Land Cover data portal. Climate data was also downloaded from National Oceanic and Atmospheric Administration (NOAA) using the station named Ostrovnoe, RS RSM00025138 located in Chukotka Autonomous Okrug, Russia. Both Sentinel products from both study areas were subjected to unsupervised and supervised classification techniques. Five (5) methods of supervised classification were used namely, *Random Forest (RF) Classifier*, *KNN Classifier*, *KDTree KNN Classifier*, *Minimum Distance (MD) Classifier* and *Maximum Likelihood (ML) Classifier*. Time series analyses were also carried out on both Sentinel products of the study areas. The use of the methods of unsupervised classification which involves *EM Cluster Analysis* and *K-Means Cluster Analysis* for Sentinel-1, and Sentinel-2 products can be described to have an average performance. It was noted that the algorithm of *K-Means Cluster Analysis* was better than that of *EM Cluster Analysis* while using Sentinel-1 and Sentinel-2 images independently and in combination. *Random Forest (RF) Classifier* proved to be the best supervised classification method for Sentinel-1, while the *Minimum Distance (MD) Classifier* had the best *Overall Accuracy (OA)* for Sentinel-2 images when analysed independently. The synergic use of both Sentinel products shown that *KDTree KNN Classifier* had the highest *Overall Accuracy (OA)*. The time series analyses carried out shown that there were some variations in the densities of land-cover types over a period of five (5) years, which indicates that there can be changes even over a short period of time in land-cover types of the Arctic region.

Keywords: Land-cover classification; Sentinel-1; Sentinel-2; Lake Illirney; Lake Khamra; Chukotka; K-Means Cluster Analysis; Random Forest classifier; KDTree KNN classifier; Minimum Distance (MD) classifier; KNN classifier; Maximum Likelihood (ML) classifier; unsupervised classification; supervised classification

ABSTRACT (German)

Der Wunsch, die Leistung verschiedener Methoden der überwachten Klassifizierung von Sentinel-1- und Sentinel-2-Datensätzen unabhängig und synergetisch in der arktischen Region zu bewerten, hat dieses Experiment hervorgebracht. Zwei (2) Untersuchungsgebiete wurden untersucht, nämlich die Illirney-See-Region des Bilibinsky-Distrikts, Chukotka Autonomous Okrug, Russland und die Khamra-See-Region, Lensky-Distrikt im südwestlichen Teil von Jakutien, Russland. Beide Untersuchungsgebiete weisen unterschiedliche Waldtypen auf. Die verwendeten Daten wurden dem Copernicus Open Access Hub entnommen. Bei diesen Daten handelte es sich um Sentinel-1- und Sentinel-2-Produkte, die den Monat Juli über einen Zeitraum von 5 Jahren (2017-2021) repräsentieren. Die geografischen Standorte von neunundzwanzig (29) Vegetationsparzellen wurden während der russisch-deutschen Expedition im Jahr 2018 in beiden Untersuchungsgebieten vor Ort erfasst. Die Referenzdaten für beide Untersuchungsgebiete wurden vom ESRI Land Cover Data Portal heruntergeladen. Klimadaten wurden auch von der National Oceanic and Atmospheric Administration (NOAA) unter Verwendung der Station namens Ostrovnoe, RS RSM00025138 im Autonomen Kreis Chukotka, Russland, heruntergeladen. Beide Sentinel-Produkte aus beiden Studienbereichen wurden unüberwachten und überwachten Klassifizierungstechniken unterzogen. Fünf (5) Methoden der überwachten Klassifizierung wurden verwendet, nämlich Random Forest (RF) Classifier, KNN Classifier, KDTree KNN Classifier, Minimum Distance (MD) Classifier und Maximum Likelihood (ML) Classifier. An beiden Sentinel-Produkten der Untersuchungsgebiete wurden auch Zeitreihenanalysen durchgeführt. Die Verwendung der Methoden der unüberwachten Klassifizierung, die die EM-Cluster-Analyse und die K-Means-Cluster-Analyse für Sentinel-1- und Sentinel-2-Produkte umfasst, kann als durchschnittliche Leistung beschrieben werden. Es wurde festgestellt, dass der Algorithmus der K-Means-Clusteranalyse besser war als der der EM-Clusteranalyse, wenn Sentinel-1- und Sentinel-2-Bilder unabhängig voneinander und in Kombination verwendet wurden. Random Forest (RF) Classifier erwies sich als die am besten überwachte Klassifizierungsmethode für Sentinel-1, während der Minimum Distance (MD) Classifier bei unabhängiger Analyse die beste Gesamtgenauigkeit (OA) für Sentinel-2-Bilder aufwies. Die synergetische Verwendung beider Sentinel-Produkte zeigte, dass der KDTree KNN-Klassifikator die höchste Gesamtgenauigkeit (OA) hatte. Die durchgeführten Zeitreihenanalysen zeigten, dass es über einen Zeitraum von fünf (5) Jahren einige Schwankungen in der Dichte der Landbedeckungstypen gab, was darauf hindeutet, dass es auch innerhalb eines kurzen Zeitraums zu Änderungen bei den Landbedeckungstypen kommen kann die arktische Region.



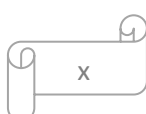
Schlüsselwörter: Landbedeckungsklassifikation; Sentinel-1; Sentinel-2; Ilirney-See; Khamra-See; Tschukotka; K-Means-Cluster-Analyse; Random Forest-Klassifikator; KDTree KNN-Klassifikator; Minimum Distance (MD)-Klassifikator; KNN-Klassifikator; Maximum-Likelihood-(ML)-Klassifikator; unbeaufsichtigte Klassifizierung; überwachte Klassifizierung

Acknowledgements

I would like to thank Birgit Heim from Alfred Wegener institute (AWI), Potsdam for giving me a chance to learn with her supervision. I thank you for the attention and expertise that you gave me through the period of my thesis. I also thank you for the opportunity you offered to be part of Polar Terrestrial Environmental Systems Research Group. I would also like to thank Taylor Smith from University of Potsdam for his time and advice. I must mention that you are the best teacher that taught me at the university. Lastly, I would like to thank my Wife, Dad, and Siblings for their moral support.

Contents

Figures	xiii
Tables	xvii
Abbreviations and Symbols	xix
1 Introduction	1
1.1 Motivation	1
1.2 Study idea	2
2 Principles	3
2.1 Remote sensing fundamentals	3
2.2 Basics of synthetic aperture radar (SAR) remote sensing	6
2.3 Sentinel-1	8
2.4 Sentinel-2	9
2.5 Fusion of images in remote sensing	9
2.6 Methods of supervised classification	15
3 Methods	16
3.1 Study area	16
3.2 Data acquisition	19
3.3 Pre-processing of Sentinel-1 images	20
3.4 Pre-processing of Sentinel-2 images	20
3.5 Pre-processing of both Sentinel products for synergic use.	21
3.6 Land-cover classification of both Sentinel products	22
3.7 Analyses of the merged product (Sentinel-1 and Sentinel-2)	23
3.8 Land-cover classification of both Sentinel products	23
3.9 Validating the training and prediction accuracy	23
3.10 Time series analyses	24



4	Results	25
4.1	Analyses of Sentinel-1 images	25
4.1.1	Unsupervised classification	25
4.1.2	Supervised classification	27
4.2	Analyses of Sentinel-2 images	35
4.2.1	Unsupervised classification	35
4.2.2	Supervised classification	37
4.3	Analyses of the merging between Sentinel-1 and Sentinel-2 products	44
4.3.1	Unsupervised classification	44
4.3.2	Supervised classification	45
4.4	Time series analyses of both Sentinel products	52
4.4.1	Time series analysis for Sentinel-1 products	52
4.4.2	Time series analysis for Sentinel-2 products	54
4.4.3	Time series analysis of fused Sentinel-1 and -2 products	57
5	Discussions	60
5.1	Analyses of Sentinel-1 images	60
5.1.1	Unsupervised classification	60
5.1.2	Supervised classification	60
5.2	Analyses of Sentinel-2 Images	61
5.2.1	Unsupervised classification	61
5.2.3	Supervised classification	62
5.3	Analyses of the merging between Sentinel-1 and Sentinel-2 products	62
5.3.1	Unsupervised classification	62
5.3.2	Supervised classification	63
5.4	Time series analyses of both Sentinel products	63
5.4.1	Time series analysis for Sentinel-1 products	63
5.4.2	Time series analysis of Sentinel-2 products	65
5.4.3	Time series analysis of fused Sentinel-1 and Sentinel-2 products	65
6	Conclusions	66
6.1	Unsupervised classification	66
6.2	Supervised classification	66
6.3	Time series analyses	66

References	68
A List of Sentinel-1 products used for the research	75
B List of Sentinel-2 products used for the research	75
C List of reference data used	76

Figures

2.1	Illustrative picture of remote sensing in details	3
2.2	Electromagnetic spectrum showing Sentinel-1 and Sentinel-2 satellites' regions	4
2.3	Pictorial representation of different remote sensing techniques	5
2.4	A mathematical expression of a SLAR imaging instrument	6
2.5A	The major symmetrical misrepresentations in radar products: Foreshortening	7
2.5B	The major symmetrical misrepresentations in radar products: Layover	7
2.5C	The major symmetrical misrepresentations in radar products: Shadow	7
2.6	Level of SAR signal penetration by sensor wavelengths, λ	7
3.1	The northern part of the mountainous Lake Illirney catchment	17
3.2	Location of Chukotka Autonomous Okrug (<i>in red colour</i>) in Russia (<i>in lemon colour</i>)	17
3.3	The evergreen forest of Lake Khamra catchment	18
3.4	Location of Khamra (<i>in point red colour</i>) in Russia (<i>in lemon colour</i>)	18
4.01	EM cluster analysis of unsupervised classification for Sentinel-1 image of Lake Illirney region (July 2017)	25
4.02	K-Means cluster analysis of unsupervised classification for Sentinel-1 image of Lake Illirney region (July 2017)	26
4.03	EM cluster analysis of unsupervised classification for Sentinel-1 image of Lake Khamra region (July 2017)	26
4.04	K-Means cluster analysis of unsupervised classification for Sentinel-1 image of Lake Khamra region (July 2017)	27
4.05	Random Forest classifier of supervised classification for Sentinel-1 image of Lake Illirney region (July 2017)	28
4.06	KDTree KNN classifier of supervised classification for Sentinel-1 image of Lake Illirney region (July 2017)	28
4.07	Minimum Distance classifier of supervised classification for Sentinel-1 image of Lake Illirney region (July 2017)	29
4.08	Maximum Likelihood classifier of supervised classification for Sentinel-1 image of Lake Illirney region (July 2017)	29

4.09	Random Forest classifier of supervised classification for Sentinel-1 image of Lake Illirney region (July 2017)	30
4.10	KDTree KNN classifier of supervised classification for Sentinel-1 image of Lake Illirney region (July 2017)	30
4.11	Minimum Distance classifier of supervised classification for Sentinel-1 image of Lake Illirney region (July 2017)	31
4.12	Maximum Likelihood classifier of supervised classification for Sentinel-1 image of Lake Illirney region (July 2017)	31
4.13	EM cluster analysis of unsupervised classification for Sentinel-2 image of Lake Illirney region (July 2017)	35
4.14	K-Means cluster analysis of unsupervised classification for Sentinel-2 image of Lake Illirney region (July 2017)	36
4.15	EM cluster analysis of unsupervised classification for Sentinel-2 image of Lake Khamra region (July 2017)	36
4.16	K-Means cluster analysis of unsupervised classification for Sentinel-2 image of Lake Khamra region (July 2017)	37
4.17	Random Forest classifier of supervised classification for Sentinel-2 image of Lake Illirney region (July 2017)	38
4.18	KDTree KNN classifier of supervised classification for Sentinel-2 image of Lake Illirney region (July 2017)	38
4.19	Minimum Distance classifier of supervised classification for Sentinel-2 image of Lake Illirney region (July 2017)	39
4.20	Random Forest classifier of supervised classification for Sentinel-2 image of Lake Khamra region (July 2017)	39
4.21	KDTree KNN classifier of supervised classification for Sentinel-2 image of Lake Khamra region (July 2017)	40
4.22	Minimum Distance classifier of supervised classification for Sentinel-2 image of Lake Khamra region (July 2017)	40
4.23	Maximum Likelihood classifier of supervised classification for Sentinel-2 image of Lake Khamra region (July 2017)	41
4.24	EM cluster analysis of unsupervised classification for Sentinel-1 and Sentinel-2 images of Lake Khamra region (July 2017)	44

4.25	K-Means cluster analysis of unsupervised classification for Sentinel-1 and Sentinel-2 images of Lake Khamra region (July 2017)	45
4.26	Random Forest classifier of supervised classification for Sentinel-1 and Sentinel-2 images of Lake Illirney region (July 2017)	46
4.27	KDTree KNN classifier of supervised classification for Sentinel-1 and Sentinel-2 images of Lake Illirney region (July 2017)	46
4.28	Minimum Distance classifier of supervised classification for Sentinel-1 and Sentinel-2 images of Lake Illirney region (July 2017)	47
4.29	Random Forest classifier of supervised classification for Sentinel-1 and Sentinel-2 images of Lake Khamra region (July 2017)	47
4.30	KDTree KNN classifier of supervised classification for Sentinel-1 and Sentinel-2 images of Lake Khamra region (July 2017)	48
4.31	KNN classifier of supervised classification for Sentinel-1 and Sentinel-2 images of Lake Khamra region (July 2017)	48
4.32	Minimum Distance classifier of supervised classification for Sentinel-1 and Sentinel-2 images of Lake Khamra region (July 2017)	49
4.33	Sentinel-1 derived backscatter time series from the vegetation plot sites in Lake Illirney region (2017-2021)	52
4.34	Backscatter of boreal forest for Sentinel-1 image for Lake Illirney region (2017-2021)	52
4.35	Backscatter of tundra for Sentinel-1 image for Lake Illirney region (2017-2021)	53
4.36	Backscatter of water for Sentinel-1 image for Lake Illirney region (2017-2021)	53
4.37	Backscatter of evergreen forest for Sentinel-1 image for Lake Khamra region (2017-2021)	53
4.38	Backscatter of tundra for Sentinel-1 image for Lake Khamra region (2017-2021)	54
4.39	Backscatter of water for Sentinel-1 image for Lake Khamra region (2017-2021)	54
4.40	Pixel values of boreal forest for Sentinel-2 images for Lake Illirney region (2017-2021)	55
4.41	Pixel values of tundra for Sentinel-2 images for Lake Illirney region (2017-2021)	55
4.42	Pixel values of water for Sentinel-2 images for Lake Illirney region (2017-2021)	55
4.43	Pixel values of evergreen forest for Sentinel-2 images for Lake Khamra region (2017-2021)	56
4.44	Pixel values of tundra for Sentinel-2 images for Lake Khamra region (2017-2021)	56
4.45	Pixel values of water for Sentinel-2 images for Lake Khamra region (2017-2021)	56
4.46	Backscatter of boreal forest for both Sentinel products for Lake Illirney region (2017-2021)	57

4.47	Backscatter of tundra for both Sentinel products for Lake Illirney region (2017-2021)	57
4.48	Backscatter of water for both Sentinel products for Lake Illirney region (2017-2021)	58
4.49	Backscatter of evergreen forest for both Sentinel products for Lake Khamra region (2017-2021)	58
4.50	Backscatter of tundra for both Sentinel products for Lake Khamra region (2017-2021)	58
4.51	Backscatter of water for both Sentinel products for Lake Khamra region (2017-2021)	59
4.52	Average temperature in July at Lake Illirney region (2017-2021)	64
4.53	Average precipitation in July at Lake Illirney region (2017-2021)	64

Tables

4.01	Training accuracy for the trained classes using Random Forest Classifier (Sentinel-1 image, Lake Illirney region, July 2017)	32
4.02	Training accuracy for the trained classes using KDTree KNN Classifier (Sentinel-1 image, Lake Illirney region, July 2017)	33
4.03	Training accuracy for the trained classes using Minimum Distance Classifier (Sentinel-1 image, Lake Illirney region, July 2017)	34
4.04	Prediction accuracy for methods of supervised classification (Sentinel-1 image)	34
4.05	Training accuracy for the trained classes using Random Forest Classifier (Sentinel-2 image, Lake Illirney region, July 2017)	41
4.06	Training accuracy for the trained classes using KDTree KNN Classifier (Sentinel-2 image, Lake Illirney region, July 2017)	42
4.07	Training accuracy for the trained classes using Minimum Distance Classifier (Sentinel-2 image, Lake Illirney region, July 2017)	43
4.08	Prediction accuracy for methods of supervised classification (Sentinel-2 image)	43
4.09	Training accuracy for the trained classes using Random Forest Classifier (Sentinel-1 and Sentinel-2 image, Lake Illirney region, July 2017)	49
4.10	Training accuracy for the trained classes using KDTree KNN Classifier (Sentinel-1 and Sentinel-2 image, Lake Illirney region, July 2017)	50
4.11	Training accuracy for the trained classes using Minimum Distance Classifier (Sentinel-1 and Sentinel-2 image, Lake Illirney region, July 2017)	51
4.12	Prediction accuracy for methods of supervised classification (Fusion of Sentinel-1 and Sentinel-2 images)	51
C.1	Vegetation plots (2018) used as reference data	77
C.2	Climate data showing average temperature (°F) and average precipitation (in)	78

Abbreviations and Symbols

~	Approximate
>=	Greater and equal to
<=	Less and equal to
%	Percent
°C	Degrees Celsius
°F	Degrees Fahrenheit
µm	Micrometre
ϵ_r	Dielectric constant
θ	Theta
λ	Wavelength
cm	Centimetre
dB	Decibel
Gb	Gigabyte
GHz	gigahertz
Km	Kilometre
m	Metre
MB	Megabyte
Mbit/s	mega-bit per second
mm	Millimetre
ALOS	Advanced Land Observing Satellite
ASAR	Advanced Synthetic Aperture Radar
AVHRR	Advanced Very High-Resolution Radiometer

AWI	Alfred-Wegener-Institute
AVNIR	Advanced Visible and Near-Infrared
BoA	Bottom of Atmosphere
CS	Component Substitution
DEM	Digital Elevation Model
DLR	Deutsches Zentrum für Luft-und Raumfahrt
DMSP	Defence Meteorological Satellite Program
DT-CWT	Dual-tree Complex Wavelet Transform
EC	European Commission
ERS	European Remote Sensing Satellites
ESA	European Space Agency
ETM+	Enhanced Thematic Mapper Plus
EW	Extra-Wide
FDBAQ	Flexible Dynamic Block Adaptive Quantization
FR	Full Resolution
GIHS	Generalized Intensity-Hue-Saturation
GLCM	Grey Level Co-occurrence Matrix
GOES	Geostationary Operational Environmental Satellite
GRD	Ground Range Detected
H	Horizontal
HH	Horizontal-horizontal
HPF	High Pass Filter
HR	High Resolution
HS	Hyperspectral
HV	Horizontal-vertical



IFOV	Instantaneous Field of View
InSAR	Interferometric Synthetic Aperture Radar
IR	Infrared
ISRO	Indian Space Research Organization
IW	Interferometric Wide
k_NN	k-Nearest Neighbors
LAI	Leaf Area Index
LC	Leaf Cover
LCC	Leaf Chlorophyll Content
LiDAR	Light Detection and Ranging
LULC	Land Use/Land Cover
MKF	Multiscale Kalman Filter
MLC	Maximum-likelihood Classification
MODIS	Moderate Resolution Imaging Spectroradiometer
MR	Medium Resolution
MRA	Multiresolution Analysis
MS	Multispectral
MSI	Multispectral Instrument
N	North
NASAR	National Aeronautics and Space Administration
NDVI	Normalized Difference Vegetation Index
NDVI_{max}	Maximum Normalized Difference Vegetation Index
NISAR	NASA-ISRO Synthetic Aperture Radar
NOAA	National Oceanic and Atmospheric Administration
OA	Overall accuracy

OCN	Ocean Colour Net
OSW	Ocean Swell
OWI	Ocean Wind
PALSAR	Phased-Array-type L-band Synthetic Aperture Radar
PAN	Panchromatic
PCA	Principal Component Analysis
POD	Precise Orbit Determination
POE	Precise Orbit Ephemerides
PROJCS	Projected Coordinate Systems
RADAR	Radio Detection and Ranging
RADARSAT	Radio Detection and Ranging Satellites
REDD	Reducing Emissions from Deforestation and Forest Degradation
RF	Random Forest
RGB	Red, Green and Blue
RMSE	Root Mean Square Error
ROIs	Region of Interests
RVL	Radial Velocities
S1	Sentinel-1
S2	Sentinel-2
SAR	Synthetic Aperture Radar
SFIM	Smoothing Filter-based Intensity Modulation
SIR	Shuttle Imaging Radar
SLAR	Side-Looking Airborne
SLC	Single Look Complex
SM	Stripmap

SNR	Signal-to-Noise Ratio
SPOT	Système Pour l'Observation de la Terre
SVM	Support Vector Machine
SWIR	Short Wave Infra-Red
TM	Thematic Mapper
TIROS-1	Television and Infrared Observation Satellite 1
USGS	United States Geological Survey
UTM	Universal Transverse Mercator
V	Vertical
VNIR	Visible and Near-Infra-Red
VH	Vertical-horizontal
VV	Vertical-vertical
WGS	World Geodetic System
WV	Wave mode
ZY-3	Ziyuan 3

1 INTRODUCTION

1.1 Motivation

There has been a significant knowledge from previous research about the land-cover classification using optical-based images in the higher latitudes and arctic regions. However, the use of radar-based products for these areas has rarely been explored for land-cover mapping. This drives the desire to carry out land-cover classification with Synthetic Aperture Radar (SAR) imagery, compare its accuracy with its optical counterpart and assess the synergic use of both Sentinel products.

Though, Sentinel-2 products are mainly used for high-resolution land-cover classification, but some regions especially the higher latitudes where cloud cover is intense might benefit from the use of Sentinel-1 products along with its Sentinel-2 counterparts in a synergic approach (Fletcher, K., 2012). The fusion of both Sentinel products may help increase the accuracy of the results and thus enhance better interpretation (Ghassemian, H., 2016). The information obtained from optical, and radar remote sensing images are complementary (Bagan, H. *et al.*, 2012); hence there is an advantage in merging the two remote sensing products which helps to achieve more improved classification precision (Herold, M. *et al.*, 2006).

The use of optical products to obtain remote sensing data in Arctic region has encountered some challenges, such as constant cloud cover, the solar geometry (Stow, D. A. *et al.*, 2004), rapidly modifying spectral characteristics, and disjointed land-cover borders (Chasmer, L. *et al.*, 2014). A radar sensor has a set of incredible characteristics that make it an important tool in Earth observation. It produces images all the time because it uses its own source of illumination on the target, unlike optical sensors. It is also weather independent, as the sensor can penetrate through clouds (Meyer, F., 2019). These abilities of SAR sensors help to compliment optical sensors.

Soria-Ruiz, J. *et al.* (2010) established a possibility of better outcomes and increased precision by exploring the combination of optical and radar imageries for the land-cover mapping in Central Mexico. He also observed a classification confusion between maize and grassland while using optical images alone, but he observed a better classification accuracy with both techniques. Ullmann, T. *et al.* (2014) showed that the overall accuracy increased up to 71 percent for unsupervised classification and 87 percent for supervised classification for some tundra landscapes in an Island in the Arctic region of Canada using Landsat 8 and Radarsat-2. The exploration of different physical properties of optical and radar images for terrain mapping

improves the efficacy of the spectral resolution and reduces greatly the demerits of using both image sources independently (Joshi, N. *et al.*, 2016).

1.2 Study idea

This study will obtain Sentinel-1 & -2 images about the summer season of a 5-year period of two regions (Lake Illirney and Lake Khamra regions) with slight difference in vegetation types. This timeline is between 2017 and 2021. The purpose is to apply fusion techniques, which involves the combination of sensing data from various satellites to utilize the matching pixel values in the data (Ghassemian, H., 2016). The data of the Sentinel products will be acquired in proximity in terms of dates, and they will be images of the same area (Pandit, V. R. & Bhiwani, R. J., 2015). The changes in the study areas within the time considered will also be observed to monitor how these Sentinel products access changes in the physical features present in the study areas.

This thesis aims at achieving the following objectives:

- to evaluate how Sentinel-1 & -2 images look at different vegetation types from both regions,
- to compare the efficacy of both Sentinel imageries to techniques in supervised land-cover classification such as Random Forest (RF) classifier, KD Tree-KNN classifier, Minimum Distance (MD) classifier, KNN classifier & Maximum Likelihood (ML) classifier,
- to assess the performance of the synergic use of both Sentinel products to supervised land-cover classification using the five (5) techniques listed above,
- to apply a verification procedure to the output data after the application of land-cover classification techniques to the Sentinel products,
- to assess the variations of the features in the study areas across the time of 5 years (2017-2021).

2 PRINCIPLES

2.1 Remote sensing fundamentals

It involves a scientific procedure that involves acquisition of information about a target of interest (usually the Earth) with no physical interaction with the target of interest. This information collection is carried out by remotely sensing and acquiring displayed light followed by handling, examining, and utilising the data for application purposes (Centre for Remote Sensing, Canada, 2015). The processes of remote sensing are described below (Fig. 2.1).

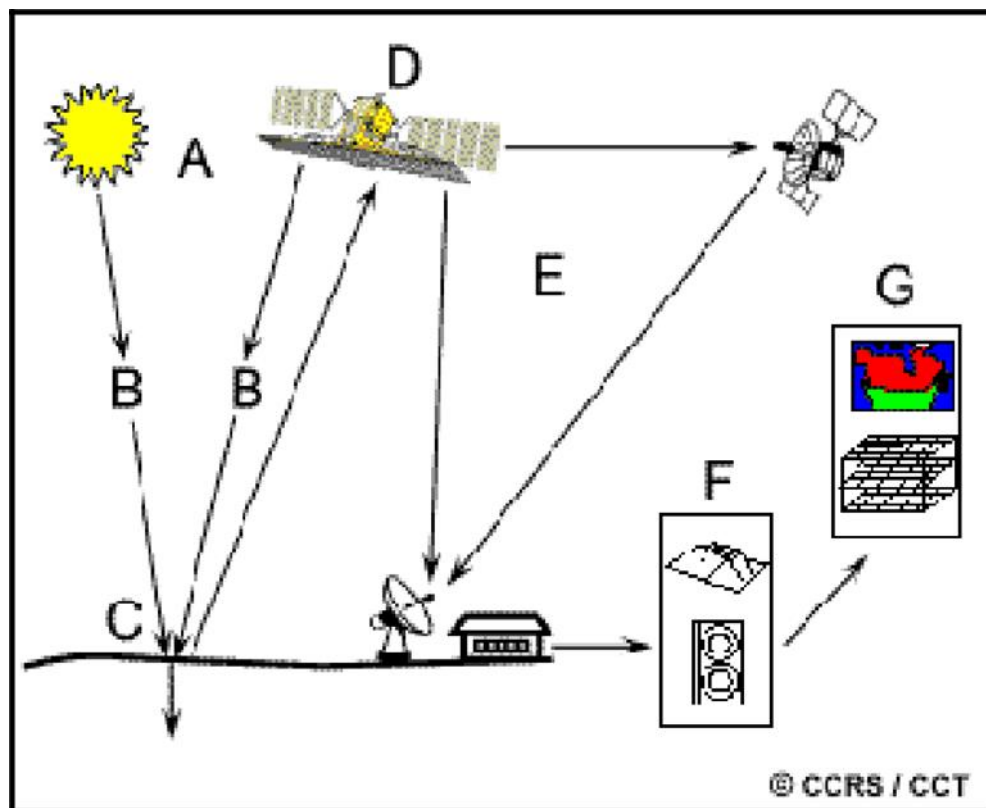


FIGURE 2.1 Illustrative picture of remote sensing in details (A) Radiance (B) Electromagnetic energy in the air (C) Contact on the Earth surface (D) Storing of radiation carried out by the satellite (E) Broadcast, reception, and handling (F) Data Interpretation and study (G) Applications (Source: National Resources Canada, Earth Sciences Sector)

The energy source or illumination highlighted earlier (in Fig. 2.1) consists of all forms of illumination which are referred to as electromagnetic waves. These electromagnetic waves comprise of electric and magnetic fields. The spectrum constitutes gamma signals, x-ray signals, ultraviolet (UV) signals, visible light signals, infrared signals, radar signals, microwaves, and radio signals (Ibrahim, S., 2007). The waves in this spectrum also possess two (2) main characteristics namely, wavelength (λ) and frequency (Hz). There are also four (4) major types of resolutions that define the characteristics of a remote sensor namely, spectral, spatial, temporal, and radiometric resolutions (Centre for Remote Sensing, Canada, 2015). These variables are inversely proportional to each other i.e., short wavelength electromagnetic waves have increased frequencies while long wavelength electromagnetic waves have decreased frequencies (Fig. 2.2). The Sentinel-1 images utilize the radar wave and microwave regions while Sentinel-2 images utilize the visible light signals and infrared signals.

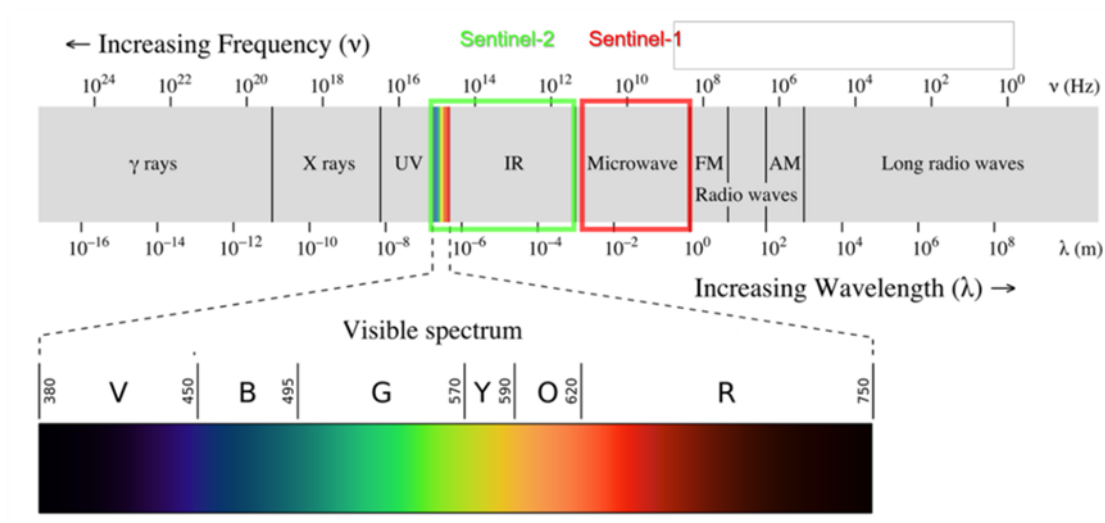


FIGURE 2.2 Electromagnetic spectrum showing Sentinel-1 and Sentinel-2 satellites' regions (Source: Ronan 2013, CC BY SA 3.0)

Remote sensing systems are categorised in two types, namely reactive and active sensing instruments. Reactive instruments measure electromagnetic energy that are naturally available. This natural available energy is the Sun, which serves as a convenient source of energy for remote sensing purposes. This limits the use of passive sensors to when the sun is available, which is mostly during daylight. Active sensors use artificial light source provided by the sensor's

manufacturer onboard the instrument and illuminated on the Earth surface been studied (Centre for Remote Sensing, Canada, 2015). Pictorial representation of different concepts of remote sensors can be seen in Figure 2.4. Active sensors can obtain information anytime or season. Light sources present in active sensor also produces enough microwaves as compared to the Sun (Centre for Remote Sensing, Canada, 2015).

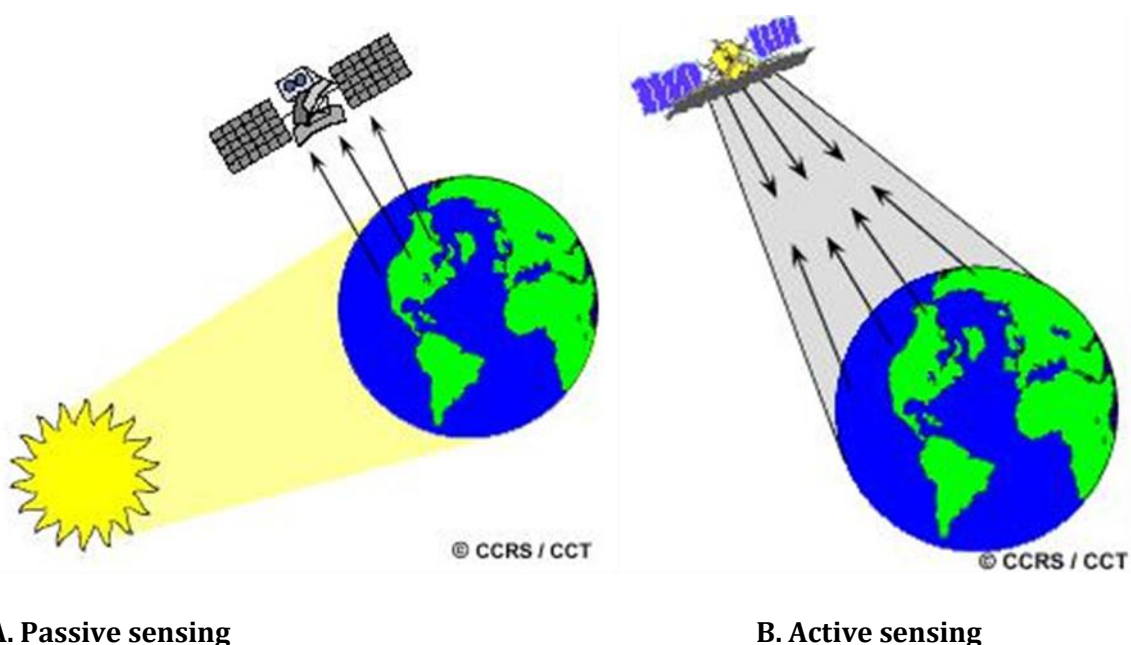


FIGURE 2.3 Pictorial representation of different remote sensing techniques (Source: National Resources Canada, Earth Sciences Sector)

Examples of passive or reactive sensors are Television and Infrared Observation Satellite -1 (TIROS-1), Advanced Very High-Resolution Radiometer (NOAA AVHRR), Système Pour l'Observation de la Terre (SPOT), Landsat program, Sentinel-2, IKONOS (offers multispectral [MS] and panchromatic [PAN] imagery), QuickBird, WorldView, DMSP (Defence Meteorological Satellite Program), Geostationary Operational Environmental Satellite (GOES) etc. Active sensing instruments include Synthetic Aperture Radar (SAR) products, Sentinel-1, Light Detection and Ranging (LiDAR) scanners, Laser fluoro-sensor, Radio Detection and Ranging Satellites (RADARSAT) systems, European Remote Sensing Satellite (ERS-1 & ERS-2). These sensors can be applied to studies involving forestry, food production, hydrology, terrain geology, arctic regions,

coastal management, mapping of physical features, land-cover & -use etc. (Centre for Remote Sensing, Canada, 2015).

2.2 Basics of synthetic aperture radar (SAR) remote sensing

Radio detection and ranging (RADAR) uses the advantage of their long signal energy to penetrate past larger particles in the atmosphere or rain cloud covering (Centre for Remote Sensing, Canada, 2015). The mid-20th century saw the use of Side-Looking Air-borne radar (SLAR) products having dependable imagery quality. This system contains a radar sensor traveling alongside a parallel line, H onboard a spaceborne platform (Fig. 2.5). The antenna of a SLAR system is pointed away from the base point directly opposite the zenith by a so-called look angle (θ_l) (Meyer, F., 2019).

Terrain features with related characteristics can cause geometric alterations in products obtained by SAR sensors because all radar sensors have tilted reflection geometry characteristic present in them. These main distortions are foreshortening, layover, and shadow (Fig. 2.6). Foreshortening occurs when the slope facing the sensor is abridged in the image. The consequences of foreshortening reduce when there is an increase in the angle of focus. Layover occurs when the top of the mountain obstructs the view of a sensor from capturing the ground ahead of the mountain. An increase in look angle decreases the effect of layover. Shadow is a type of distortion that occur when the ground behind the mountain is not visible to the sensing instrument. A rise in the angle of focus increases shadow effects (Meyer, F., 2019).

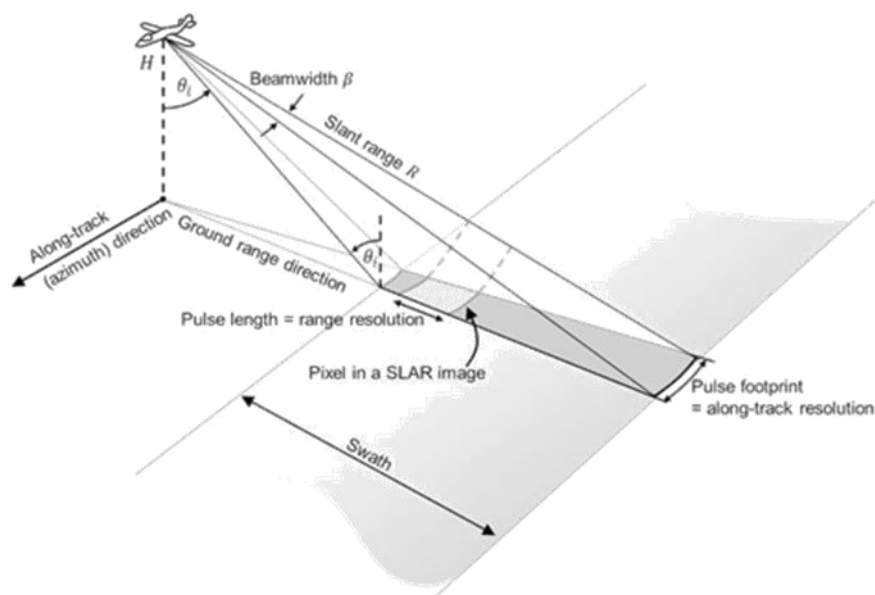


FIGURE 2.4 A mathematical expression of a SLAR imaging instrument (Source: Meyer, F., 2019)

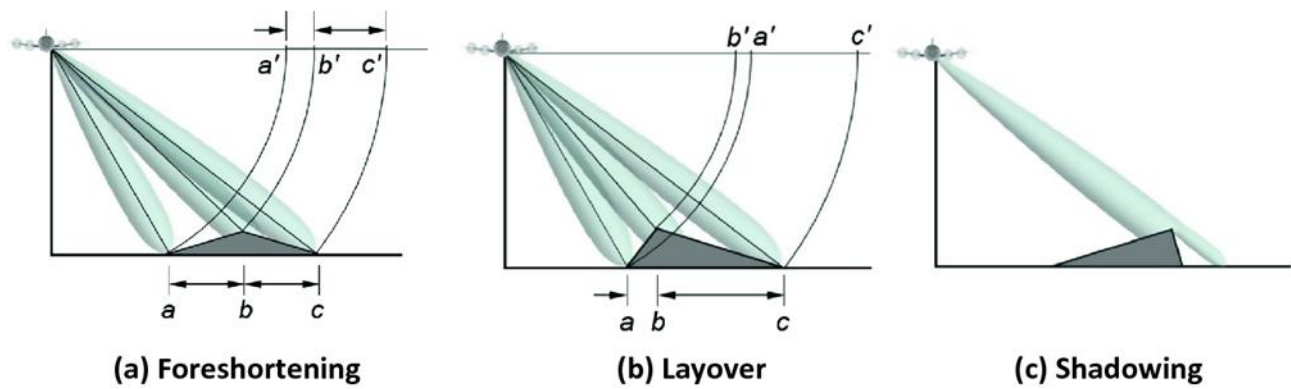


FIGURE 2.5 The major symmetrical misrepresentations in radar products: (A) Foreshortening, (B) Layover, and (C) Shadow (Source: Environmental Geoinformatics, Joseph Awange and John Kiema, 2018, pp 137-148)

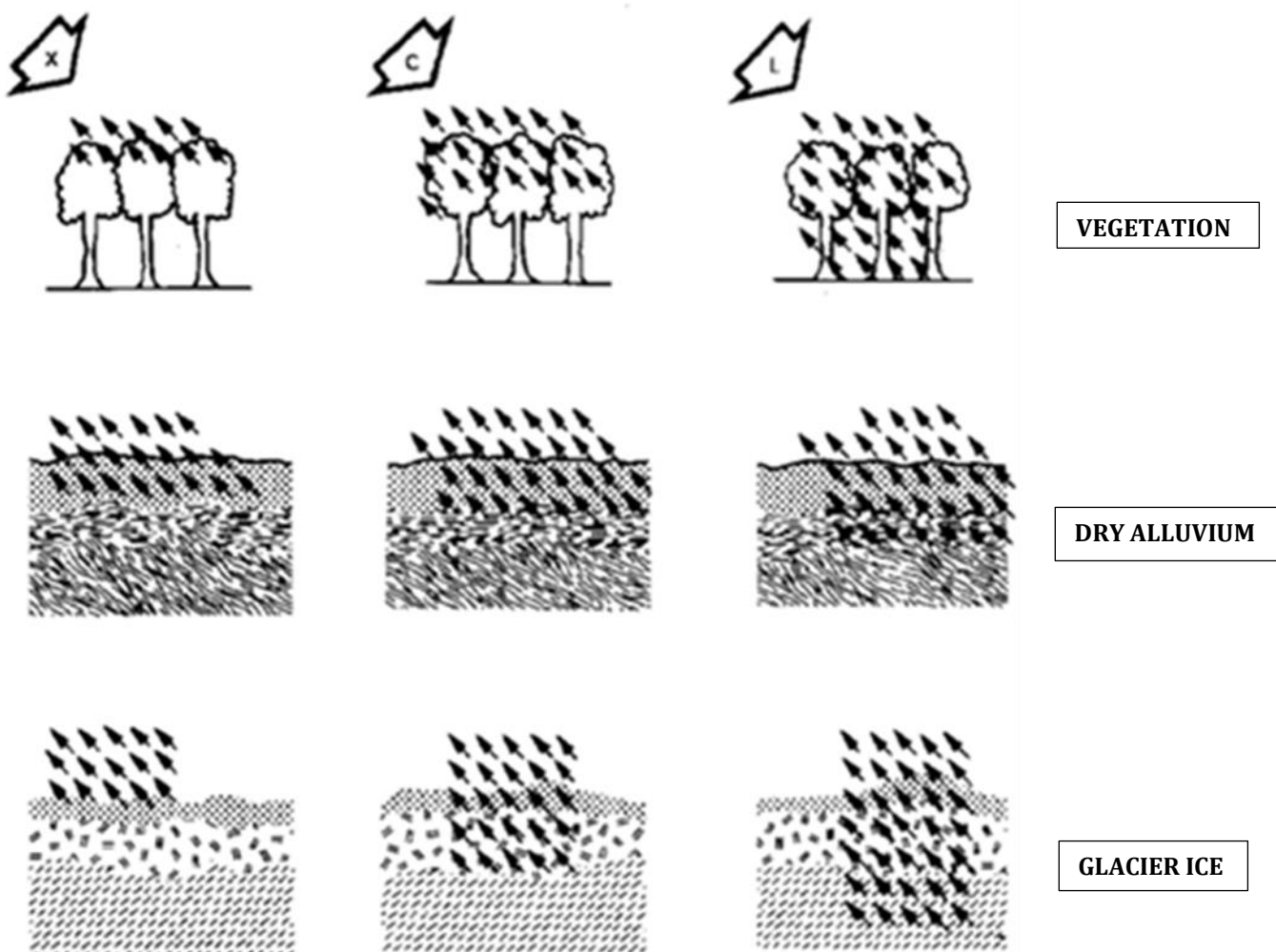


FIGURE 2.6 Level of SAR signal penetration by sensor wavelengths, λ (Source: Meyer, F., 2019)

Fig. 2.7 shows how signals penetrated a variety of surface types due to the influence of signal wavelength, λ . The increase in sensor wavelength enhances deeper penetration of radar signals. The signal polarization of SAR sensors is controlled by the user on the transfer and the obtain directions (Westphal, W. H., 1970). Most of the SAR sensors are polarized in straight direction and broadcast in x- or y-directional signal types. These sensing instruments usually function in HH- or VV- or HV- or VH-polarization (Meyer, F., 2019).

SAR sensors propagate electromagnetic radiation in a particular band of microwave signal. The SAR sensing instrument's wavelength is fundamentally attached to its abilities to penetrate with its propagated microwave energy. For instance, the signals of L- and P-band travel more into forested structures and the ground. The usefulness of radar sensing products is dependent on the bands utilized (Meyer, F., 2019). C-band images are regarded as good fit used in lieu of X-band and L-band sensing instruments because of its medium- to high-level resolution abilities and enhanced flora access. Most radar images operate in C-band, though L-band is regarded as the future of radar because of its deeper penetration reach of vegetation canopies, particularly the beneath canopy layers (Meyer, F., 2019).

2.3 Sentinel-1

The fundamentals of Sentinel-1 are built majorly on C-band radar products combining two sensors to prevent omitting an area during observation of the Earth surface (Meyer, F., 2019). Images having dual polarisation are suitable for terrain features mapping and its application in arctic regions. Sentinel-1 products function in Extra-Wide (EW) swath, Strip Map (SM), Wave mode (WV) and Interferometric Wide (IW) swath (Fletcher, K., 2012).

The characteristics of images from Sentinel-1 has brought about various applications in SAR remote sensing. This is because Sentinel-1 products can record information of a large area and repeating occurrence found in the matching pixel values of the sensing products. It also possesses a high-level ability that methodically handles, records, and make available the output images in an organized format to the users (Potin, P. *et al.*, 2016). These abilities make Sentinel-1 a better option over some other satellite products.

Radar sensors can efficiently map Earth surfaces as well as monitor the magnitude of changes that occur on it, especially if a reference data is provided. The Sentinel-1 products are mostly utilized in land, marine, and atmospheric monitoring. They are also applied to security, emergency response and climate. Sentinel-1 mission can also be employed while investigating terrain feature mapping, food production management etc. (Fletcher, K., 2012).

2.4 Sentinel-2

It consists of a twin satellite that orbit round its axis at the poles of the orbit, located 180° apart from one and other and intended to give a high revisit frequency. The revisit of these satellites independently is ten (10) days, and five (5) days is the revisit time when merged. Sentinel-2 has high-resolution, wide-swath, multi-spectral imaging systems. Sentinel-2 products can examine 13 spectral bands with an optical swath width of about 290 km (Hoersch, B., 2015). Sentinel-2 mission was designed to observe irregularity in terrain cover situations and supports observation of the variations to flora in the period of crop cultivation. It is also involved in emergency management, security, and climate change (Hoersch, B., 2015).

2.5 Fusion of images in remote sensing

The varieties of satellite products like radar products, hyperspectral (HS), multispectral (MS), panchromatic (PAN) etc. have advantages to combine their strong qualities. This can be accomplished by different techniques of image fusion. The interpretation of remotely sensed images may be better improved or reliable for application purposes when these images are fused together. The merging of images has been important technique in combining data acquired from various remote sensing instruments with various spatial, temporal, spectral, and radiometric resolutions (Mitchell, H. B., 2010; Zheng, Y., 2011 & Ghassemian, H., 2016). Three (3) techniques occur in merging of images which include; pixel, feature and decision levels (Ghassemian, H., 2016). The images formed at the pixel-level fusion provides more precise image data that is then utilised for evaluation and managing when the terrain characteristics are explored and mapping are carried out (Dawei, Z. & Fang, Z., 2007; Hui, T. & Binbin, W., 2009). Loss of information in the images are minimal during pixel-level image fusion, but this procedure processes the biggest quantity of data, so making the speed of the processing instrument to be slow and place high demand on the memory of the instrument (Wang, Z. *et al.*, 2010).

There have been various researches in the past utilizing images from optical and radar satellite instruments. The merging of WorldView-2 and TerraSAR-X products was used by Xu, Y. *et al.* (2015) to obtain data in relation to the height of built-up areas in selected cities. Their results revealed a decreased average absolute height retrieval error when the images of the different Earth study tools are fused together compared its errors when used separately. Their proposed fusion approach is appropriate for the study of retrieval of the height of built-ups in urban areas.

Landsat satellites offer good resolution images for land-cover classification (Knorn, J. *et al.*, 2009; Masek, J. G. *et al.*, 2006) but the revisit time of sixteen (16) days place a restriction from the atmosphere to their use in monitoring terrain feature variabilities when considering a longer

timeline (González-Sanpedro, M. C. *et al.*, 2008). Also, NOAA sensing instruments which has medium resolution imaging spectro-radiometer (MODIS) data is collected two times per day, therefore the temporal resolution make it useful for managing active variations of terrain features (Walker, J. J. *et al.*, 2012; Strugnell, N. C. *et al.*, 2001).

Simone, G. *et al.* (2002) studied the combination of optical(Landsat) and radar products of the same study area obtained at different periods making use of neural systems. They also used a processor to merge multiple SAR images with different characteristics, centred on multiscale Kalman filter (MKF) and wavelet transform. The multiscale Kalman filters are system that utilize simulations of dynamics and onboard satellite instrument measurements to acquire evaluation of the state vectors (Ovchinnikov, M. & Barrington-Brown, J., 2021).

Garzelli, A. & Nencini, F. (2006) suggested a pan-sharpening model for multi-band multi-spectral images. This model uses a Generalized Intensity-Hue-Saturation (GIHS) conversion to the multi-spectral bands. A genetic model was also used to determine the misplaced high-pass data from the panchromatic image. The fitness function of the natural procedure which offers the procedure variables running the merging method was established on a quality indicator particularly created for quality evaluation of multi-band multispectral images. Both photographic and unbiased comparisons with advanced merging procedures were presented on QuickBird image data.

The merging of images techniques were used in analysing panchromatic (PAN) and multispectral (MS) images for a study carried out by Jing, Y. *et al.* (2008). These techniques include Principle Component Analysis (PCA), High Pass Filter (HPF), Smoothing Filter-based Intensity Modulation (SFIM), and other methods. The result revealed that HPF and SFIM had the best quality in preserving spectral data of the preliminary data. It was also noticed that PCA had the worst performance. The study also concluded that using merged data had an increment in spatial resolution compared to the spatial resolutions of the individual images when landcover classification methods were applied to both the fused images and individual images separately. Also, SFIM Transform method had the highest performance in preserving spectral data of the initial data.

Piella, G. (2003) proposed a broad structure for the merging of multi-resolution (MR) image. The suggested structure allows for the creation of new image fusion techniques as well as integrating the existing techniques. The merging of multi-resolution images based on regions technique used by this researcher is an expansion of the conventional pixel-centred techniques. Her plan was to carry out the merging of multi-resolution/multi-spectral data using several data. So she created a technique centred on pyramid linking and she recommended a fusion algorithms which made use of the segmentation outcomes. The findings obtained suggested that her methodology may be of

use when conducting researches that involves the merging of sensing data. She indicated that work is in progress on the impact of the various factors on the merging procedures.

The fragmentation of the characteristics of input images carried out with the utilization of a Dual-tree Complex Wavelet Transform (DT-CWT), either in combination or independently, to create a landcover outline were carried out by Lewis, J. J. *et al.* (2004). The results revealed that their method performed in a way that can be matched to pixel-based fusion methods. Though the processes employed by these researchers had some intricacies, it also has some improvements over the existing methods. These improvements consist of the capability to make use of additional logical semantic merging rules; and for zones containing specific features to be reduced or increased.

A new merging technique used for the merging at pixel level of transmitted data as well as data structures was recommended by Rockinger, O. in 1996. This merging technique was built using change invariant expansion of isolated wavelet transform that produced a perfect wave description known as wavelet frames. The benefit of his suggested merging is the enhanced temporal constancy and how the merged image structures are reliable. He displayed illustrations of the purpose of the wavelet frame merging system in cooperation with both the actual images and image structures (Rockinger, O., 1996).

Image processing and image fusion to generate high-resolution multispectral images in remote sensing are considered as distinct procedures. The subsequent errors caused by applying these procedures separately can be able to lead to major mistakes which can impact the quality of the resulting output products of the merging process (Zhang, Q. *et al.*, 2015). They created a novel image processing and fusion procedures for panchromatic (PAN) and multi-spectral (MS) products using Ziyuan 3 (ZY-3) and GeoEye-1 data. This methodology uses the implementation of the merging technique to assess the image processing precision and creates an actual function to iteratively fill in the process factors. It was observed that the results achieved with their suggested method had better image processing accuracy and fusion quality.

The research regarding the combined application of the Sentinel-1 & -2 remote sensing instruments for terrain features mapping was carried out by Clerici, N. *et al.* (2017). This experiment applied radar and optical data, using a region in Colombia as an area of interest. The authors used three (3) various supervised classification methods such as; Support Vector Machine (SVM), k-Nearest Neighbors (k-NN), and Random Forest to assess the functionalities of these distinct mapping techniques. The synergic application of Sentinel-1 & -2 products for land-cover classification produced more accurate result compared to using both images separately. Also, their result shown that visible-near infrared and radar unified images grouped with the technique

of Support Vector Machine (SVM) yielded a very precise land cover classification compared to the other two techniques (Clerici, N. *et al.*, 2017).

The ability of merging an optical and radar sensing products used for terrain features mapping was recommended by Bagan, H. *et al.* (2012). They proposed that land-cover mapping precision can be more enhanced by means of merging an optical product, AVNIR-2, PALSAR (radar product), as well as some polarimetric factors in one dataset. The authors used Maximum Likelihood (ML) classifier and subspace method, support vector machine (SVM). They concluded that the merging between both optical and radar datasets used produced a better precise output products for both supervised classification techniques utilized than the use of same supervised classification methods on optical and radar data independently.

Ban, Y. *et al.* (2010) assessed the fusion of Quickbird MS and RADARSAT SAR for urban terrain features classification. The researchers categorized the remotely sensed data by utilizing a methodology centred on objects and rules. The results revealed that the methodology is objective and knowledge-centred have being efficient in obtaining municipal terrain feature types "from Quickbird MS data (16 classes, overall accuracy: 87.9%; kappa 0.868) and multi-temporal RADARSAT fine-beam SAR data (11 classes, overall accuracy of 86.6%; kappa: 0.852)". The merging of the optical and radar mapping outcomes was capable to utilize the benefits of both different characteristics peculiar to these products, in order words greatly improving the precisions of the different terrain features (Ban, Y. *et al.*, 2010). However, the researchers recommended that potential research is necessary to create improved procedures to differentiate between the highly metropolitan areas and smaller towns and villages with low residential areas in both optical and radar instruments' classification.

A comparative assessment of Advanced Land Observing Satellite (ALOS), Landsat imagery and PALSAR sources utilized in the terrain features mapping of the vegetation in the Brazilian Amazon was achieved by Walker, W. S. *et al.* (2010). The researchers achieved a thorough relative assessment centred on twenty (20) distinct PALSAR- and Landsat categories. Their relative assessment analyses and approves capacities of recent radar sensing systems in producing precise as well as suitable classification and the observation of the vegetative terrain, with concentration on the rainforest areas that usually limits the performances of optical sensing instruments due to the occurrence of clouds and other substances affecting the performance of these sensors. It was also observed that existing and scheduled implementations of different bands of radar instruments remain perfectly situated by offering continuous information flows at present and in future (Walker, W. S. *et al.*, 2010).

Chu, H. T. *et al.* (2010) performed an experiment with optical and radar images while working on terrain features classification using the municipal town of Ho Chi Minh located in Vietnam. The

products used are SPOT, PALSAR and ALOS multispectral instruments. The researchers utilized some SPOT multispectral images and PALSAR for the terrain feature mapping. Their results recommended that the combination of radar and optical products provides substantially better mapping precision than when the data were utilized independently. The Support Vector Machine (SVM) classifier likewise outshine the Maximum Likelihood (ML) classifier in instances entailing the mapping for the merged products. This is due to its non-parametric kind that is regarded as most suitable in categorizing spatially numerical information (Chu, H. T. *et al.*, 2010).

The terrain features mapping of a humid tropics using Central Sulawesi, Indonesia as a case study was carried out by Erasmi, S. & Twele, A. (2009). The authors examined the products of Landsat ETM+ (Enhanced Thematic Mapper Plus) and Envisat-ASAR remotely sensed instruments which has the capacity to measure small-scale landcover terrain in a humid natural environment. The outcome of this experiment proved the benefits of multi-temporal radar images as matched with one-dimensional temporal radar-centred land-cover classification. So, a full terrain features classification in a municipal town with a diverse low-scale land-cover terrain can not be accomplished without the use of optical sensing instruments, but can be enhanced with a SAR-based product like Envisat ASAR in the case of the case study carried out by Erasmi, S. and Twele, A. (2009).

The multi-sensor terrain features classification of an area in West Africa using ASAR, TanDEM-X/TerraSAR-X and MODIS data was achieved by Gessner, U. *et al.* (2015). These enhanced land-cover information with spatial resolution around 250m for the region of West Africa, was built centred around information using MODIS, ASAR as well as TanDEM-X/TerraSAR-X products. The optical and radar data were utilized to describe stable and seasonal streams, rivers and oceans. Structures and paved surfaces in the region were identified with regards to a smooth coverage of SAR information compiled by the SAR sensors used (Gessner, U. *et al.*, 2015). Their results shown that the precision valuation in the multiple sensing instrument land cover map yielded a total precision of “80% at legend level 1 (9 classes) and 73% at the more detailed legend level 2 (14 classes)”. Multiple sensing instruments as well as provincially improved terrain features maps, like the data information provided by the authors can bring evidence that is appropriate in provincial usefulness when using it in aquatic and terrestrial resource supervision, also it can then be utilized in sufficiently describing the terrestrial outward for provincial-level algorithm researches (Gessner, U. *et al.*, 2015).

Haack, B. & Bechdol, M. (2000) used Landsat Thematic Mapper (TM) and Shuttle Imaging Radar (SIR-C) to assess multisensor spaceborne data for East African terrains involving cultivation lands, communities, and plant life. The research analyzed the efficacy of the radar data in order to precisely detect the zones of cultivation lands, communities, and plant life. It was noted that SAR products alone produced outstanding classification precisions. The combination of SAR (SIR-C) and

Landsat TM (optical product), also enhanced classification capacity, also it was observed that L-band proved to be more valuable than C-band. The outcome of this experiment indicated that a potential is present in merging both optical and radar sensing instruments for land-cover classification of natural terrains (Haack, B. & Bechdol, M., 2000).

A study on the merging of optical and radar images for land-cover classification was carried out by Herold, N. D. & Haack, B. N. (2002). They assessed Landsat Thematic Mapper (TM) multispectral and Spaceborne radar datasets separately and also merging those two different products to perform terrain features mapping using an area of interest close Wad Medani, Sudan. The independent use of Landsat Thematic Mapper (TM) multispectral image created an improved result than the independent use of SAR image. The synergic use of both image products created an enhanced output products, resulting in flawless grouping of all terrain features categories representing the environment of the area of interest (Herold, N. D. & Haack, B. N., 2002). This study also revealed the possible benefit in combining the use of optical and radar and images in terrain features mapping.

Qin, Y. *et al.* (2016) created a method in an experiment to classify a forested area in 2010. The researcher experimented with "Advanced Land Observation System (ALOS) Phased Array L-band Synthetic Aperture Radar (PALSAR) and MODerate Resolution Imaging Spectroradiometer (MOD13Q1 and MOD09A1) products". They utilized the composition and biomass data from the SAR products and the phenological data from the optical products. The L-band PALSAR products were important because it is needed to obtain the land forms and ground biomass of vegetation, because it has the ability to penetrate into the vegetation (Imhoff, M. L., 1995). The Maximum NDVI ($NDVI_{max}$) derived from MOD13Q1 in 2010 have been utilized in order to decrease prospective error from sparingly forested terrain area including large buildings and bumpy land forms and rough land surfaces, which gave elevated PALSAR backscatter amounts comparable to the forested areas. They fused the radar and optical products utilized in the research to attain an improved classification precision (Qin, Y. *et al.*, 2016).

The experiment involving integration of Sentinel-1 & -2 for the classification of the terrain in the metropolitan area of Belém, in Eastern Brazilian Amazon was carried out by Tavares, P. A. *et al.* (2019). They chose top terrain features classification methodologies meant for humid zones make use of Sentinel remote sensing instruments with data whose dates of acquisition are close to each other to create a machine learning land-cover mapping out of a Random Forest (RF) classifier. Their outcome revealed a better overall accuracy (OA) was discovered to be in the fusion of Sentinel-1 and -2 images, which yielded an accuracy of 91.07. They also shown that the combination of the vegetation and water body indicators as well as SAR textural characteristics reduced the overall accuracy (OA) (Tavares, P. A. *et al.*, 2019).

2.6 Methods of supervised classification

Supervised classification is a type of land-cover classification that involves the provision of training data by the user in order for the specified algorithm to analyse and aggregate the clusters of pixel values with the same characteristics into land-cover classes as specified by the training data. The other method of land-cover classification is unsupervised classification. Unsupervised classification uses only the in-built algorithm without the need of a training data to merge pixel information of related characteristics (Braun, A., 2020). Unsupervised classification constitutes *Expectation Maximization (EM) Cluster Analysis* and *K-Means Cluster Analysis*.

The methods of supervised classification utilized in this study are as follows; *Random Forest (RF) Classifier*, *Minimum Distance (MD) Classifier*, *KNN Classifier*, *KDTree KNN Classifier* and *Maximum Likelihood (ML) Classifier*. *Random Forest (RF) Classifier* was created by Leo Breiman, an American statistician. The algorithms in RF randomly choose pixels based on the training data provided by the user and aggregate them in clusters of identical characteristics (Breiman, L, 2001). The use of different methods of supervised classification in the research work conducted by Barrett Lowe and Arun D. Kulkarni in 2015 and 2016 indicated that RF classifier outperformed other methods of supervised classification when using multispectral optical images (Lowe, B. & Kulkarni, A. D., 2015; Kulkarni, A. D. & Lowe, B., 2016). Liaw, A. and Wiener, M. (2002) used the RF algorithm for both terrain features mapping and regression for satellite images. Barrett, B. *et al.* (2016) assessed the utilization of optical data with average spatial resolution and radar images, for detecting and classifying plateau plant life utilizing the Random Forest (RF) classifier. They also accomplished a very high precision and improved outputs while monitoring the changes in the upland vegetation of Mount Brandon, the Comeragh Mountains and the Galtee Mountains.

Hou, W. *et al.* (2018) carried out a research work by utilizing *KD-Tree KNN Classifier* algorithm to complement for the processing period required if only *KNN Classifier* was used for supervised classification. It was concluded that the use of *KD-Tree KNN Classifier* increased the efficacy of the classification (Hou, W. *et al.*, 2018). Xue, S. *et al.* (2019) used the algorithm of *KDTree KNN Classifier* to improve Iterative Closest Point (ICP) algorithm for a more precise fitting to acquire point cloud registration. *Minimum Distance (MD) Classifier* was employed by Abinaya, V. and Poonkuntran, S. (2019) to make sure all pixel values were classified as well as to reduce the processing time. They concluded that *MD Classifier* was an improvement on other methods of supervised classification used in their study.

3 METHODS

3.1 Study area

In this research work, two (2) study areas were considered namely; Lake Illirney region of Bilibinsky district, Chukotka Autonomous Okrug, Russia (Fig. 3.1) and Lake Khamra region, Lensky district in the south-western part of Yakutia, Russia (Fig. 3.3). The Lake Illirney region consists of northern tree-line biome largely composing of boreal forest. This district is sparsely populated with 7866 inhabitants (2010 Census). Most of the population are involved in animal husbandry like reindeer, fish hunting and crop farming (Official Website of Bilibinsky District, 2021). The Autonomous Okrug is mainly comprises of Bilibinsky and Anadyrsky districts (Kryžanovskij, O. L. 1995). The daily mean temperature in the month of July, which is the warmest month of the year in Lake Illirney region is 13.2C while the daily mean for month of January (coldest month of the year in that region) is -35.6C (Climatebase.ru.).

The Lake Khamra region consists of northern taiga constituting of densely distributed evergreen forest. The weather and climate of south-western Yakutia can be described by a brief, moderate farming time of year and exceedingly freezing wintry weather. It has an average temperature in July of approximately 18C and the average temperature in January, which is the coldest month of the year can go as low as -40C (Fedorov, *et al.*, 2018). The climate around Lake Khamra is majorly impacted by huge amount of Arctic Oscillation (AO) form rising in the middle of winter high-latitude with moderate mid-latitude atmospheric forms (Wu, B. & Wang, J., 2002).

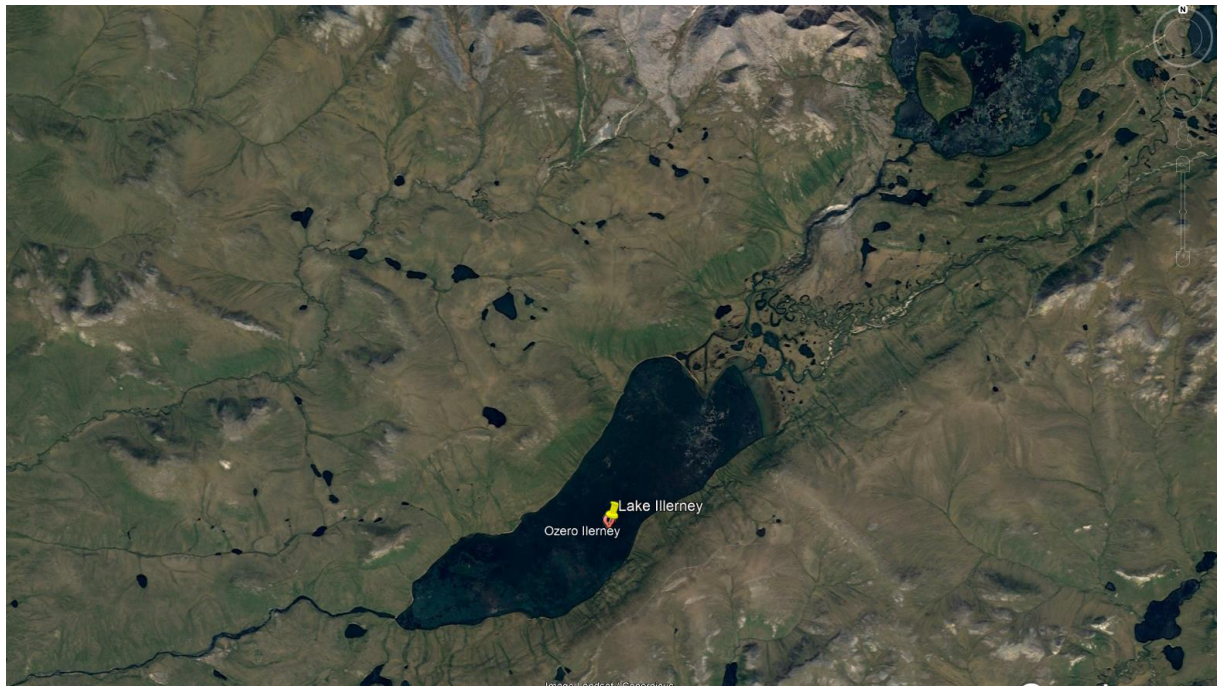


FIGURE 3.1 The northern part of the mountainous Lake Illirney catchment Lake Illirney region of Bilibinsky district, Chukotka Autonomous Okrug, Russia (Source: Google Earth Pro, US Geological Survey)



FIGURE 3.2 Location of Chukotka Autonomous Okrug (in red colour) in Russia (in lemon colour) (Source: Illirney, From Wikipedia, the free encyclopedia)



FIGURE 3.3 The evergreen forest of Lake Khamra catchment Lake Khamra region, Lensky district in the south-western part of Yakutia, Russia (Source: Google Earth Pro, US Geological Survey)

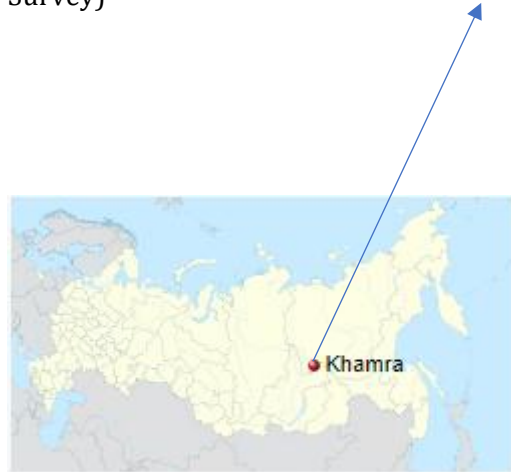


FIGURE 3.4 Location of Khamra (in point red colour) in Russia (in lemon colour) (Source: Khamra, From Wikipedia, the free encyclopedia)

3.2 Data acquisition

The imagery data utilized for this research were accessed through the Copernicus Open Access Hub. One of the data used was gotten from German Aerospace Center e. V. (DLR, Deutsches Zentrum für Luft-und Raumfahrt), Oberpfaffenhofen, Germany. The Digital Elevation Model (DEM) was provided by the Polar Terrestrial Environmental Systems research group in Alfred-Wegener-Institute, (AWI), Potsdam. These download data were Sentinel-1 and -2 images which represented the peak summer month in the year, July. Sentinel-1 and -2 products were downloaded of a timeline of five (5) years from 2017- 2021. July is the month when the vegetation is very dense. These acquisitions enabled me to analyse the efficacy of Sentinel-1 and -2 images to different methods of landcover classification when used separately and synergically. Sentinel-1 products represents a SAR remote sensing instruments while Sentinel-2 represents an optical remote sensing instrument.

The essence of the analyses is to compare the products' performance individually and in combination to the study area. I also assessed how the different methods of supervised classification reacted to both Sentinel products and the changes in the land-cover of the areas of interest over a period of five (5) years. The geographic locations of twenty-seven (29) vegetation plots were also collected from the areas of interest in-situ during the expedition of the research group in conjunction with Russia in 2018. Twenty-seven (27) vegetation plots were collected from Lake Illirney region while only two (2) plots were collected from Lake Khamra (*Shevtsova, I. et al., 2020; Kruse, S. et al., 2021*). Reference data for both study areas were also downloaded from ESRI Land Cover data portal. Climate data were accessed through National Oceanic and Atmospheric Administration (NOAA) using the station named Ostrovnoe, RS RSM00025138 located in Chukotka Autonomous Okrug, Russia.

The amount of factors that can be utilized while predicting land-cover types for Sentinel-1 data is reduced in comparison to Sentinel-2 data (*Braun, A., 2020*). Therefore, five (5) images of Sentinel-1 data were used, with each image representing a date in July of 2017-2021. The properties of the Sentinel-1 products used are as follows:

- Product type: GRD
- Mission: Sentinel-1B
- Polarization: VV+VH
- Sensor mode: IW
- Orbit direction: descending

3.3 Pre-processing of Sentinel-1 images

Subsets of the images were created to concentrate on the areas of interest. This also reduces the sizes of the images to enhance faster processing time during analyses. The following geographic coordinates were entered in the “Geo Coordinates” interface for the Lake Illirney region:

- Latitude point (North): 67.448
- Longitude point (West): 168.839
- Latitude point (South): 67.329
- Longitude point (East): 167.823

The following geographic coordinates were entered for te Lake Khamra region:

- Latitude point (North): 60.038
- Longitude point (West): 113.209
- Latitude point (South): 59.963
- Longitude point (East): 112.775

The following pre-procesing steps were carried out on the subsets of both areas of study:

- Application of orbit information
- Radiometric calibration
- Terrain correction
- Speckle filtering
- Thermal noise removal
- Creating a multi-temporal stack for the time series analysis

3.4 Pre-processing of Sentinel-2 images

The sub-set of Sentinel-2 images were created in order to decrease the dimension in the data been processed and to concentrate on the area of interest. The following geographic coordinates were entered in the “Geo Coordinates” interface:

- Latitude point (North): 67.484
- Longitude point (West): 167.942
- Latitude point (South): 67.276
- Longitude point (East): 168.752

The following geographic coordinates were entered for te Lake Khamra region:

- Latitude point (North): 60.061
- Longitude point (West): 112.821
- Latitude point (South): 59.944
- Longitude point (East): 113.187

The bands 2, 3, 4, 5, 6, 7, 8, 11 and 12 were selected for the subset. Resampling was also performed to 10 m to put all the bands in the same size. The calculation of Normalized Difference Vegetation Index (NDVI) was carried out and added to the bands in the subsets.

3.5 Pre-processing of both Sentinel products for synergic use

These data from different products have close dates of acquisition. The Sentinel products of the identical years were merged. The Sentinel-2 images were standardized to Bottom of Atmosphere reflectance (BoA). A number of process were needed before the Sentinel products can be fused together in a stack:

Sentinel-1 products:

- Sub-set
- Radiometric standardization
- Removal of Speckle through filtering
- Range Doppler Terrain Correction and projecting it to the UTM coordinate system of Sentinel-2

Sentinel-2 products:

- Sub-set
- Re-sampling

In the initial phase, a band in the Sentinel-2 images was selected in the dialog box of *Product Explorer* then, the *Geo-Coding* tool was opened to examine the co-ordinate location in the image (Braun, A., 2020). This Sentinel-2 images for Lake Illirney region has a co-ordinate projection of PROJCS["WGS 84 / UTM zone 58N" while the UTM zone for Lake Khamra region is PROJCS["WGS 84 / UTM zone 52N". Sentinel-1 products used were also projected into the same coordinate reference system as Sentinel-2 products.

Subsets of both Sentinel data were created in line with co-ordinates stated above for the study area. Radiometric calibration is applied to the subset of the Sentinel-1 product. Speckles were filtered from the calibrated data. The filtered Sentinel-1 products were then converted to dB scale.

Terrain correction was applied to the resulting products (Braun, A., 2020). The map was projected to match the Sentinel-2 product. Ratio bands were created with the terrain corrected data to decrease the disparity of bands (3 bands of Sentinel-1 and 10 bands of Sentinel-2).

The following numbers described in the pre-processing steps of Sentinel-2 products above were used for the “*Geo Coordinates*” interface for the Sentinel-2 product. It should be noted that the *Geo Coordinates* were different for both Sentinel images, this is because of the different principles employed by those products.

The two products were merged each for the areas of interest into one stack after ensuring that they possess identical spatial resolution, which is 10 metres, comparable dimensional range and projected in the identical co-ordinate system of UTM zone 58N for Lake Illirney region and (UTM zone 52N) for Lake Khamra region. The master product was Sentinel-1 data because of the high-level geo-location precision it possesses after *Range Doppler Terrain Correction*. *Bilinear interpolation resampling* was selected for the resampling method.

3.6 Land-cover classification of both Sentinel products

The two broad techniques of land-cover classification were performed with the datasets. Unsupervised classification comprises of the *EM Cluster Analysis* and *K-Means Cluster Analysis*. These different types of algorithms detect and combine related attributes. The benefit of unsupervised classification is that it does not need a preceding information on the area of interest or the data and still sets pixels of related attributes. Five (5) methods of the supervised classification were used namely: *Random Forest Classifier*, *KNN Classifier*, *Maximum Likelihood Classifier*, *KDTree KNN Classifier* and *Minimum Distance Classifier*. Land-cover types for Lake Illirney region are Boreal Forest, Tundra, Bare Ground and Water while the land-cover types for Lake Khamra region are Evergreen Forest, Tundra and Water. The above land-cover types for both study areas were referenced from ESRI Land Cover reference maps.

Grey Level Co-occurrence Matrix (GLCM) and Principal Component Analysis (PCA) were carried out on the datasets. GLCM textures are used as additional elements for the supervised classification (Haralick, R. M. *et al.*, 1973). The supervised classification was carried out on the datasets using the following products as inputs; Terrain Corrected stack, Principal Component Analysis (PCA), and Image textures.

The digitization of training areas was carried out on the datasets. This training data defines land-cover classes (Boreal Forest, Tundra, Bare Ground and Water) is needed by supervised classification. Numerous polygonal shapes were digitalized for every land-cover type to boost the

precision of the classification. The option of Evaluate classifier was also selected to obtain a review on the training accuracy on each classifier.

3.7 Analyses of the merged product (Sentinel-1 and Sentinel-2)

Visual interpretation was carried out by combining different bands in the stack of the merged product. The combinations sampled uncovered forms that are unseen by optical data only. Masking was also applied to the data using Mask Manager. This helps to utilize rational representations of the pixel values of a particular image to find out which one will fulfil specific requirements. Firstly, a mask was created for identical areas of both Sentinel products using this expression:

```
collocationFlags == 1
```

The above expression is true for all the areas that fall within the expression and false for area that fall outside the expression.

Principal Component Analysis (PCA) and Grey Level Co-occurrence Matrix (GLCM) were also carried out on the merged datasets. Vector containers were built to digitalize training areas. The training data constitutes the physical features that lie in this area of research and was used for supervised landcover classification and statistical purposes.

3.8 Land-cover classification of both Sentinel products

Unsupervised classification was carried out on both Sentinel products to detect and gather pixels with comparable characteristics using *EM Cluster Analysis* and *K-Means Cluster Analysis*. Principal Component Analysis (PCA), Grey Level Co-occurrence Matrix (GLCM) and Supervised classification were also carried out on the datasets using the process described above.

3.9 Validating the training and prediction accuracy

The training accuracy was carried out to show how the training data reacted when applied to different methods of supervised classification for both study areas. Prediction accuracy was also carried out to better assess the actual output data centred on an unbiased reference data rather than the training data.

3.10 Time series analyses

The temporal performance of pixels representing the vegetation plots gathered during expeditions (2016 & 2018) were analysed using *Pin manager* dialog box. Mathematical expressions using the *Mask Manager* were created for the various landcover classes to estimate statistical properties for the time-scale considered in the study. These analyses were carried out using both Sentinel products.

4 RESULTS

4.1 Analyses of Sentinel-1 images

4.1.1 Unsupervised classification

The images produced contain four land-cover types (Boreal Forest, Tundra, Water body and Bare Ground) for Lake Illirney region and three land-cover types (Evergreen Forest, Tundra and Water body) for Lake Khamra region. The outcome of this classification had some usefulness as the backscatter was divided into the classes specified and as it was in the reference data. Though, the application of unsupervised classification to these data did not fully represent the exact area of the land-cover types (Figures 4.1-4.4).

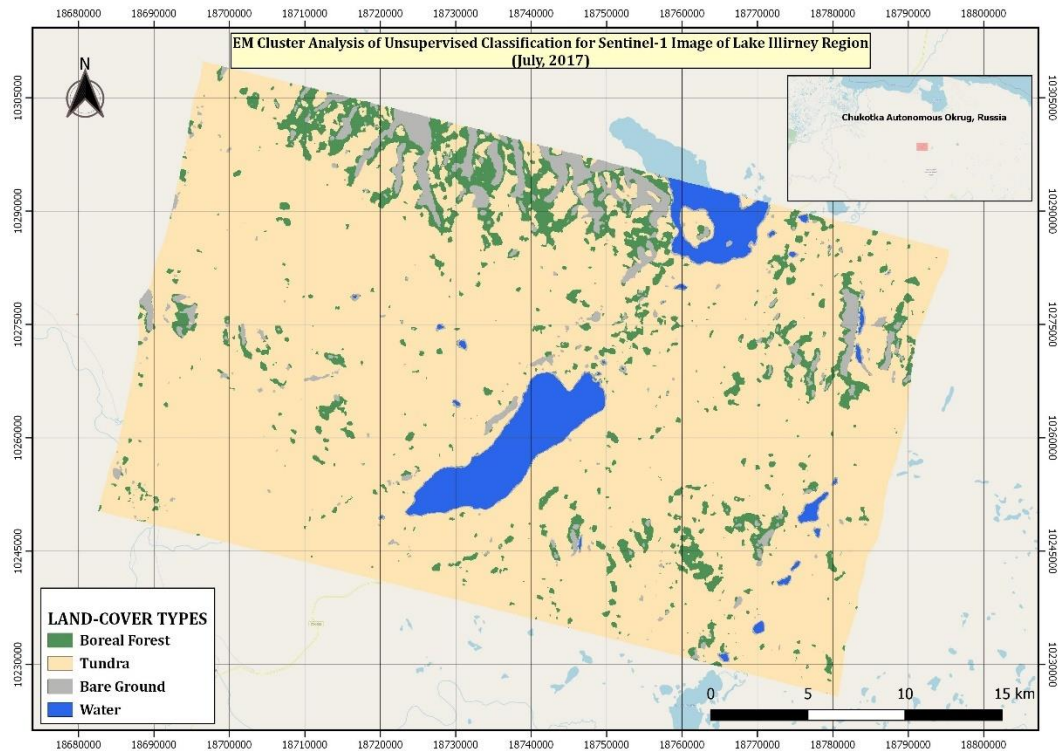


FIGURE 4.01 EM cluster analysis of unsupervised classification for Sentinel-1 image of Lake Illirney region (July 2017)

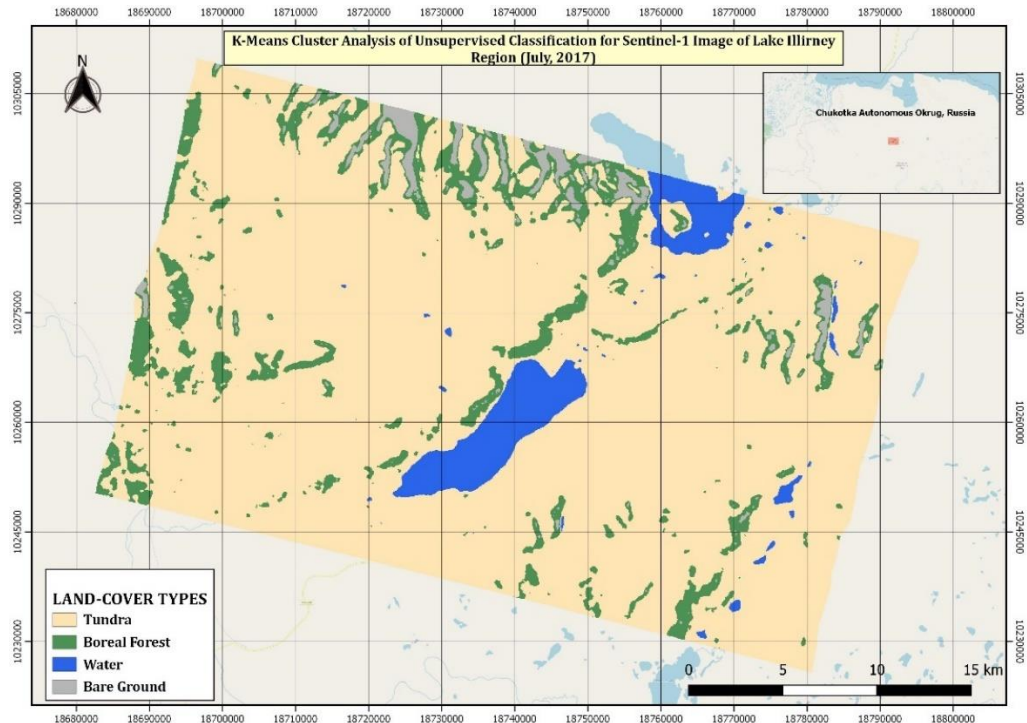


FIGURE 4.02 K-Means cluster analysis of unsupervised classification for Sentinel-1 image of Lake Illirney region (July 2017)

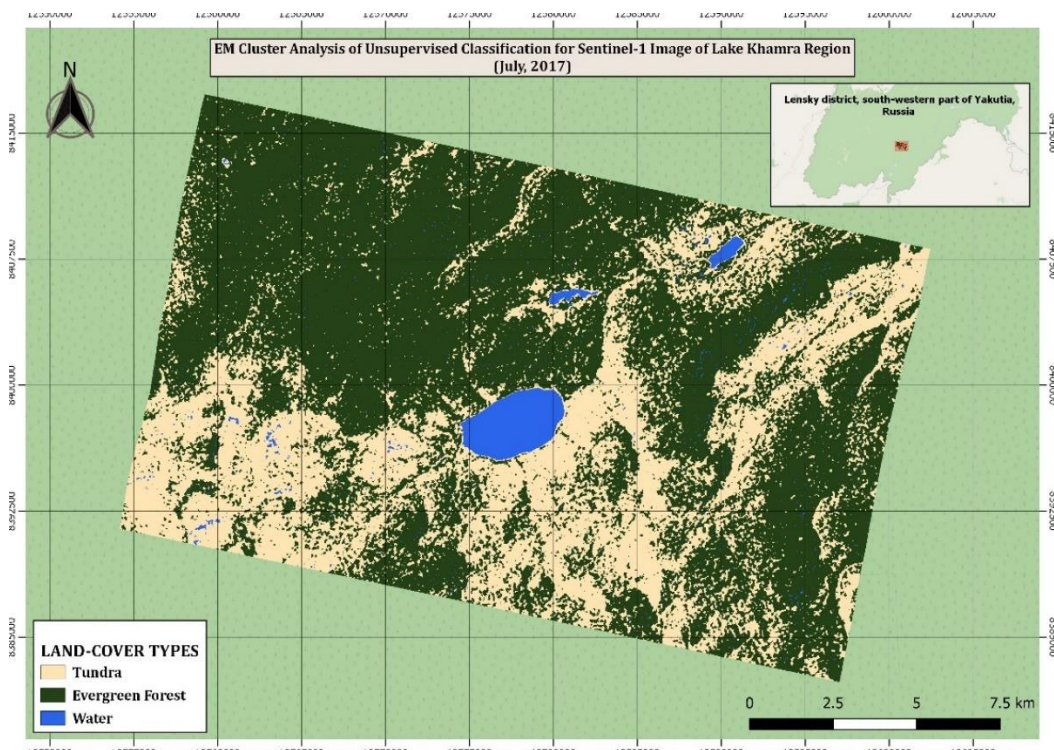


FIGURE 4.03 EM cluster analysis of unsupervised classification for Sentinel-1 image of Lake Khamra region (July 2017)

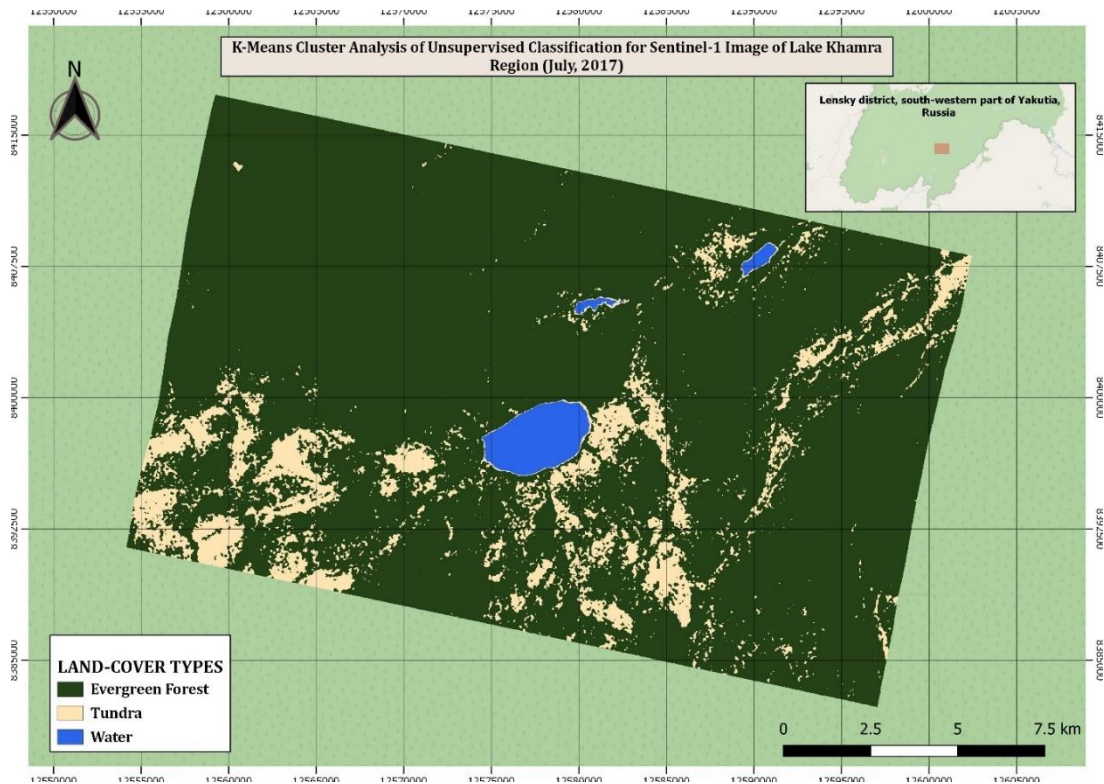


FIGURE 4.04 K-Means cluster analysis of unsupervised classification for Sentinel-1 image of Lake Khamra region (July 2017)

4.1.2 Supervised classification

The supervised classification was carried out on the Sentinel-1 images of both study areas using five (5) different methods in supervised classification analysis namely, *Random Forest (RF) Classifier*, *KDTree KNN Classifier*, *KNN Classifier*, *Minimum Distance (MD) Classifier* and *Maximum Likelihood (ML) Classifier*. Output maps for the different algorithms of the land-cover classification can be seen below (Figures 4.5-4.12). The new products were created comprising of a band called *LabeledClasses*, which is the result of the classification and *Confidence* band as side products. It was noticed that the *Random Forest Classifier* does not spontaneously assign a class to each pixel – some of the pixels remained transparent. This is for all pixels which could not be classified with a confidence higher than 0.5. To display classes with low confidence values, the *Valid-Pixel Expression* of the *LabeledClasses* dataset was changed from *Confidence >= 0.5* to *Confidence >=0.2*. Tables 4.1-4.3 presents different accuracy for the four (4) trained land-cover types for the three (3) different methods of supervised classification which had optimum performance. Table 4.4 shows the prediction accuracy of different methods of supervised classification for Sentinel-1 products.

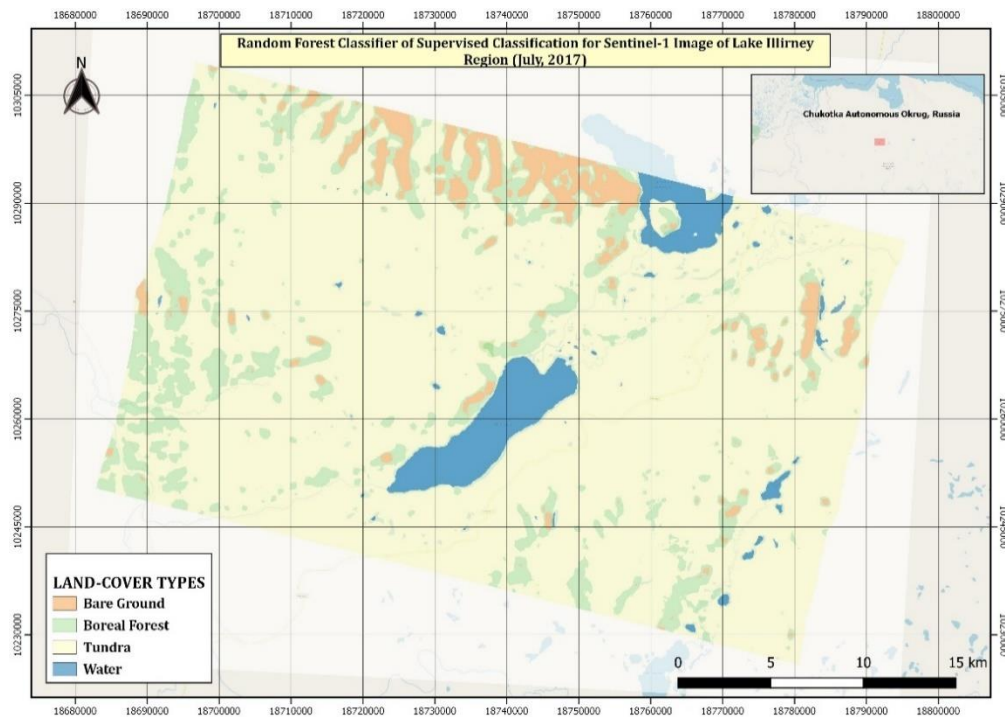


FIGURE 4.05 Random Forest classifier of supervised classification for Sentinel-1 image of Lake Illirney region (July 2017)

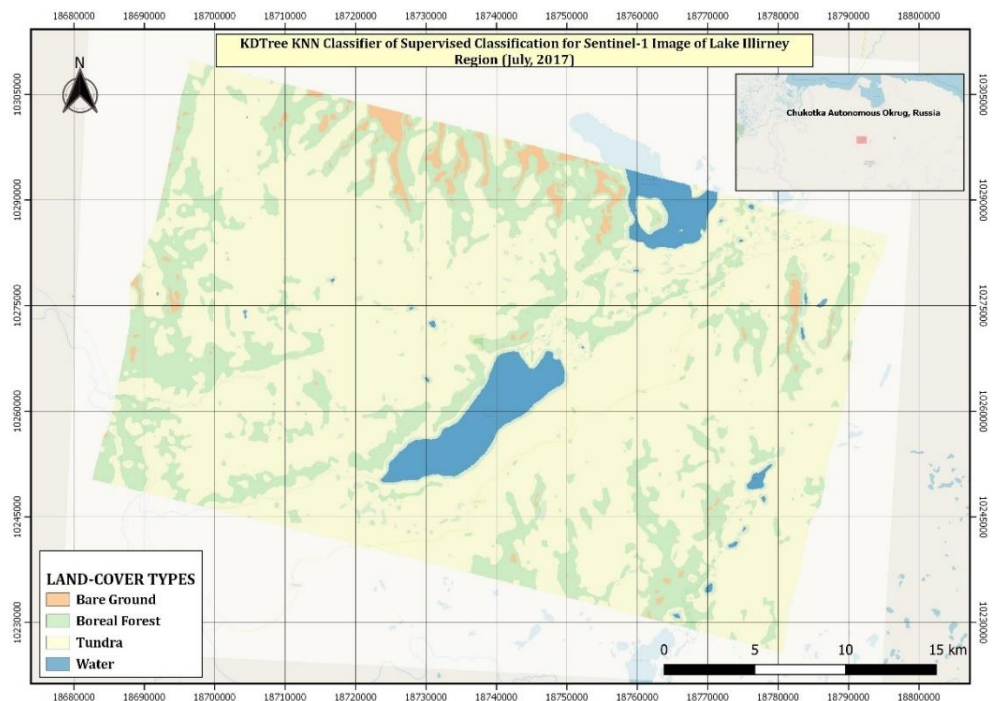


FIGURE 4.06 KDTree KNN classifier of supervised classification for Sentinel-1 image of Lake Illirney region (July 2017)

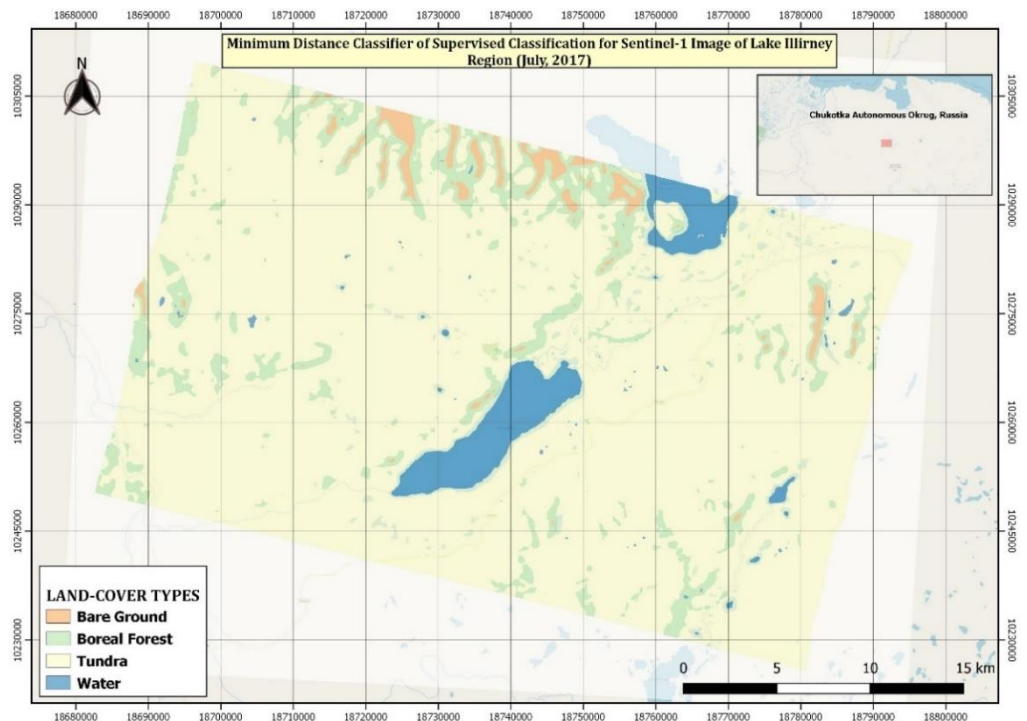


FIGURE 4.07 Minimum Distance classifier of supervised classification for Sentinel-1 image of Lake Illirney region (July 2017)

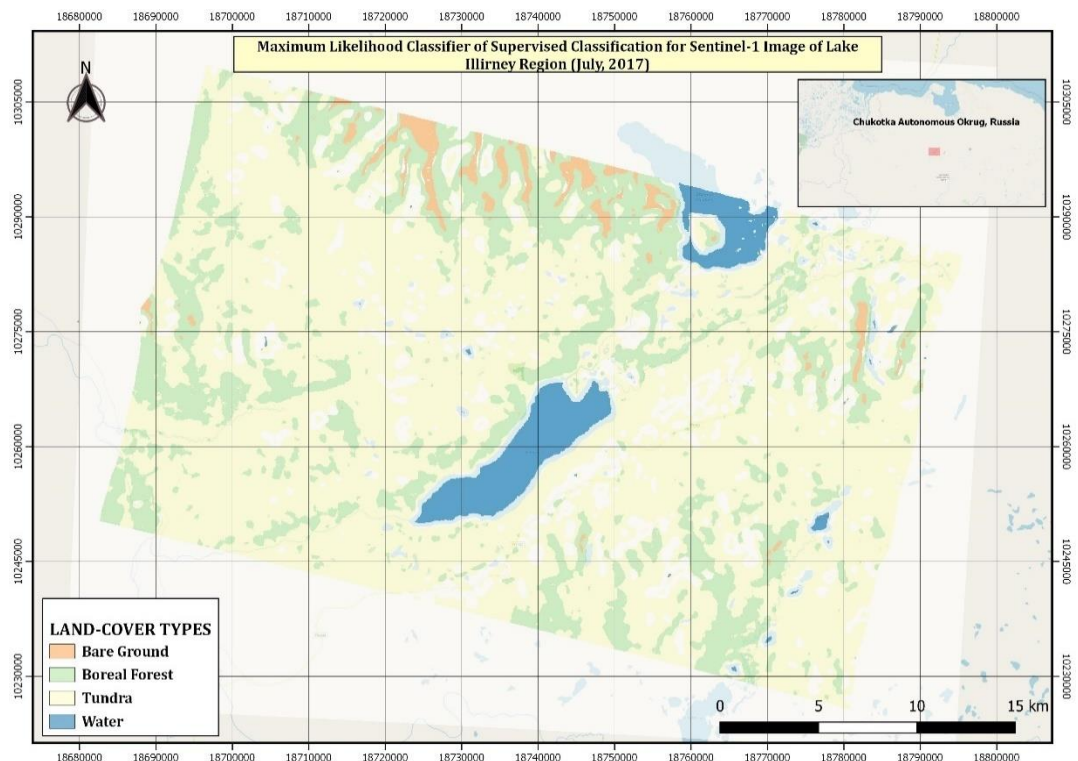


FIGURE 4.08 Maximum Likelihood classifier of supervised classification for Sentinel-1 image of Lake Illirney region (July 2017)

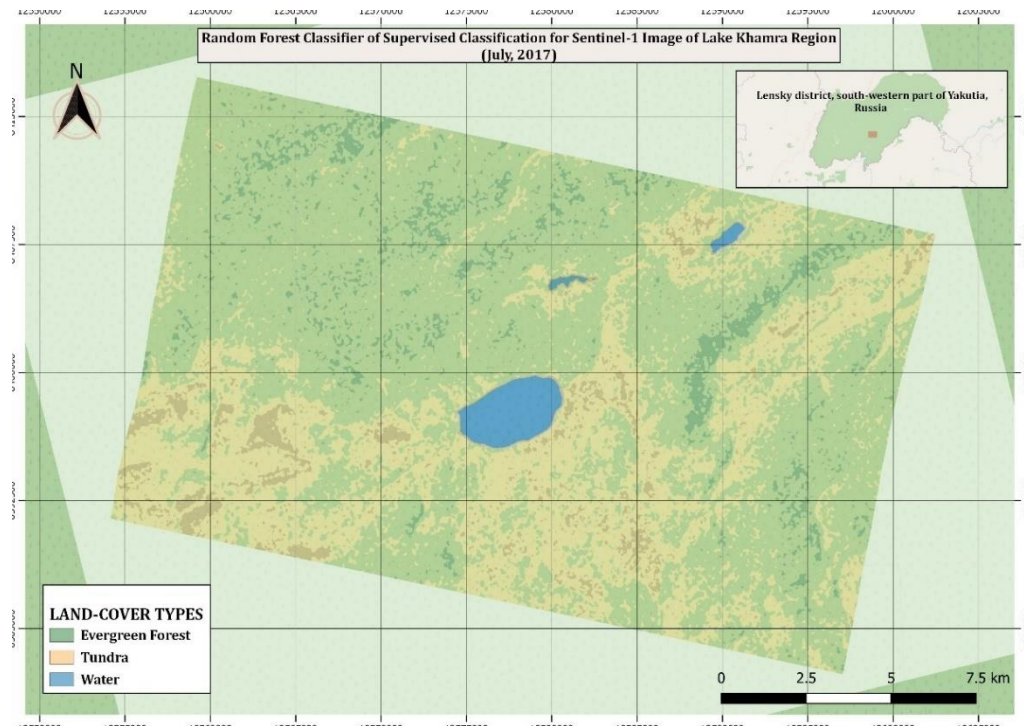


FIGURE 4.09 Random Forest classifier of supervised classification for Sentinel-1 image of Lake Khamra region (July 2017)

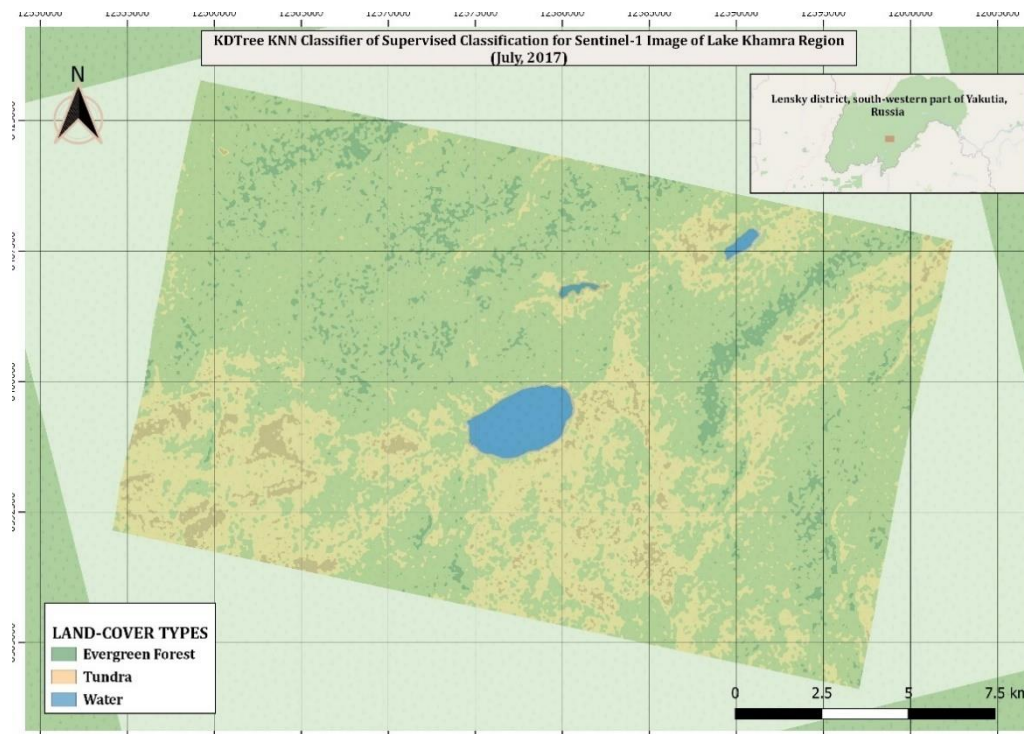


FIGURE 4.10 KDTree KNN classifier of supervised classification for Sentinel-1 image of Lake Khamra region (July 2017)

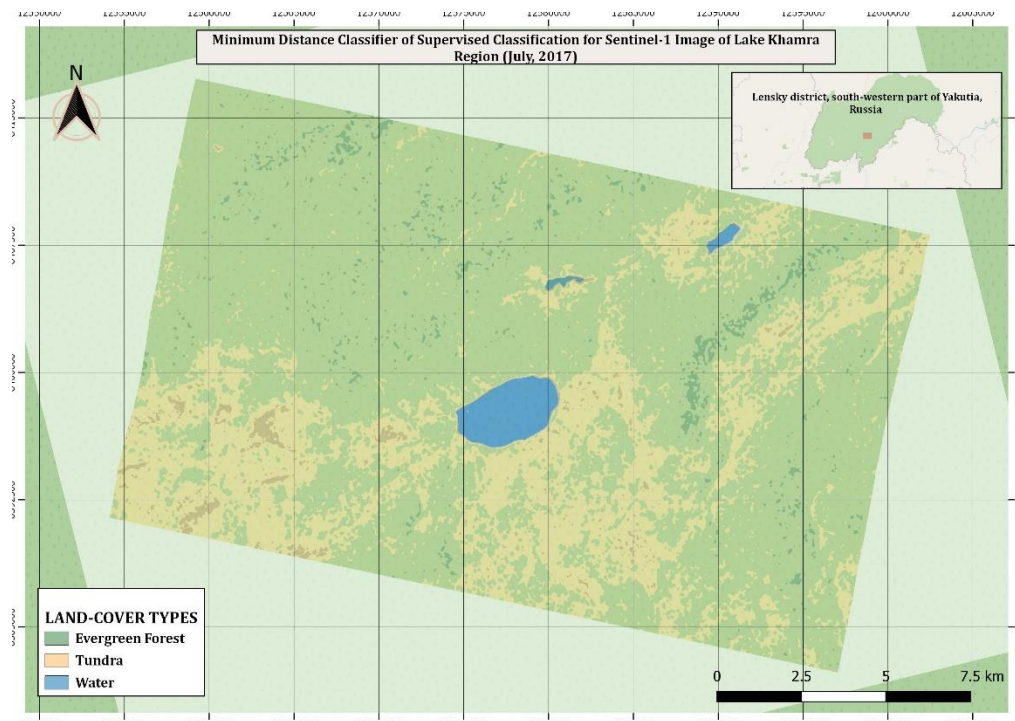


FIGURE 4.11 Minimum Distance classifier of supervised classification for Sentinel-1 image of Lake Khamra region (July 2017)

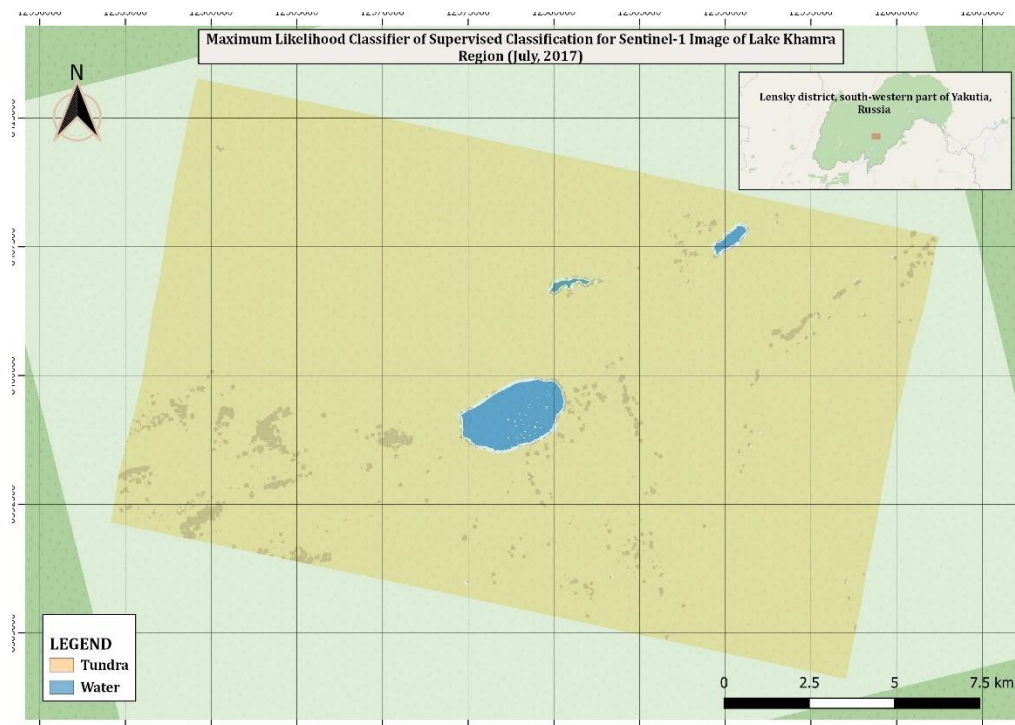


FIGURE 4.12 Maximum Likelihood classifier of supervised classification for Sentinel-1 image of Lake Khamra region (July 2017)

TABLE 4.01 Training accuracy for the trained classes using Random Forest Classifier (Sentinel-1 image, Lake Illirney region, July 2017)

	<i>Boreal Forest</i>	<i>Tundra</i>	<i>Bare Ground</i>	<i>Water</i>
Accuracy	0.9991	1.0000	0.9991	1.0000
Precision	0.9853	1.0000	1.0000	1.0000
Correlation	0.9922	1.0000	0.9964	1.0000
Error rate	0.0009	0.0000	0.0009	0.0000
True positives	134.0000	1238.0000	320.0000	650.0000
False positives	2.0000	0.0000	0.0000	0.0000
True negatives	2208.0000	1106.0000	2022.0000	1694.0000
False negatives	0.0000	0.0000	2.0000	0.0000

Using Testing dataset, % correct predictions = 99.9147

Total samples = 4689

RMSE = 0.0292103118918493

Bias = 8.532423208189588E-4

Distribution:

- Boreal Forest: 269 (5.7368%)
- Tundra: 2476 (52.8044%)
- Bare Ground: 644 (13.7343%)
- Water: 1300 (27.7245%)

TABLE 4.02 Training accuracy for the trained classes using KDTree KNN Classifier (Sentinel-1 image, Lake Illirney region, July 2017)

	<i>Boreal Forest</i>	<i>Tundra</i>	<i>Bare Ground</i>	<i>Water</i>
Accuracy	0.9915	0.9996	0.9919	1.0000
Precision	0.8958	0.9992	0.9871	1.0000
Correlation	0.9247	0.9991	0.9657	1.0000
Error rate	0.0085	0.0004	0.0081	0.0000
True positives	129.0000	1238.0000	307.0000	650.0000
False positives	15.0000	1.0000	4.0000	0.0000
True negatives	2195.0000	1105.0000	2018.0000	1694.0000
False negatives	5.0000	0.0000	15.0000	0.0000

Using Testing dataset, % correct predictions = 99.1468

Total samples = 4689

RMSE = 0.09237111674214579

Bias = 0.005119453924914641

Distribution:

- Boreal Forest: 269 (5.7368%)
- Tundra: 2476 (52.8044%)
- Bare Ground: 644 (13.7343%)
- Water: 1300 (27.7245%)

TABLE 4.03 Training accuracy for the trained classes using Minimum Distance Classifier (Sentinel-1 image, Lake Illirney region, July 2017)

	<i>Boreal Forest</i>	<i>Tundra</i>	<i>Bare Ground</i>	<i>Water</i>
Accuracy	0.9590	0.9804	0.9723	0.9936
Precision	0.6696	0.9753	0.9105	0.9774
Correlation	0.6070	0.9614	0.8849	0.9843
Error rate	0.0410	0.0196	0.0277	0.0064
True positives	75.0000	1223.0000	285.0000	650.0000
False positives	37.0000	31.0000	28.0000	15.0000
True negatives	2173.0000	1075.0000	1994.0000	1679.0000
False negatives	59.0000	15.0000	37.0000	0.0000

Using Testing dataset, % correct predictions = 95.2645

Total samples = 4689

RMSE = 0.21761192248004416

Bias = 0.023464163822525475

Distribution:

- Boreal Forest: 269 (5.7368%)
- Tundra: 2476 (52.8044%)
- Bare Ground: 644 (13.7343%)
- Water: 1300 (27.7245%)

TABLE 4.04 Prediction accuracy for methods of supervised classification (Sentinel-1 image)

<i>Methods of Supervised Classification</i>	<i>Overall Accuracy (OA) (%)</i>
Random Forest Classifier	76.80
KDTree KNN Classifier	74.40
KNN Classifier	56.00
Minimum Distance (MD) Classifier	74.40
Maximum Likelihood (ML) Classifier	66.15

4.2 Analyses of Sentinel-2 images

4.2.1 Unsupervised classification

The images below contain four (4) land-cover types using the two (2) methods of unsupervised classification as described in the previous section (4.1.1) (Fig. 4.13-4.16).

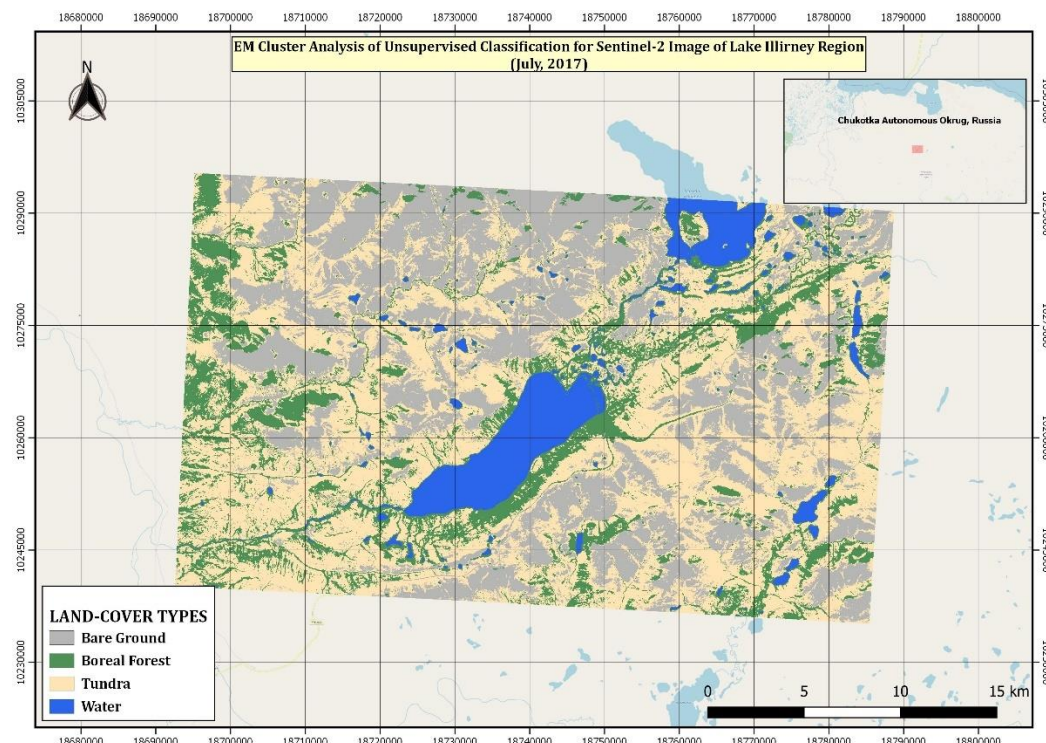


FIGURE 4.13 EM cluster analysis of unsupervised classification for Sentinel-2 image of Lake Illirney region (July 2017)

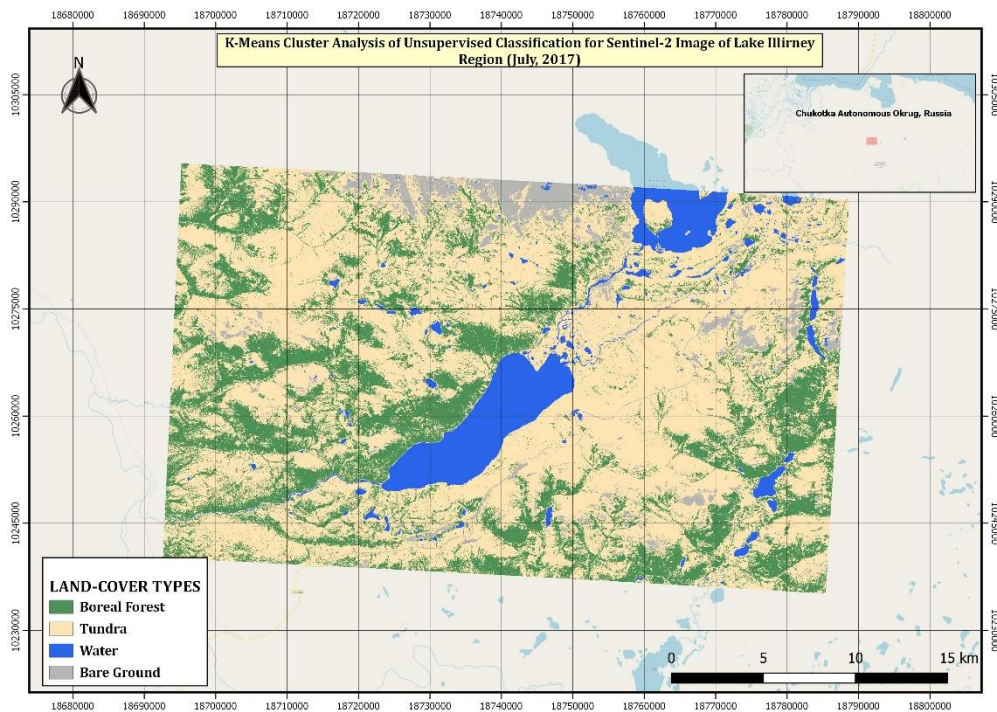


FIGURE 4.14 K-Means cluster analysis of unsupervised classification for Sentinel-2 image of Lake Illirney region (July 2017)

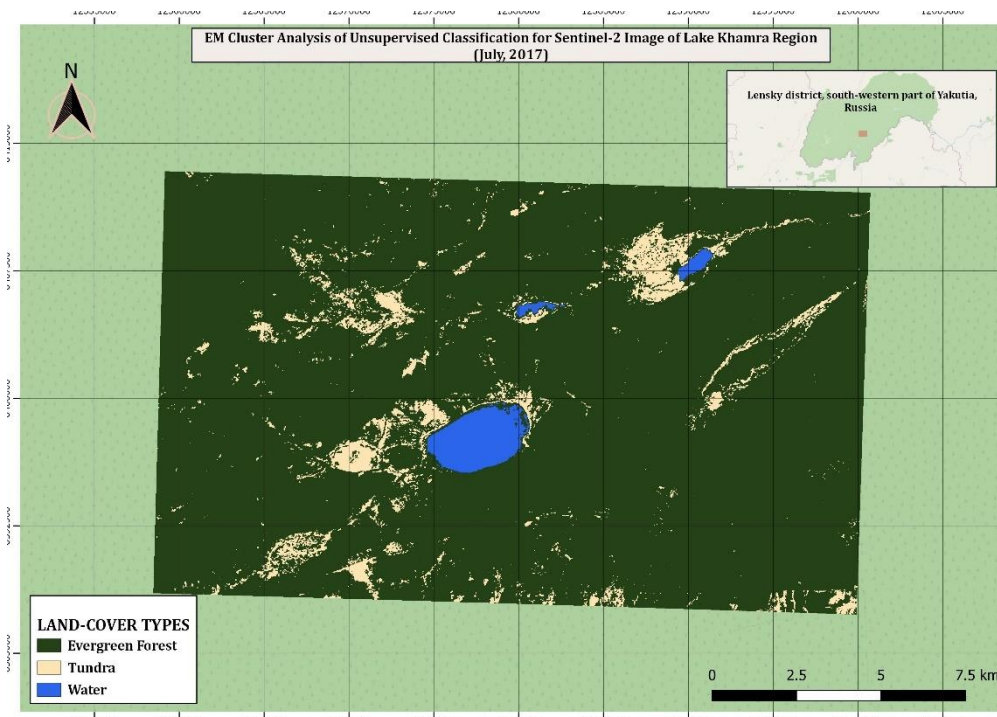


FIGURE 4.15 EM cluster analysis of unsupervised classification for Sentinel-2 image of Lake Khamra region (July 2017)

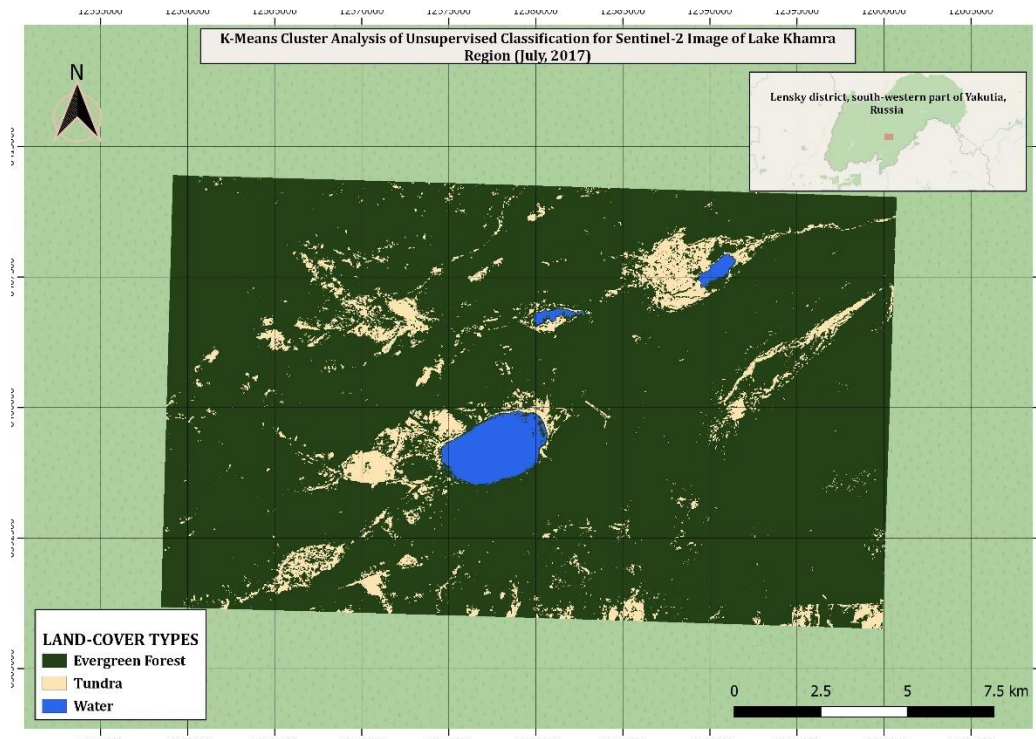


FIGURE 4.16 K-Means cluster analysis of unsupervised classification for Sentinel-2 image of Lake Khamra region (July 2017)

4.2.2 Supervised classification

The analysis was performed on the Sentinel-2 images of both areas of interest using five (5) different methods in supervised classification analysis namely, *Random Forest (RF) Classifier*, *KDTree KNN Classifier*, *KNN Classifier*, *Minimum Distance (MD) Classifier* and *Maximum Likelihood (ML) Classifier*. The output maps for the different algorithms of the land-cover classification can be seen below (Figures 4.17-4.23). Tables 4.5-4.7 presents different accuracy for the four (4) trained land-cover types of Sentinel-2 products for the three (3) different methods of supervised classification which had optimum performance. Table 4.8 shows the prediction accuracy of different methods of supervised classification for Sentinel-2 products.

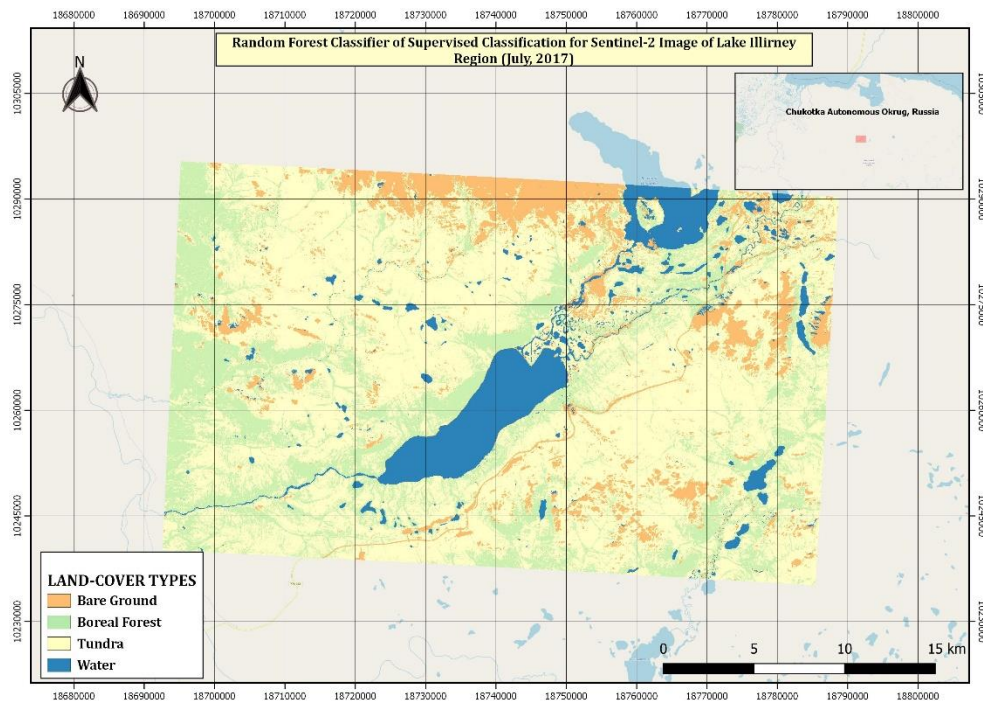


FIGURE 4.17 Random Forest classifier of supervised classification for Sentinel-2 image of Lake Illirney region (July 2017)

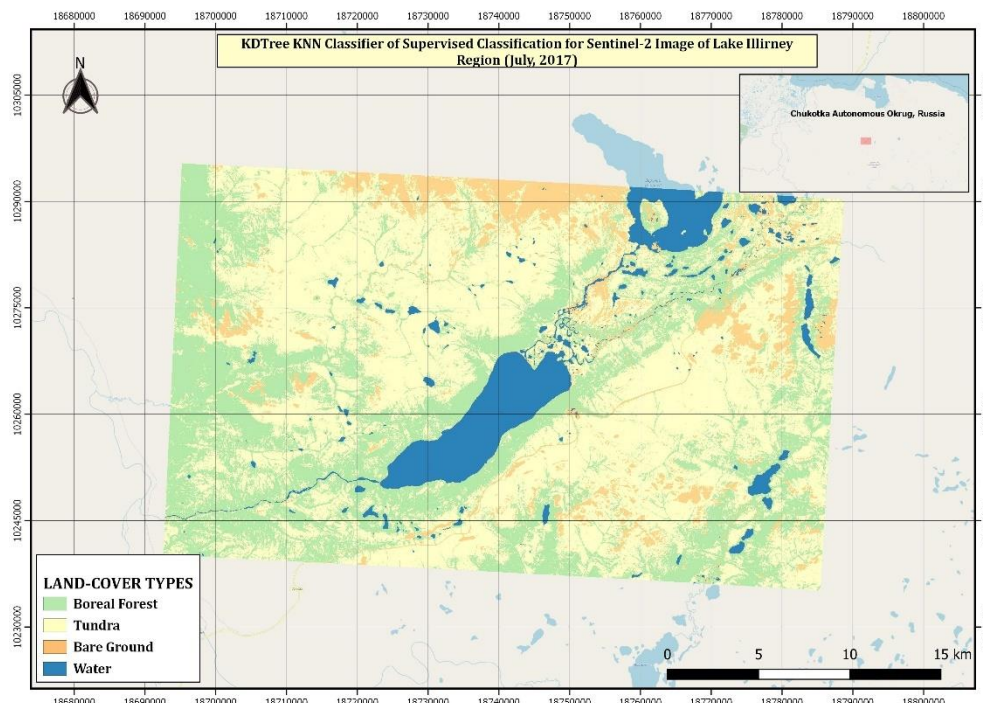


FIGURE 4.18 KDTree KNN classifier of supervised classification for Sentinel-2 image of Lake Illirney region (July 2017)

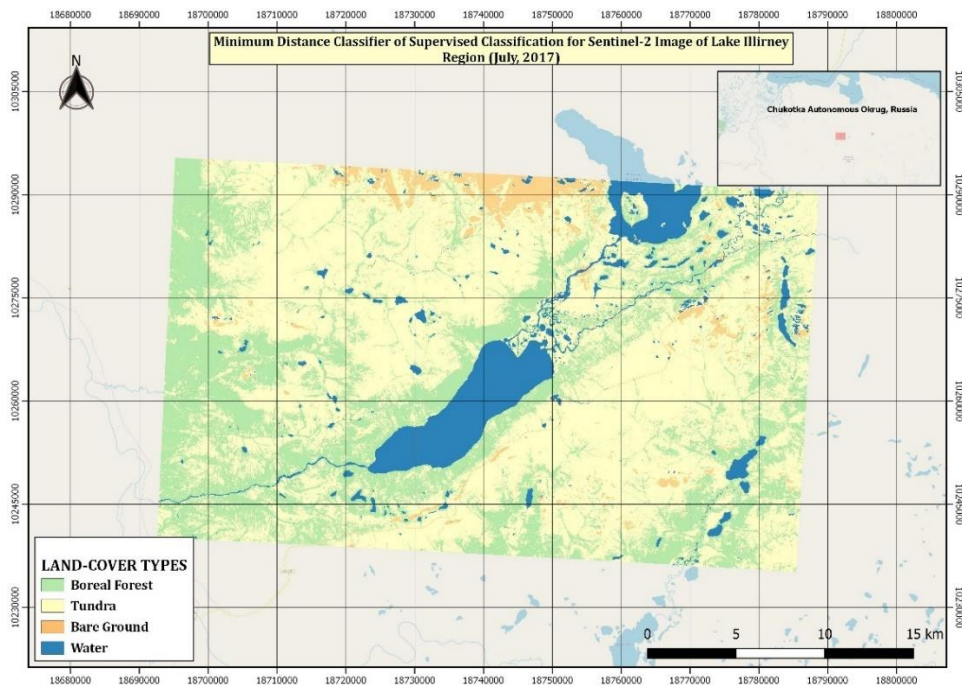


FIGURE 4.19 Minimum Distance classifier of supervised classification for Sentinel-2 image of Lake Illirney region (July 2017)

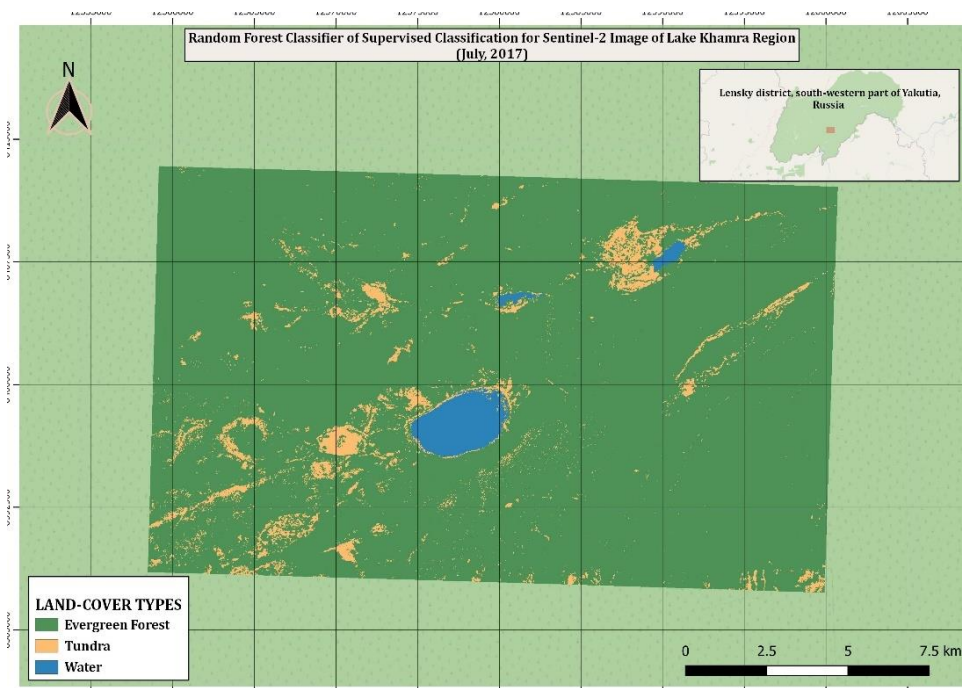


FIGURE 4.20 Random Forest classifier of supervised classification for Sentinel-2 image of Lake Khamra region (July 2017)

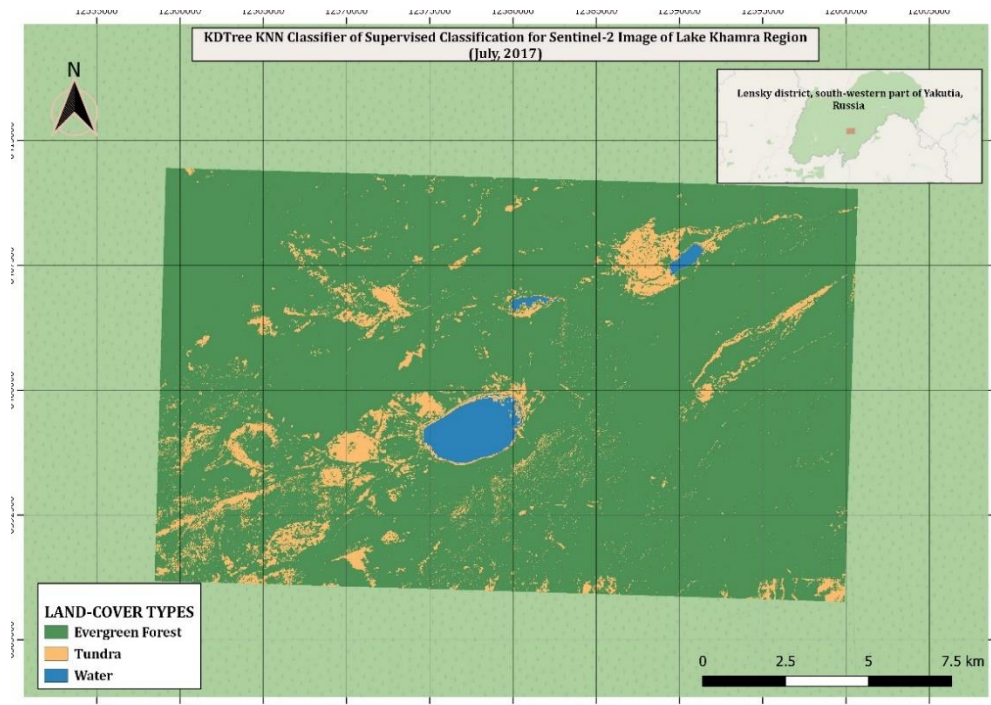


FIGURE 4.21 KDTree KNN classifier of supervised classification for Sentinel-2 image of Lake Khamra region (July 2017)

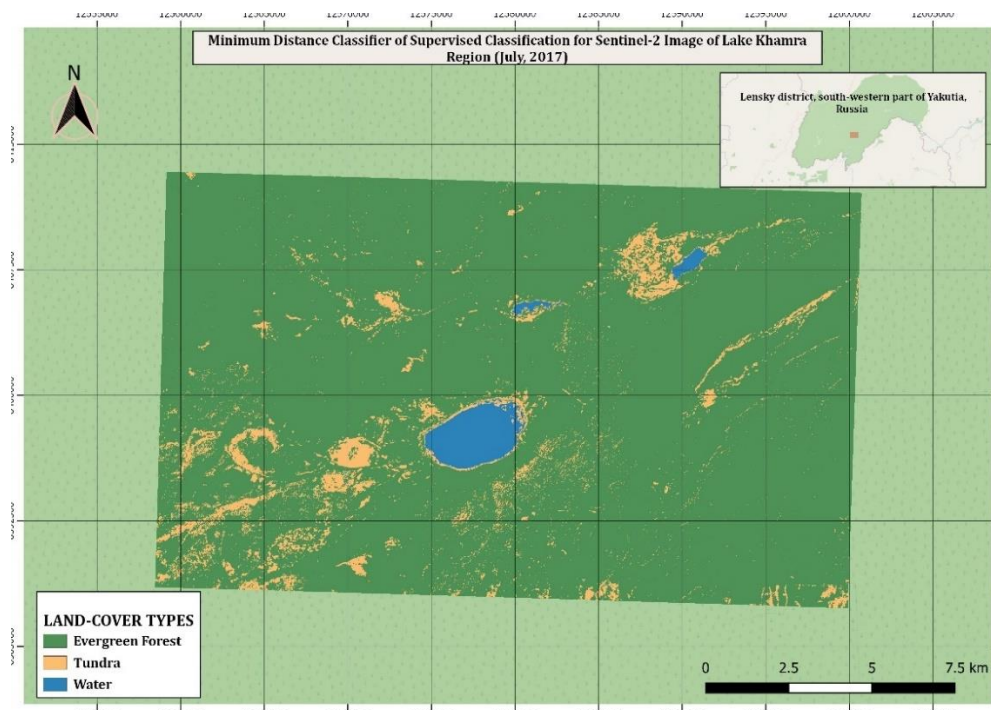


FIGURE 4.22 Minimum Distance classifier of supervised classification for Sentinel-2 image of Lake Khamra region (July 2017)

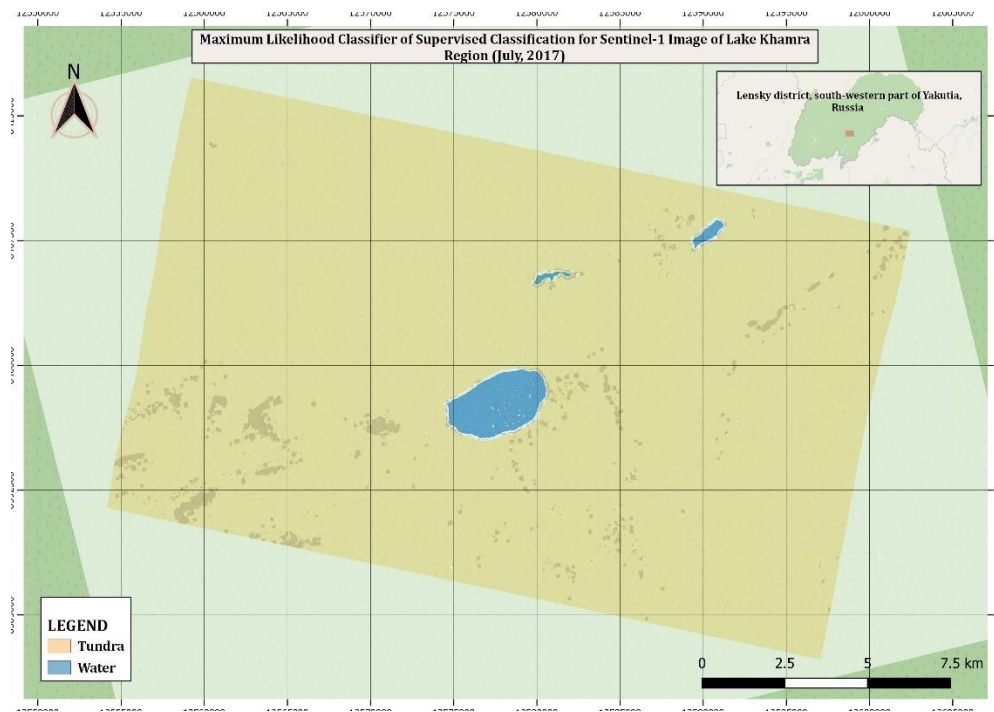


FIGURE 4.23 Maximum Likelihood classifier of supervised classification for Sentinel-2 image of Lake Khamra region (July 2017)

TABLE 4.05 Training accuracy for the trained classes using Random Forest Classifier (Sentinel-2 image, Lake Illirney region, July 2017)

	<i>Boreal Forest</i>	<i>Tundra</i>	<i>Bare Ground</i>	<i>Water</i>
<i>Accuracy</i>	0.9998	0.9998	1.0000	1.0000
<i>Precision</i>	1.0000	0.9992	1.0000	1.0000
<i>Correlation</i>	0.9993	0.9994	1.0000	1.0000
<i>Error rate</i>	0.0002	0.0002	0.0000	0.0000
<i>True positives</i>	956.0000	1250.0000	972.0000	1250.0000
<i>False positives</i>	0.0000	1.0000	0.0000	0.0000
<i>True negatives</i>	3472.0000	3178.0000	3457.0000	3179.0000
<i>False negatives</i>	1.0000	0.0000	0.0000	0.0000

Using Testing dataset, % correct predictions = 99.9774

Total samples = 8859

RMSE = 0.015026130622691205

Bias = 2.2578460149036417E-4

Distribution:

- Boreal Forest: 1915 (21.6164%)
- Tundra: 2500 (28.2199%)
- Bare Ground: 1944 (21.9438%)
- Water: 2500 (28.2199%)

TABLE 4.06 Training accuracy for the trained classes using KDTree KNN Classifier (Sentinel-2 image, Lake Illirney region, July 2017)

	<i>Boreal Forest</i>	<i>Tundra</i>	<i>Bare Ground</i>	<i>Water</i>
Accuracy	0.9998	0.9977	0.9980	1.0000
Precision	1.0000	0.9921	1.0000	1.0000
Correlation	0.9993	0.9945	0.9941	1.0000
Error rate	0.0002	0.0023	0.0020	0.0000
True positives	956.0000	1250.0000	963.0000	1250.0000
False positives	0.0000	10.0000	0.0000	0.0000
True negatives	3472.0000	3169.0000	3457.0000	3179.0000
False negatives	1.0000	0.0000	9.0000	0.0000

Using Testing dataset, % correct predictions = 99.7742

Total samples = 8859

RMSE = 0.04751679718690838

Bias = -0.001806276811921581

Distribution:

- Boreal Forest: 1915 (21.6164%)
- Tundra: 2500 (28.2199%)
- Bare Ground: 1944 (21.9438%)
- Water: 2500 (28.2199%)

TABLE 4.07 Training accuracy for the trained classes using Minimum Distance Classifier (Sentinel-2 image, Lake Illirney region, July 2017)

	<i>Boreal Forest</i>	<i>Tundra</i>	<i>Bare Ground</i>	<i>Water</i>
Accuracy	0.9998	0.9761	0.9729	0.9966
Precision	1.0000	0.9218	1.0000	0.9881
Correlation	0.9993	0.9440	0.9204	0.9917
Error rate	0.0002	0.0239	0.0271	0.0034
True positives	956.0000	1250.0000	852.0000	1250.0000
False positives	0.0000	106.0000	0.0000	15.0000
True negatives	3472.0000	3073.0000	3457.0000	3164.0000
False negatives	1.0000	0.0000	120.0000	0.0000

Using Testing dataset, % correct predictions = 97.2680

Total samples = 8859

RMSE = 0.16528743684960326

Bias = -0.02009482953262598

Distribution:

- Boreal Forest: 1915 (21.6164%)
- Tundra: 2500 (28.2199%)
- Bare Ground: 1944 (21.9438%)
- Water: 2500 (28.2199%)

TABLE 4.08 Prediction accuracy for methods of supervised classification (Sentinel-2 image)

<i>Methods of Supervised Classification</i>	<i>Overall Accuracy (OA) (%)</i>
<i>Random Forest Classifier</i>	79.20
<i>KDTree KNN Classifier</i>	80.00
<i>KNN Classifier</i>	-
<i>Minimum Distance (MD) Classifier</i>	83.20
<i>Maximum Likelihood (ML) Classifier</i>	-

4.3 Analyses of the merging between Sentinel-1 and Sentinel-2 products

4.3.1 Unsupervised classification

The images below contain four (4) land-cover types using the two (2) methods of unsupervised classification as described in the previous section (4.1.1) (Fig. 4.24-4.25).

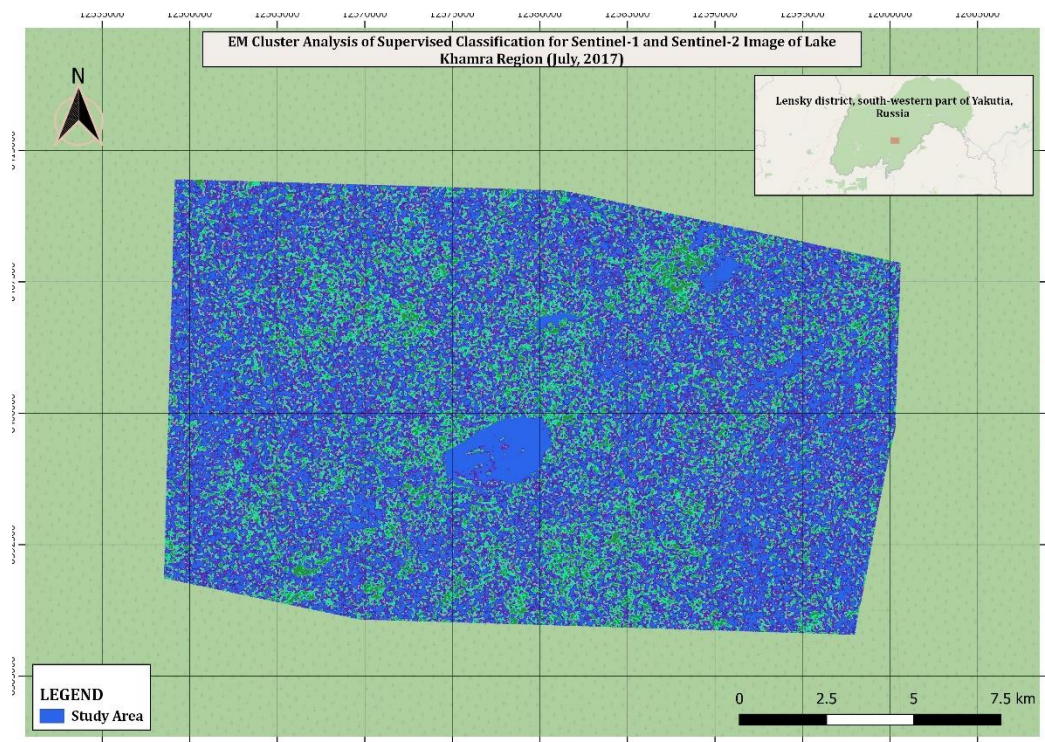


FIGURE 4.24 EM cluster analysis of unsupervised classification for Sentinel-1 and Sentinel-2 images of Lake Khamra region (July 2017)

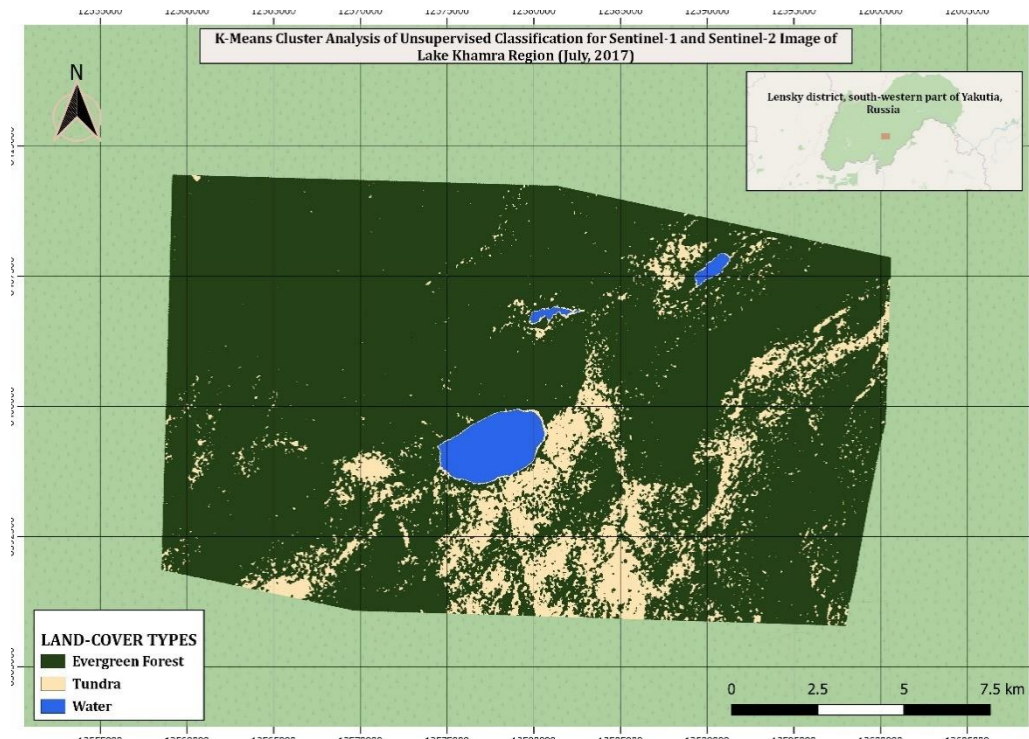


FIGURE 4.25 K-Means cluster analysis of unsupervised classification for Sentinel-1 and Sentinel-2 images of Lake Khamra region (July 2017)

4.3.2 Supervised classification

The supervised classification was carried out on the merging of the Sentinel products of both areas of interest utilizing five (5) different methods in supervised classification analysis namely, *Random Forest (RF) Classifier*, *KDTree KNN Classifier*, *KNN Classifier*, *Minimum Distance (MD) Classifier* and *Maximum Likelihood (ML) Classifier*. The output maps for the different algorithms of the land-cover classification can be seen below (Figures 4.26-4.32). Tables 4.9-4.11 presents different accuracy for the four (4) trained land-cover types of Sentinel-2 products for the three (3) different methods of supervised classification which had best performance. Table 4.12 shows the prediction accuracy of different methods of supervised classification for the combined use of the two Sentinel image products.

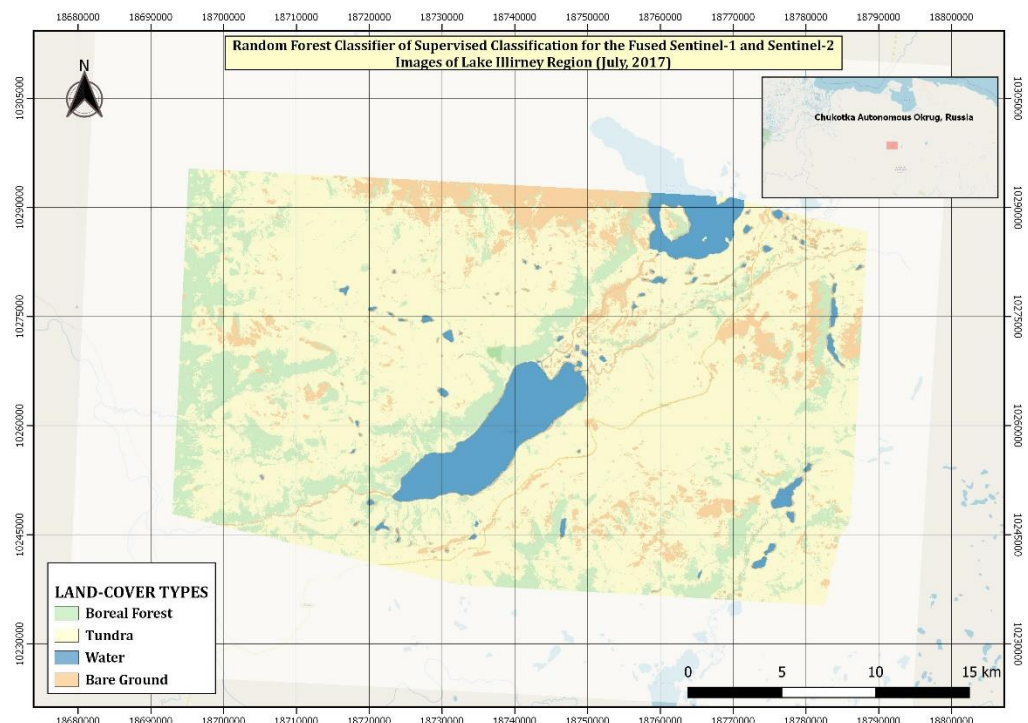


FIGURE 4.26 Random Forest classifier of supervised classification for Sentinel-1 and Sentinel-2 images of Lake Illirney region (July 2017)

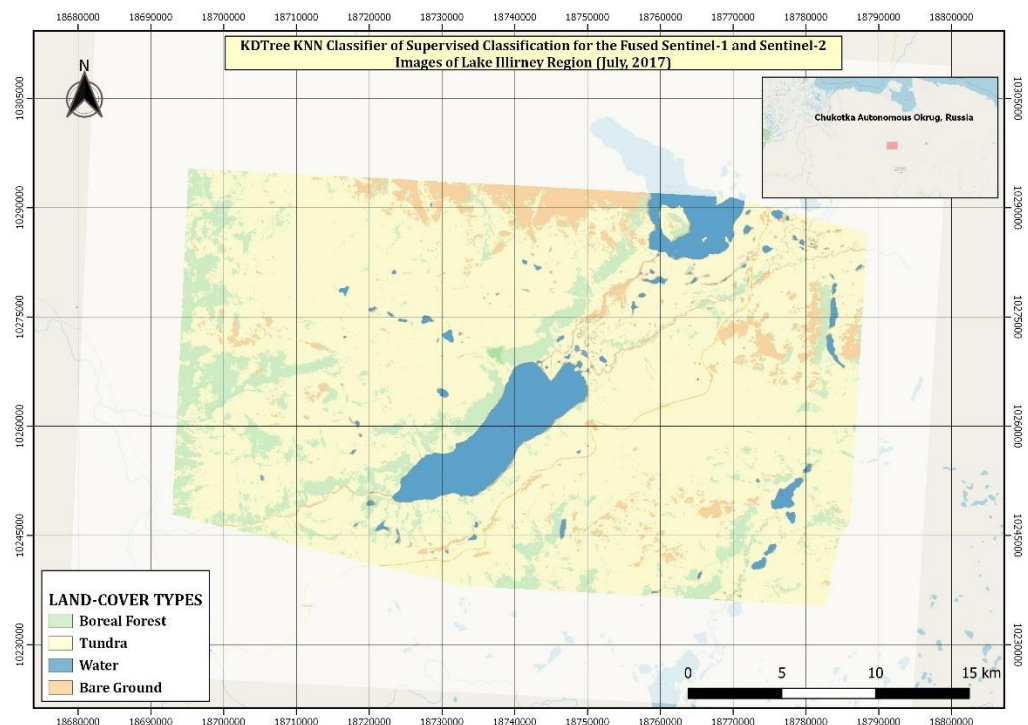


FIGURE 4.27 KDTree KNN classifier of supervised classification for Sentinel-1 and Sentinel-2 images of Lake Illirney region (July 2017)

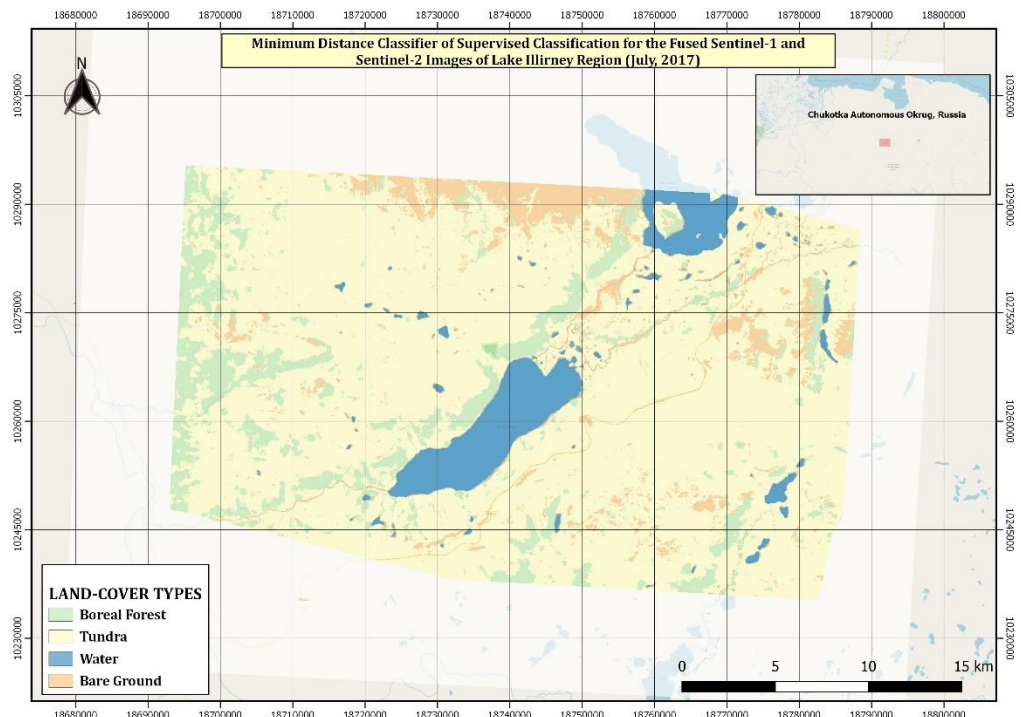


FIGURE 4.28 Minimum Distance classifier of supervised classification for Sentinel-1 and Sentinel-2 images of Lake Illirney region (July 2017)

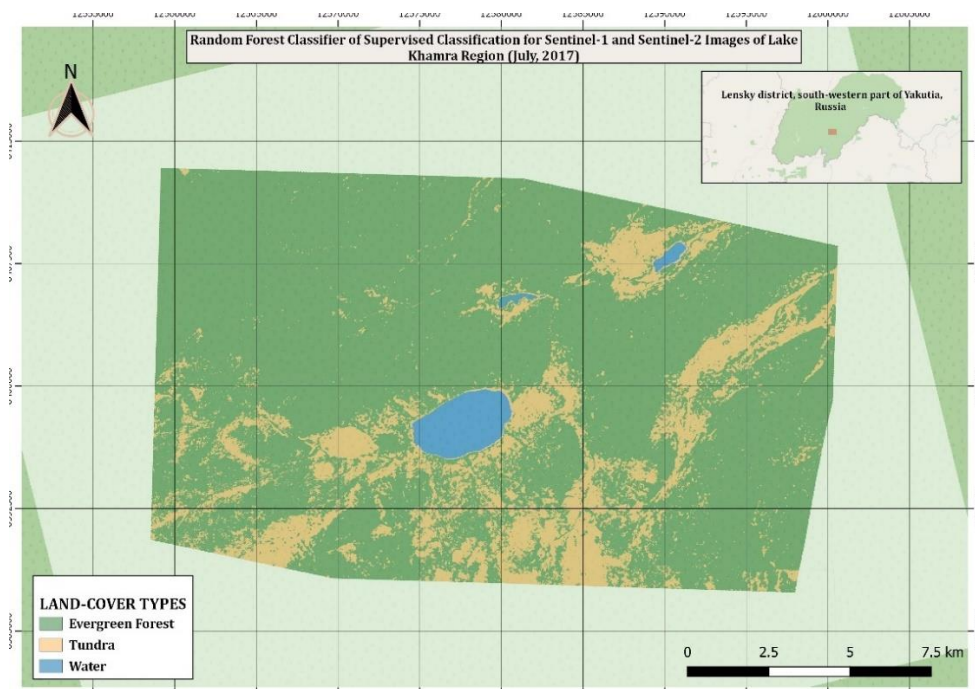


FIGURE 4.29 Random Forest classifier of supervised classification for Sentinel-1 and Sentinel-2 images of Lake Khamra region (July 2017)

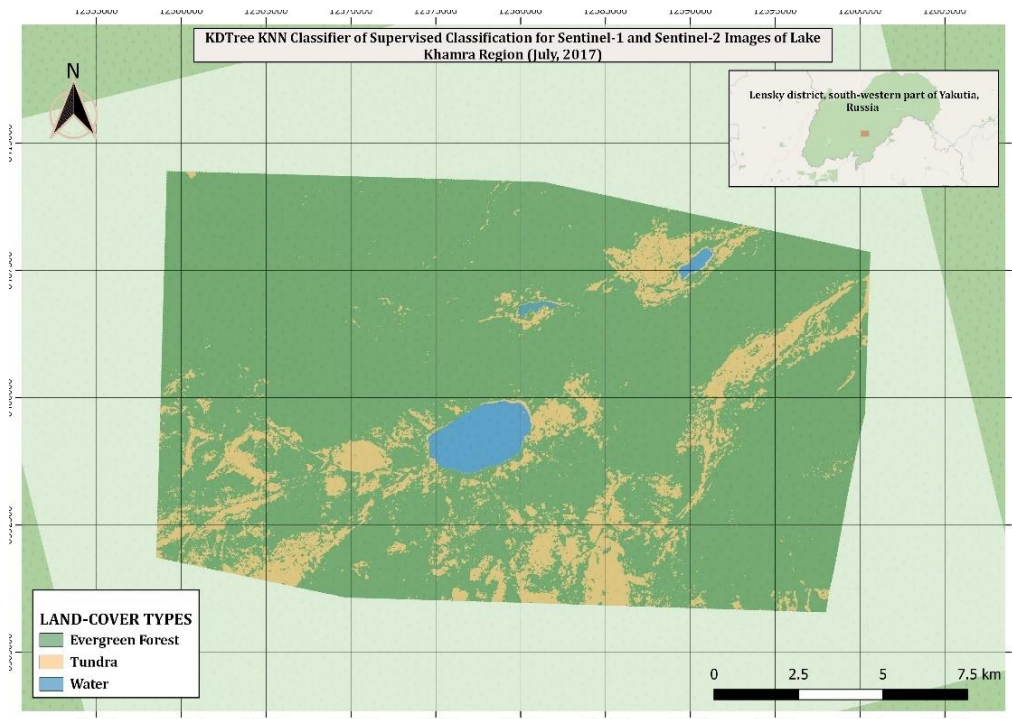


FIGURE 4.30 KDTree KNN classifier of supervised classification for Sentinel-1 and Sentinel-2 images of Lake Khamra region (July 2017)

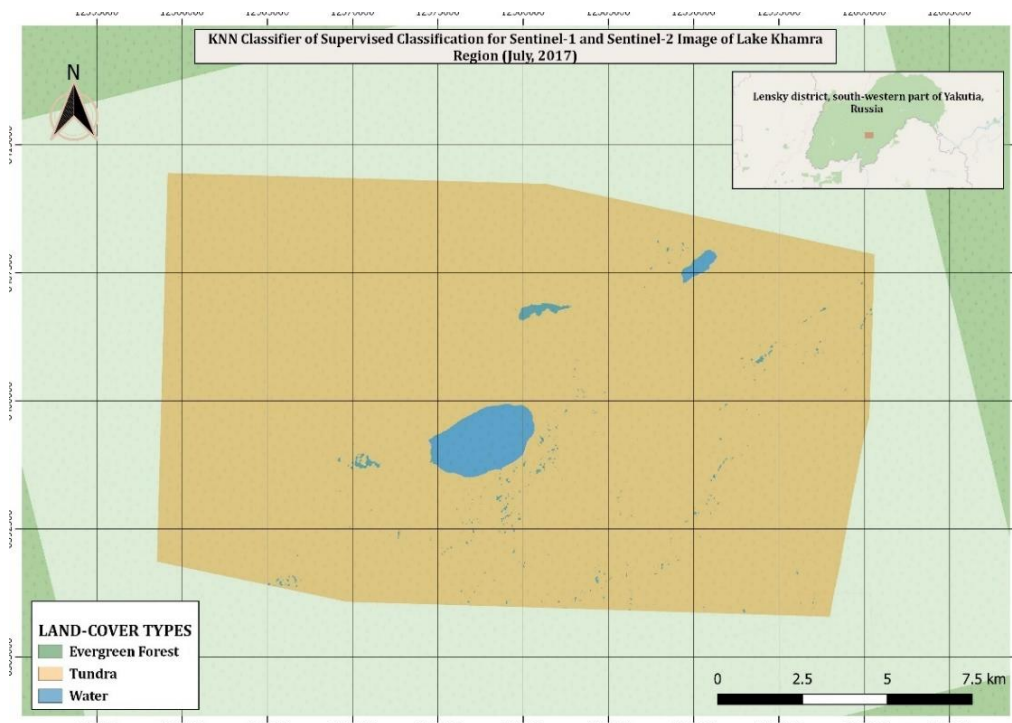


FIGURE 4.31 KNN classifier of supervised classification for Sentinel-1 and Sentinel-2 images of Lake Khamra region (July 2017)

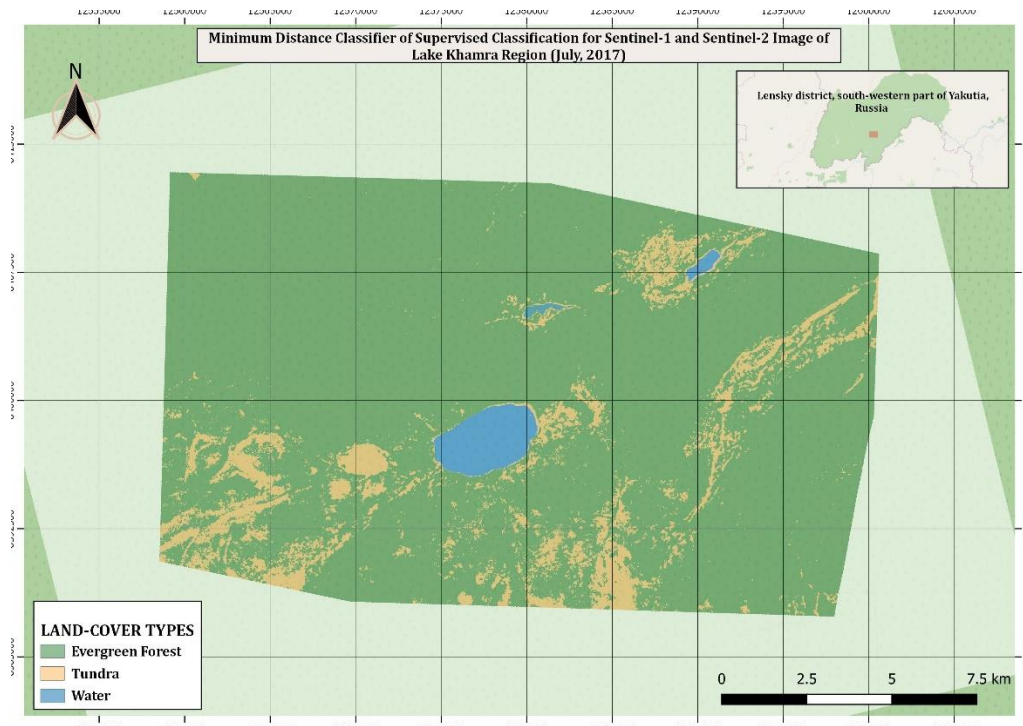


FIGURE 4.32 Minimum Distance classifier of supervised classification for Sentinel-1 and Sentinel-2 images of Lake Khamra region (July 2017)

TABLE 4.09 Training accuracy for the trained classes using Random Forest Classifier (Sentinel-1 and Sentinel-2 image, Lake Illirney region, July 2017)

	<i>Boreal Forest</i>	<i>Tundra</i>	<i>Bare Ground</i>	<i>Water</i>
Accuracy	1.0000	0.9983	0.9983	1.0000
Precision	1.0000	0.9901	1.0000	1.0000
Correlation	1.0000	0.9941	0.9864	1.0000
Error rate	0.0000	0.0017	0.0017	0.0000
True positives	135.0000	301.0000	116.0000	1250.0000
False positives	0.0000	3.0000	0.0000	0.0000
True negatives	1670.0000	1501.0000	1686.0000	555.0000
False negatives	1.0000	0.0000	3.0000	0.0000

Using Testing dataset, % correct predictions = 99.8338

Total samples = 3611

RMSE = 0.08153649149910351

Bias = -0.003324099722991747

Distribution:

- Boreal Forest: 271 (7.5048%)
- Tundra: 602 (16.6713%)
- Bare Ground: 238 (6.5910%)
- Water: 2500 (69.2329%)

TABLE 4.10 Training accuracy for the trained classes using KDTree KNN Classifier (Sentinel-1 and Sentinel-2 image, Lake Illirney region, July 2017)

	<i>Boreal Forest</i>	<i>Tundra</i>	<i>Bare Ground</i>	<i>Water</i>
Accuracy	0.9978	0.9945	0.9967	1.0000
Precision	1.0000	0.9678	1.0000	1.0000
Correlation	0.9839	0.9805	0.9727	1.0000
Error rate	0.0022	0.0055	0.0033	0.0000
True positives	131.0000	301.0000	113.0000	1250.0000
False positives	0.0000	10.0000	0.0000	0.0000
True negatives	1670.0000	1494.0000	1686.0000	555.0000
False negatives	4.0000	0.0000	6.0000	0.0000

Using Testing dataset, % correct predictions = 99.4460

Total samples = 3611

RMSE = 0.12454904806525507

Bias = -0.004432132963988922

Distribution:

- Boreal Forest: 271 (7.5048%)
- Tundra: 602 (16.6713%)
- Bare Ground: 238 (6.5910%)
- Water: 2500 (69.2329%)

TABLE 4.11 Training accuracy for the trained classes using Minimum Distance Classifier (Sentinel-1 and Sentinel-2 image, Lake Illirney region, July 2017)

	<i>Boreal Forest</i>	<i>Tundra</i>	<i>Bare Ground</i>	<i>Water</i>
Accuracy	0.9972	0.9917	0.9945	1.0000
Precision	1.0000	0.9525	1.0000	1.0000
Correlation	0.9798	0.9711	0.9542	1.0000
Error rate	0.0028	0.0083	0.0055	0.0000
True positives	130.0000	301.0000	109.0000	1250.0000
False positives	0.0000	15.0000	0.0000	0.0000
True negatives	1670.0000	1489.0000	1686.0000	555.0000
False negatives	5.0000	0.0000	10.0000	0.0000

Using Testing dataset, % correct predictions = 99.1690

Total samples = 3611

RMSE = 0.15789473684210525

Bias = -0.008310249307479145

Distribution:

- Boreal Forest: 271 (7.5048%)
- Tundra: 602 (16.6713%)
- Bare Ground: 238 (6.5910%)
- Water: 2500 (69.2329%)

TABLE 4.12 Prediction accuracy for methods of supervised classification (Fusion of Sentinel-1 and Sentinel-2 images)

<i>Methods of Supervised Classification</i>	<i>Overall Accuracy (OA) (%)</i>
<i>Random Forest Classifier</i>	77.60
<i>KDTree KNN Classifier</i>	81.60
<i>KNN Classifier</i>	-
<i>Minimum Distance (MD) Classifier</i>	80.80
<i>Maximum Likelihood (ML) Classifier</i>	-

4.4 Time series analyses of both Sentinel products

4.4.1 Time series analysis for Sentinel-1 products

The plot for time series analysis showing the temporal variability of the vegetation plots from the Expedition in 2018 can be seen in Figure 4.33. The temporal analysis of various land-cover groups in the area of research is highlighted in Figures 4.34-4.39.

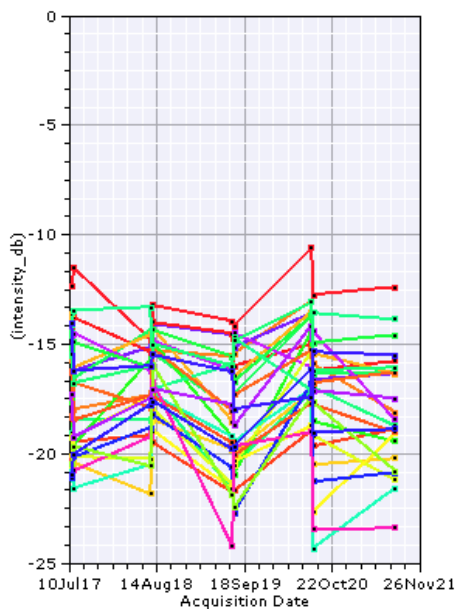


FIGURE 4.33 Sentinel-1 derived backscatter time series from the vegetation plot sites in Lake Illirney region (2017-2021)

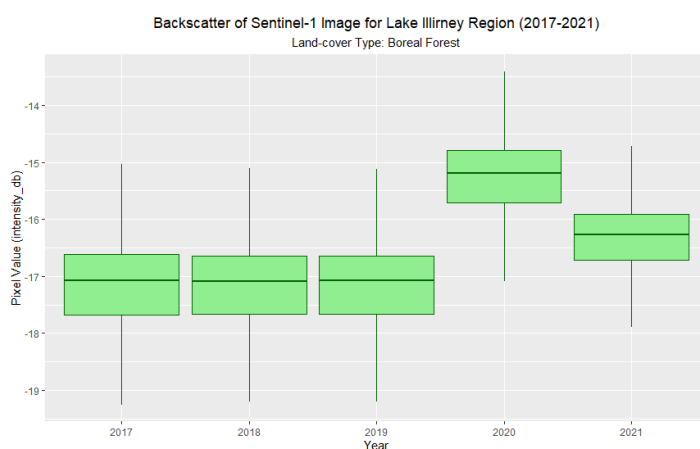


FIGURE 4.34 Backscatter of boreal forest for Sentinel-1 image for Lake Illirney region (2017-2021)

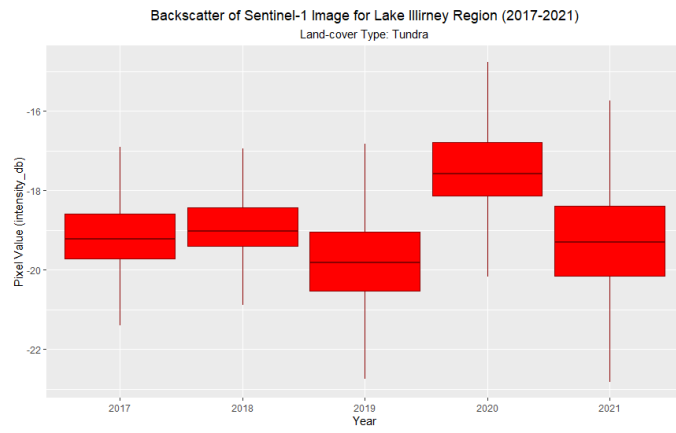


FIGURE 4.35 Backscatter of tundra for Sentinel-1 image for Lake Illirney region (2017-2021)

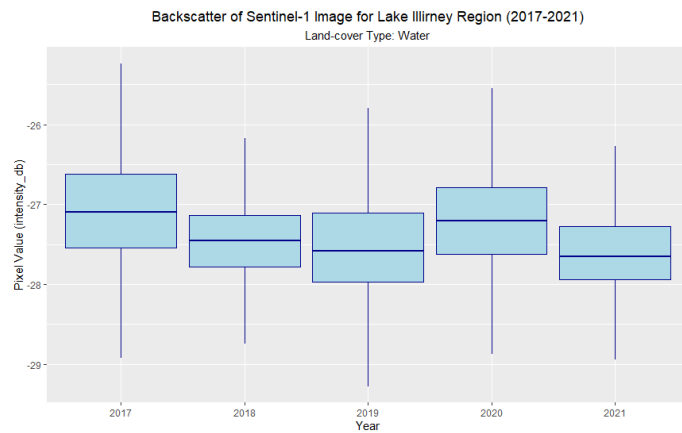


FIGURE 4.36 Backscatter of water for Sentinel-1 image for Lake Illirney region (2017-2021)

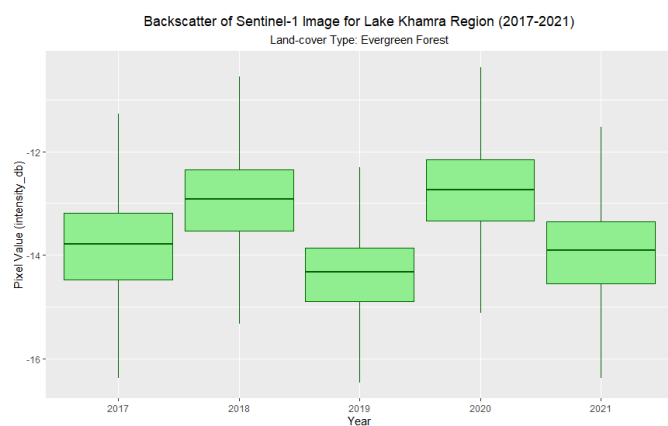


FIGURE 4.37 Backscatter of evergreen forest for Sentinel-1 image for Lake Khamra region (2017-2021)

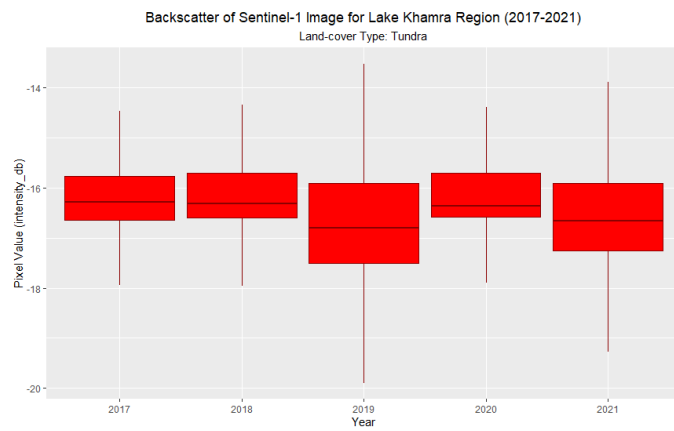


FIGURE 4.38 Backscatter of tundra for Sentinel-1 image for Lake Khamra region (2017-2021)

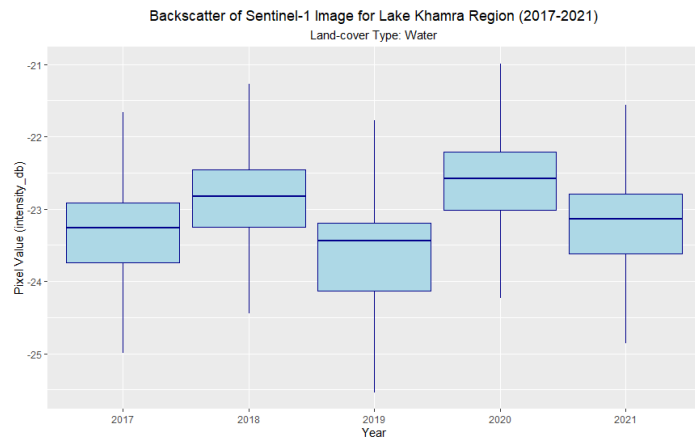


FIGURE 4.39 Backscatter of water for Sentinel-1 image for Lake Khamra region (2017-2021)

4.4.2 Time series analysis for Sentinel-2 products

The temporal analysis of several land-cover types in the areas for interest for Sentinel-2 images can be seen in Figures 4.40-4.45.

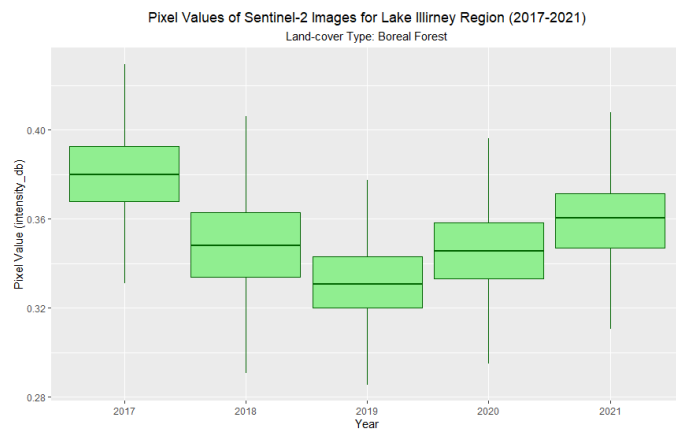


FIGURE 4.40 Pixel values of boreal forest for Sentinel-2 images for Lake Illirney region (2017-2021)

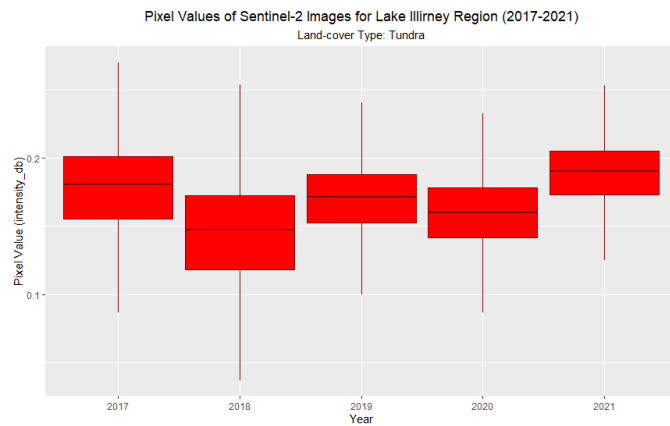


FIGURE 4.41 Pixel values of tundra for Sentinel-2 images for Lake Illirney region (2017-2021)

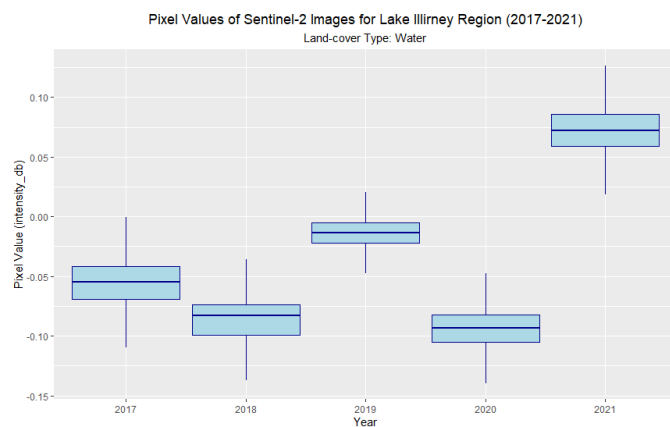


FIGURE 4.42 Pixel values of water for Sentinel-2 images for Lake Illirney region (2017-2021)

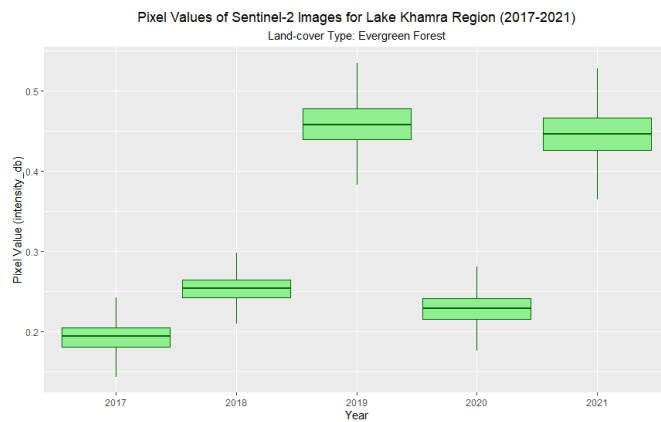


FIGURE 4.43 Pixel values of evergreen forest for Sentinel-2 images for Lake Khamra region (2017-2021)

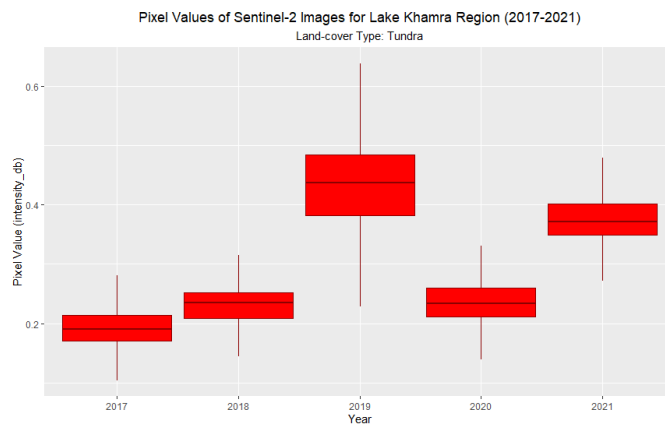


FIGURE 4.44 Pixel values of tundra for Sentinel-2 images for Lake Khamra region (2017-2021)

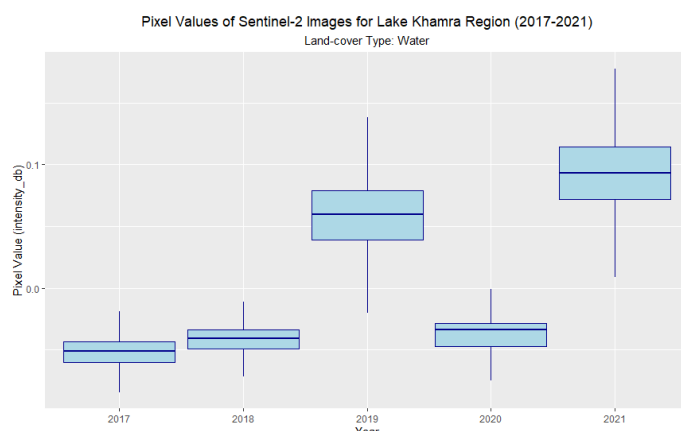


FIGURE 4.45 Pixel values of water for Sentinel-2 images for Lake Khamra region (2017-2021)

4.4.3 Time series analysis of fused Sentinel-1 and -2 products

The temporal analysis of various land-cover groups in the study areas for the fusion of both Sentinel products can be examined in Figures 4.46-4.51.

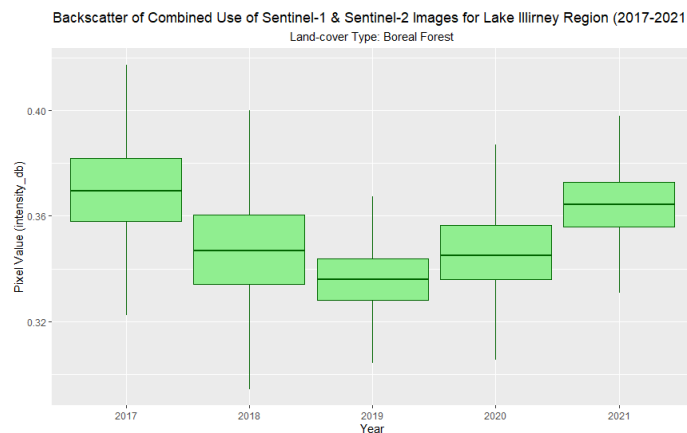


FIGURE 4.46 Backscatter of boreal forest for both Sentinel products for Lake Illirney region (2017-2021)

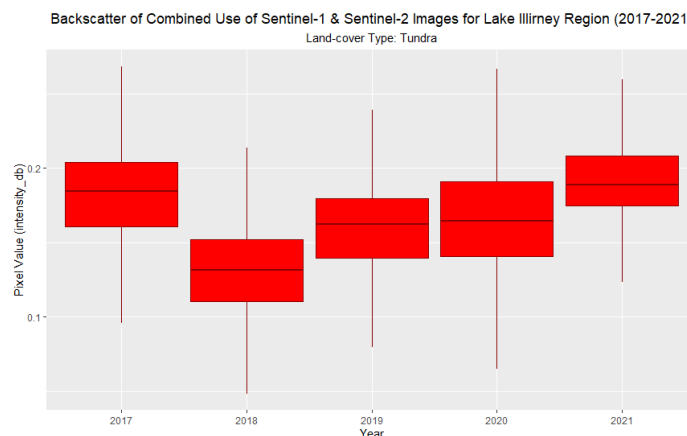


FIGURE 4.47 Backscatter of tundra for both Sentinel products for Lake Illirney region (2017-2021)

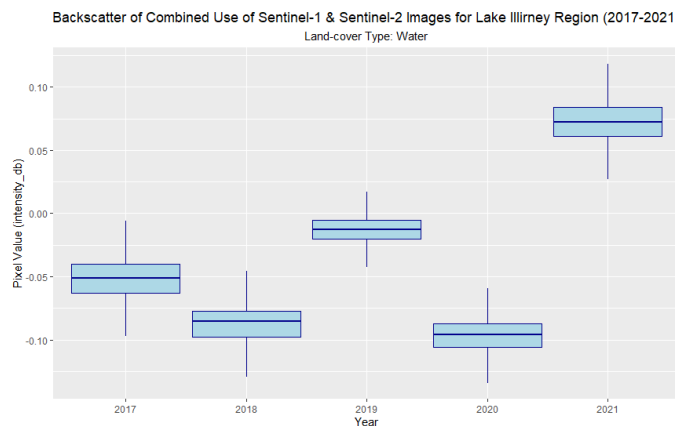


FIGURE 4.48 Backscatter of water for both Sentinel products for Lake Illirney region (2017-2021)

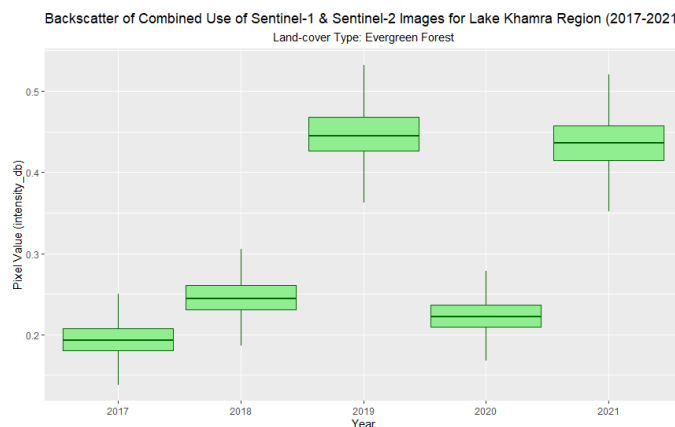


FIGURE 4.49 Backscatter of evergreen forest for both Sentinel products for Lake Khamra region (2017-2021)

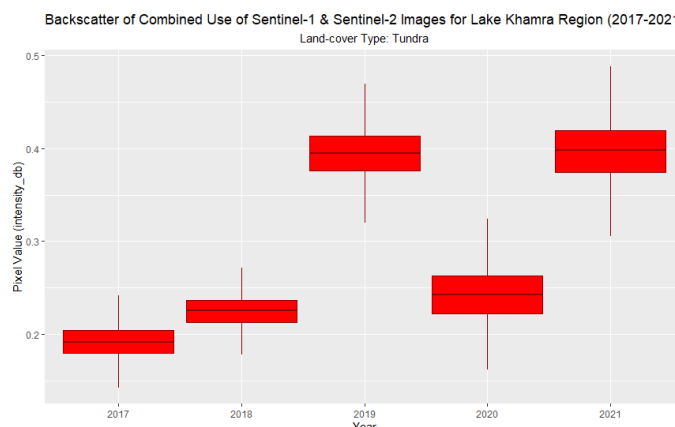


FIGURE 4.50 Backscatter of tundra for both Sentinel products for Lake Khamra region (2017-2021)

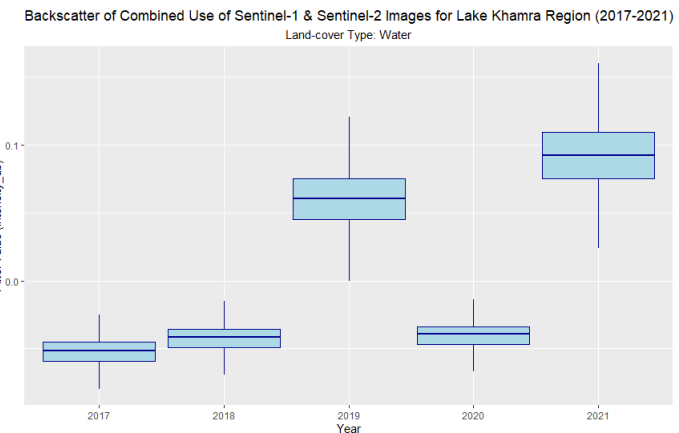


FIGURE 4.51 Backscatter of water for both Sentinel products for Lake Khamra region (2017-2021)

5 DISCUSSIONS

5.1 Analyses of Sentinel-1 images

5.1.1 Unsupervised classification

In unsupervised land-cover classification, pixels were not grouped based on prior information but based on many unidentified data points and divides them into classes related to the properties possessed by the data themselves. The algorithm of *EM Cluster Analysis* assigns pixels based on the sum of rear possibility values which usually tend to unity. The algorithm in *K-means clustering* assigns each pixel to the cluster whose centre is nearest, and the centre is the arithmetic mean of all pixels belonging to that cluster.

It can be noted that Figures 4.2 and 4.4, which represent the *K-Means Cluster Analysis* better interpret the land-cover classes in the image of Sentinel-1 product than the *EM Cluster Analysis* represented in Figures 4.1 and 4.3. This indicates that by assigning every pixel to the cluster whose centre is nearest proved to be a better algorithm than assigning every pixel to posterior possibility values. However, the *K-Means Cluster Analysis* does not consider the different scales and correlations in the data, which is a major disadvantage. It should be mentioned that both methods of unsupervised classification were faster to run. Furthermore, despite the slight difference in the land-cover types of both study areas, the methods of unsupervised classification seem to react to both study areas the same way. It was also noted that these algorithms predicted the land-cover types of Sentinel-1 products as seen in the reference data to a good extent, especially for the *K-Means Cluster Analysis*.

5.1.2 Supervised classification

The methods of supervised classification used in this analysis are namely, *Random Forest (RF) Classifier*, *KDTree KNN Classifier*, *KNN Classifier*, *Minimum Distance (MD) Classifier* and *Maximum Likelihood (ML) Classifier*. The output images are seen in Figures 4.5-4.12. The algorithm of *Random Forest (RF) Classifier* did not identify all valid pixels with the default *Valid-Pixel Expression*. The confidence level had to be reduced to *Confidence >= 0.2* from *Confidence >= 0.5* for all the pixels to be assigned. The other methods of supervised classification do not require the change of pixel values in the expression of confidence level. The output products of *Random Forest (RF) Classifier*, *KDTree KNN Classifier* and *Minimum Distance (MD) Classifier* show that all the pixels

located in the study areas were duly classified into each land-cover types regarding the training data and parameters provided. The *Maximum Likelihood (ML) Classifier* did not classify all the pixels in the study areas into the land-cover classes, while the *KNN Classifier* performed the worse in the process. The failure of Maximum Likelihood (ML) Classifier could be centred on the insufficient number of training data for each land-cover class which led to the inaccuracy of the valuation of covariance matrix, hereby in turn leading to inadequate classification. The other methods of supervised classification considered in this study does not depend on covariance matrix.

The training accuracy for the trained land-cover classes as shown in Tables 4.1-4.3 illustrated how training data created for all land-cover groupings reacted to the algorithms of the three (3) different methods in supervised classification that were effective. The *Root Mean Square Error (RMSE)* represents the misclassification rate inaccuracy. *Random Forest (RF) Classifier* shown the lowest amount of RSME and biasness towards the training data followed by the *KDTree KNN Classifier*, while the *Minimum Distance (MD) Classifier* had the highest amount of RMSE and biasness. Table 4.4 illustrated the prediction accuracy for the methods of supervised classification. In this table, *Random Forest (RF) Classifier* had the highest overall accuracy, while *KDTree KNN Classifier* and *Minimum Distance (MD) Classifier* followed same level of overall accuracies. *Maximum Likelihood (ML) Classifier* had a lower level of accuracy, while *KNN Classifier* had the lowest level of overall accuracy. The outcome of this analysis is comparable to the study conducted by Barrett Lowe and Arun D. Kulkarni where they concluded that Random Forest (RF) Classifier outperformed other methods of supervised classification (Lowe, B. & Kulkarni, A. D., 2015; Kulkarni, A. D. & Lowe, B., 2016). Barrett, B. *et al.* (2016) also assessed the use of radar images, for detecting and classifying highland plant life utilizing the algorithm in Random Forests (RF) classifier. They also accomplished a very high precision and improved output products while examining the changes in the upland vegetation of Mount Brandon, Comeragh Mountains, and the Galtee Mountains.

5.2 Analyses of Sentinel-2 images

5.2.1 Unsupervised classification

It was observed that the algorithm of *EM Cluster Analysis* did not aggregate the pixels in the Sentinel-2 image into the proper land-cover classes when compared with the Sentinel-1 product. Part of the land-cover area representing the tundra in the reference data were wrongly classified as bare ground in the first study area (Lake Illirney region) (Fig. 4.13). This can mostly be due to closeness of the values of pixels between both land-cover classes and since the algorithm of *EM Cluster Analysis* reacted based on the posterior probability values, it might be interpreting tundra

class posterior pixel values for bare ground class pixel values. It was noted that the algorithm of *EM Cluster Analysis* reacted better to the second study area (Lake Khamra region) (Fig. 4.15). The region of Lake Khamra used for this study does not have bare ground class. This further solidifies the assumption made for the algorithm's reaction to the Lake Illirney region. Figures 4.14 and 4.16 show the *K-Means Cluster Analysis* for both study areas. The algorithm of *K-Means Cluster Analysis* reacted better than its *EM Cluster Analysis* counterpart for both study areas.

5.2.2 Supervised classification

The application of the methods of supervised classification to Sentinel-2 products show that the algorithms of *Random Forest (RF) Classifier*, *KDTree KNN Classifier* and *Minimum Distance (MD) Classifier* produced useful output products. The algorithms of *KNN Classifier* and *Maximum Likelihood (ML) Classifier* did not produce useful output products (Fig. 4.17-4.23). The training accuracy for the trained classes for Sentinel-2 products shown that *Random Forest (RF) Classifier* had the lowest amount of RSME, followed by *KDTree KNN Classifier* and *Minimum Distance (MD) Classifier* respectively (Tab. 4.5-4.7). The prediction accuracy using the reference data indicated that *Minimum Distance (MD) Classifier* had the highest level of *Overall Accuracy (OA)*, followed by *KDTree KNN Classifier* and *Random Forest (RF) Classifier* respectively (Tab. 4.8). The algorithm of *Minimum Distance (MD) Classifier* usually ensure that all misclassified pixels are classified, as it was also concluded by Abinaya, V. and Poonkuntran, S. (2019) to have outperformed other methods of supervised classification for optical images.

5.3 Analyses of the merging between Sentinel-1 and Sentinel-2 products

5.3.1 Unsupervised classification

The use of both methods of unsupervised mapping to the merging of Sentinel-1 and -2 images does not improve the output images. This is likely due to the conflicting principles of the algorithms under these forms of land-cover classification. *EM Cluster Analysis* take into consideration the posterior probability values while *K-Means Cluster Analysis* considers the centre of the clusters to allocate a pixel to a certain class. Though, the *K-Means Cluster Analysis* created a result for the fused Sentinel products, its output product still appeared worse than performing *K-Means Cluster Analysis* on each Sentinel products separately (Fig. 4.25). *EM Cluster Analysis* produced a result that cannot be interpreted (Fig. 4.24).

5.3.2 Supervised classification

The application of the methods of supervised classification on the fusion of Sentinel-1 and Sentinel-2 images of both study areas produced similar results to that which was produced when the same methods were applied to the Sentinel products individually. *Random Forest (RF) Classifier*, *KDTree KNN Classifier* and *Minimum Distance (MD) Classifier* produced useful outputs. The algorithms of *KNN Classifier* and *Maximum Likelihood (ML) Classifier* failed to produce useful outputs based on same parameters (Fig. 4.26-4.32).

The *Root Mean Square Error (RMSE)* was lowest for *Random Forest (RF) Classifier*, followed by *KDTree KNN Classifier* and *Minimum Distance (MD) Classifier* respectively (Tab. 4.9-4.11). It was also noted that the RMSE for the fused Sentinel products did not improve compared to the outputs of the Sentinel products when analysed independently. The ability of the algorithms of the methods of supervised classification to better predict the land-cover classes using reference data showed that *KDTree KNN Classifier* had the highest accuracy. This is followed by *Minimum Distance (MD) Classifier* and *Random Forest (RF) Classifier* respectively (Tab. 4.12).

5.4 Time series analyses of both Sentinel products

5.4.1 Time series analysis for Sentinel-1 products

The vegetation plots measured in-situ during the Expedition of 2018 were analysed to highlight the changes that occurred over the period of five (5) years considered in this study. It was noticed that some plots situated in the boreal forest land-cover class changed to tundra class over the period of five (5) years (Fig. 4.33). These changes can be detected by observing the intensity (db) of the backscatter in the y-axis. These changes were more prominent in 2019, but these changes reversed as well in 2020 when some of the vegetation plots appeared to have changed from tundra back to boreal forest. These changes in land-cover type from boreal forest to tundra coincided with the decrease in temperature and precipitation in 2019 for Lake Illirney region (Fig. 4.52-4.53). The drop of average precipitation from 2018 high in 2021 also corresponded with the changes of most of the vegetation plots from boreal forest to tundra land-cover class (Fig. 4.53).

The boxplots which illustrate the trends of the backscatter for the land-cover types for Sentinel-1 products of Lake Illirney region between 2017-2021 can be seen in Figures 4.34-4.36. The boreal forest in the Lake Illirney region appeared to have flourished more in 2020 compared to the earlier years (2017-2019) in the period considered in the study. The intensity of the pixel values was between -14.5 and -15.8 which show a very healthy vegetation of boreal forest (Fig. 4.34). The same healthy trend continued into 2021 but slightly on the downward trend. The boreal forest in the summer of 2017-2019 tends toward the intensity of pixel values for tundra land-

cover class. Though the average precipitation was seen to be declining from its 2018 peak in 2020 (Fig. 4.53), the healthy nature of the vegetation in 2020 could be more influenced by other anthropogenic factors as well as the effect of the remote sensing instrument used. The tundra land-cover class in Lake Illirney region during these five (5) years period also confirmed the 2020 vegetation boom as it is seen in Figure 4.35. This boxplot shows the distribution of the intensity of pixel values in 2020 towards the boreal forest class. Overall, the Sentinel-1 products did not seem to monitor the changes of land-cover types very well.

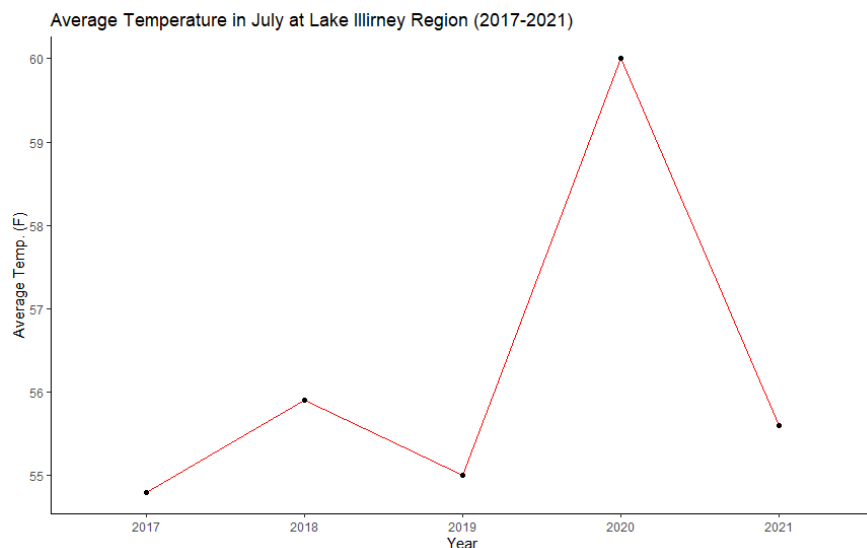


FIGURE 4.52 Average temperature in July at Lake Illirney region (2017-2021)

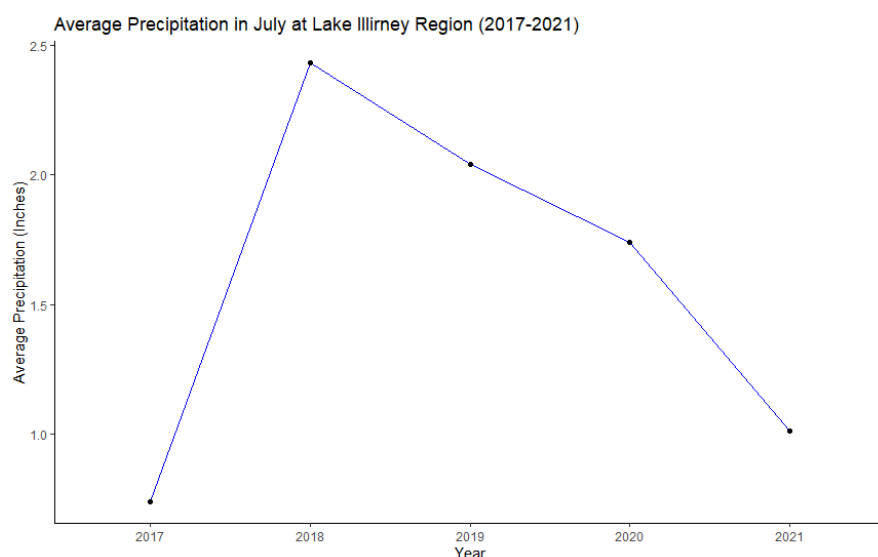


FIGURE 4.53 Average precipitation in July at Lake Illirney region (2017-2021)

The evergreen forest land-cover class of Lake Khamra region also had a surge in 2020. It was also observed that the evergreen forest had a surge in 2018 as well (Fig. 4.37), which coincided with the increase in average precipitation of the region (Fig. 4.53). The tundra land-cover class for this region had a high amount of distribution in 2019 (Fig. 4.38) which coincided with the decrease in intensity of pixel values for the evergreen forest land-cover class of the same year (Fig. 4.37).

5.4.2 Time series analysis of Sentinel-2 products

The backscatter pixel intensity values look to be on a steady decline from 2017 to 2019 where it bottomed and rose steadily back up towards 2021 for the boreal forest in Lake Illirney region (Fig. 4.40). A similar trend can be noticed in the tundra class of Lake Illirney region (Fig. 4.41). The backscatter pixel intensity values had a noticeable increase in 2019 and 2021 for the evergreen forest and tundra land-cover classes of Lake Khamra region (Fig. 4.43-4.44). It can be observed that the abundance of vegetation (e.g., boreal forest and evergreen forest) coincided with lower levels of average temperature for most of the data studied (Fig. 4.40). This is comparable to the study by Gomez-Martinez F. *et. al.* (2021), where they compared the surface temperature and vegetation in Mexico and concluded that an increase in vegetation of the area led to a significant decrease in surface temperature of the study area. The effect of a sharp increase in average temperature (Fig. 4.52) also corresponded with the decrease in the intensities of boreal forest and tundra in Lake Illirney region (Fig. 4.40-4.41). Baumbach, L. *et. al.* (2017) studied the effect of extreme temperatures on vegetations in Europe and highlighted how temperature affects some vegetative land-cover types. These analyses indicated that Sentinel-2 products produced more useful results in monitoring changes of land-cover types in the Arctic region.

5.4.3 Time series analysis of fused Sentinel-1 and Sentinel-2 products

The outcome obtained from the fusion of Sentinel-1 and Sentinel-2 products can be seen in Figures 4.46-4.51. These temporal analyses appeared like the ones derived when time series analyses were carried out on Sentinel-2 products independently. this indicates that Sentinel-1 images did not significantly improve the outcome of the time series analyses when fused with Sentinel-2 images.

6 CONCLUSION

6.1 Unsupervised classification

The use of the methods of unsupervised classification which involves *EM Cluster Analysis* and *K-Means Cluster Analysis* of Sentinel-1 & Sentinel-2 products can be described to have an average performance. It was noted that the algorithm of *K-Means Cluster Analysis* was better than the algorithm of *EM Cluster Analysis* while using unsupervised classification for analysing both Sentinel images independently and in combination. It can also be concluded that the fusion of the Sentinel products does not improve the output products.

6.2 Supervised classification

The application of the algorithms of different methods of supervised classification to the Sentinel products produced similar outcomes. *Random Forest (RF) Classifier* showed to have being the best technique for Sentinel-1, while the *Minimum Distance (MD) Classifier* had the best *Overall Accuracy (OA)* for Sentinel-2 images when analysed independently. The synergic use of both Sentinel products shown that *KDTree KNN Classifier* had the highest *Overall Accuracy (OA)*. Based on the parameters used, *Maximum Likelihood (ML) Classifier* and *KNN Classifier* failed to produce desired outcomes. Considering the training data accuracy, prediction accuracy (using reference images), the Root Mean Square Error (RMSE) and biasness of all the method of supervised classification, the merging of both Sentinel acquisitions did not improve the outcome of the land-cover mapping of both area of interest. It can be concluded that only Sentinel-2 images are sufficient to generate good quality products for the terrain features classification of forested areas in the Arctic region. It was also noticed that the difference in forest types of the study areas did not affect the outcome of the results when subjected to the methods of supervised classification considered.

6.3 Time series analyses

The temporal analyses carried out show that there were some variations in the densities of land-cover types over a period of five (5) years, which indicates that there can be changes even over a short period of time in land-cover types of the Arctic region. Some of these changes noticed were changes between land-cover types, for instance, changes occurring between boreal forest and tundra and vice versa. The different Sentinel products were used independently and synergically

for these analyses. It was concluded that Sentinel-1 products independently did not perform well in highlighting the changes in land-cover types thereby revealing misleading information. Sentinel-2 products on the other hand performed better in analysing the changes of land-cover types over a timeline. The fusion of both Sentinel products did not seem to improve the outcome of the time series analysis.

REFERENCES

- Abinaya, V., & Poonkuntran, S. (March 2019). Classification of Satellite Image using Minimum Distance Classification Algorithm. *SSRG International Journal of Computer Science and Engineering (SSRG-IJCSE)*, S. 15-18.
- Bagan, H., Kinoshita, T., & Yamagata, Y. (2012). Combination of AVNIR-2, PALSAR, and Polarimetric Parameters for Land Cover Classification. *IEEE Transactions on Geoscience and Remote Sensing*, 50(4), S. 1318–1328. doi:10.1109/TGRS.2011.2164806.
- Ban, Y., Hu, H., & Rangel, I. M. (20. March 2010). Fusion of Quickbird MS and RADARSAT SAR Data for Urban Landcover Mapping: Object-based and Knowledge-based Approach. *International Journal of Remote Sensing Vol. 31, No. 6*, S. 1391–1410.
- Barrett, B., Raab, C., Cawkwell, F., & Green, S. (2016). Upland Vegetation Mapping using Random Forests with Optical and Radar Satellite Data. *Remote Sensing in Ecology and Conservation*, S. 2, 212–231.
- Baumbach, L., Siegmund, J. F., Mittermeier, M., & Donner, R. V. (2017). Impacts of temperature extremes on European vegetation during the growing season. *Biogeosciences*, 14, S. 4891–4903. <https://doi.org/10.5194/bg-14-4891-2017>.
- Braun, A. (2020). SAR-based landcover classification with Sentinel-1 GRD products. *Sentinel-1 Toolbox. STEP ESA*.
- Breiman, L. (2001). Random Forests. *Machine Learning*, S. 45: 5-32.
- Canada Centre for Remote Sensing. (2015). Fundamentals of Remote Sensing.
- Chasmer, L., Hopkinson, C., Veness, T., Quinton, W., & Baltzer, J. (2014). A Decision-tree Classification for Low-lying Complex Land Cover Types within the Zone of Discontinuous Permafrost. . *Remote Sens. Environ.*, S. 143, 73-84.
- Chu, H. T., & Ge, L. (2010). Synergistic Use of Multi-temporal ALOS/PALSAR with SPOT Multispectral Satellite Imagery for Land Cover Mapping in the Ho Chi Minh City Area, Vietnam. *IEEE International Geoscience and Remote Sensing Symposium*, S. 1465-1468.
- Clerici, N., Calderón, C. A., & Posada, J. M. (2017). Fusion of Sentinel-1A and Sentinel-2A Data for Land Cover Mapping: a Case Study in the Lower Magdalena Region, Colombia. *Journal of Maps*, 13:2, S. 718-726. DOI: 10.1080/17445647.2017.1372316.

Climatebase.ru. (kein Datum). Illirney, Russia. <http://climatebase.ru/station/25248/?lang=en>, S. Retrieved 16 May 2022.

Dawei, Z., & Fang, Z. (2007). A New Improved Hierarchical Model of Image Fusion. *The Eighth International Conference on Electronic Measurement and Instruments, ICEMI'2007. IEEE.*, S. 2-853 to 2-857.

Erasmi, S., & Twele, A. (20. May 2009). Regional Land Cover Mapping in the Humid Tropics using Combined Optical and SAR Satellite Data—a Case Study from Central Sulawesi, Indonesia. *International Journal of Remote Sensing Vol. 30, No. 10*, S. 2465–2478.

Fedorov, A. N., Vasilyev, N. F., Torgovkin, Y. I., Shestakova, A. A., Varlamov, S. P., Zheleznyak, M. N., . . . Kunitsky, V. V. (2018). Permafrost-Landscape Map of the Republic of Sakha (Yakutia) on a Scale 1 : 1 500 000. *Geosciences*, 8, S. 1-17. <https://doi.org/10.3390/geosciences8120465>.

Fletcher, K. (2012). Sentinel-1: ESA's Radar Observatory Mission for GMES Operational Services. *Paris, France: ESA SP-1322/1*.

Fletcher, K. (2012). Sentinel-1: ESA's Radar Observatory Mission for GMES Operational Services. S. Paris, France: ESA SP-1322/1.

Garzelli, A., & Nencini, F. (2006). Fusion of Panchromatic and Multispectral Images by Genetic Algorithms. *IEEE International Geoscience and Remote Sensing Symposium, Department of Information Engineering, University of Siena, Siena Italy*, S. 3810-3813.

Gessner, U., Machwitz, M., Esch, T., Tillack, A., Naeimi, V., Kuenzer, C., & Dech, S. (24. April 2015). Multi-sensor Mapping of West African Land Cover using MODIS, ASAR and TanDEM-X/TerraSAR-X Data. *Remote Sensing of Environment (164), Science Direct*, S. 282-297. doi:10.1016/j.rse.2015.03.029.

Ghassemian, H. (2016). A review of remote sensing image fusion methods. *Elsevier Information Fusion*, S. Vol. 32, Part A, 75-89.

Ghassemian, H. (2016). A Review of Remote Sensing Image Fusion Methods. *Elsevier Information Fusion*, S. Vol. 32, Part A, 75-89.

Ghassemian, H. (2016). A Review of Remote Sensing Image Fusion Methods. *Elsevier Information Fusion*, S. Vol. 32, Part A, 75-89.

Gomez-Martinez, F., de Beurs, K. M., Koch, J., & Widener, J. (2021). Multi-Temporal Land Surface Temperature and Vegetation Greenness in Urban Green Spaces of Puebla, Mexico. *Land 2021, 10, 155.*, S. <https://doi.org/10.3390/land10020155>.

- González-Sanpedro, M., Le Toan, T., Moreno, J., Kergoat, L., & Rubio, E. (18. March 2008). Seasonal Variations of Leaf Area Index of Agricultural Fields retrieved from Landsat Data. *Remote Sensing of Environment, Volume 112, Issue 3*, S. 810-824.
- Haack, B., & Bechdol, M. (2000). Integrating Multisensor Data and RADAR Texture Measures for Land Cover Mapping. *Computers & Geosciences, 26*, S. 411-421. doi: 10.1016/S0098-3004(99)00121-1.
- Haralick, R. M., Shanmugam, K., & Dinstein, I. (6. November 1973). Textural Features for Image Classification. *IEEE Transactions on Systems, Man, and Cybernetics (Volume: SMC-3, Issue: 6)*, S. 610 - 621.
- Herold, M., Woodcock, C., Di Gregorio, A., Mayaux, P., Belward, A., Latham, J., & Schmullius, C. C. (2006). A Joint Initiative for Harmonization and Validation of Land Cover Datasets. *IEEE Transactions on Geoscience and Remote Sensing, 44 (7)*, S. 1719–1727.
- Herold, N. D., & Haack, B. N. (2002). Fusion of Radar and Optical Data for Land Cover Mapping. *Geocarto International, 17:2*, S. 21-30. doi: 10.1080/10106040208542232.
- Hoersch, B. (2015). Sentinel-2 Use Handbook. *ESA Standard Document, European Space Agency*.
- Hou, W., Li, D., Xu, C., Zhang, H., & Li, T. (December 2018). An Advanced k Nearest Neighbor Classification Algorithm Based on KD-tree. *2018 IEEE International Conference of Safety Produce Informatization (IICSPI)*, S. DOI: 10.1109/IICSPI.2018.8690508.
- Hui, T., & Binbin, W. (2009). Discussion and Analyze on Image Fusion Technology. *Second International Conference on Machine Vision (ICMV'09)*. IEEE, S. 246 – 250.
- Ibrahim, S. (January 2007). The Electromagnetic Spectrum. *ResearchGate*, S. DOI: 10.13140/RG.2.2.34731.44325.
- Imhoff, M. L. (1995). A Theoretical-Analysis of the Effect of Forest Structure on Synthetic-Aperture Radar Backscatter and the RemoteSensing of Biomass. *IEEE T Geosci Remote*, S. 33, 341–352, doi: 10.1109/36.377934.
- Jing, Y., Wenbo, W., & Tingjun, K. (2008). Study of Remote Sensing Image Fusion and its Application in Image Classification. *Beijing: The International Archives of the Photogrammetry, Remote Sensing and Spatial Information Sciences. Vol. XXXVII. Part B7*.
- Joshi, N., Baumann, M., Ehammer, A., Fensholt, R., Grogan, K., Hostert, P., & Waske, B. (16. January 2016). A Review of the Application of Optical and Radar Remote Sensing Data Fusion to Land use Mapping and Monitoring. *Remote Sensing*, S. 8, 70. doi:10.3390/rs8010070.

- Knorn, J., Rabe, A., Radeloff, V. C., Kuemmerle, T., Kozak, J., & Hostert, P. (15. May 2009). Land Cover Mapping of Large Areas using Chain Classification of Neighboring Landsat Satellite Images. *Remote Sensing of Environment*, S. Volume 113, Issue 5, pp. 957-964.
- Kruse, S., Farkas, L., Brieger, F., Geng, R., Heim, B., Pestryakova, L. A., . . . van Geffen, F. (2021). SiDroForest: Orthomosaics, SfM point clouds and products from aerial image data of expedition vegetation plots in 2018 in Central Yakutia and Chukotka, Siberia. *PANGAEA*.
- Kryžanovskij, O. L. (1995). A Checklist of the Ground-beetles of Russia and Adjacent Lands (Insecta, Coleoptera, Carabidae). *Sofia, Bulgeria: Pensoft Publishers*.
- Kulkarni, A. D., & Lowe, B. (2016). Random Forest Algorithm for Land Cover Classification. *Computer Science Faculty Publications and Presentations. Paper 1.*, S. <http://hdl.handle.net/10950/341>.
- Liaw, A., & Wiener, M. (2002). Classification and Regression by randomForest. *R News*, vol. 2, no. 3, S. 18–22.
- Lowe, B., & Kulkarni, A. (February 2015). Multispectral Image Analysis using Random Forest. *International Journal on Soft Computing (IJSC) Vol.6, No. 1*, S. DOI: 10.5121/ijsc.2015.6101.
- Masek, J. G., Vermote, E. F., Saleous, N. E., Wolfe, R., Hall, F. G., Huemmrich, K. F., & ...Lim, T. K. (2006). A Landsat Surface Reflectance Dataset for North America, 1990-2000. *IEEE Geosciences and Remote Sensing Letters* 3 (1), S. 68-72.
- Meyer, F. (2019). SAR Handbook: Comprehensive Methodologies for Forest Monitoring and Biomass Estimation. *E. NASA*.
- Mitchell, H. (2010). Image Fusion: Theories, Techniques And Applications. *Berlin Heidelberg: Springer-Verlag e-ISBN 978-3-642-11216-4*.
- Official Website of Bilibinsky District.* (kein Datum). Von Retrieved at 16 August, 2021.: <http://www.bilchao.ru/index.php?newsid=34> abgerufen
- Ovchinnikov, M., & Barrington-Brown, J. (2021). 14 - Attitude Determination and Control Systems. *In Cubesat Handbook. Academic Press.*, S. 263-281.
- Pandit, V. R., & Bhiwani, R. (2015). Image Fusion in Remote Sensing Applications: A Review. *International Journal of Computer Applications*.
- Piella, G. (1. April 2003). A General Framework for Multiresolution Image Fusion: from Pixels to Regions. *Elsevier Information Fusion* 4, S. 259–280.

- Potin, P., Rosich, B., Grimont, P., Miranda, N., Shurmer, I., O'Connell, A., & ...Krassenburg, M. (2016). Sentinel-1 mission status, in Proceedings EUSAR 2016: 11th European Conference on Synthetic Aperture Radar, Proceedings of 2016. S. VDE, 1-6.
- Qin, Y., Xiao, X., Dong, J., Zhang, G., Roy, P. S., Joshi, P. K., & ...Moore III, B. (2016). Mapping Forests in Monsoon Asia with ALOS PALSAR 50-m Mosaic Images and MODIS Imagery in 2010. *Scientific Reports*, S. 6(1). doi: 10.1038/srep20880.
- Rockinger, O. (kein Datum). Pixel - Level Fusion of Image Sequences using Wavelet Frames. *Leeds, England: the 16th Leeds Applied Shape Research workshop, Leeds University Press*.
- Shevtsova, I., Kruse, S., Herzschuh, U., Brieger, F., Schulte, L., Stuenzi, S. M., . . . Zakharov, E. S. (2020). Total above-ground biomass of 39 vegetation sites of central Chukotka from 2018. *PANGAEA*, S. <https://doi.org/10.1594/PANGAEA.923719>.
- Simone, G., Farina, A., Morabito, F. C., Serpico, S. B., & Bruzzone, L. (March 2002). Image Fusion Techniques for Remote Sensing Applications. *Elsevier Information Fusion, Volume 3, Issue 1*, S. 3-15.
- Soria-Ruiz, J., Fernandez-Ordonez, Y., & Woodhouse, I. (2010). Land-cover Classification using Radar and Optical Images: a Case Study in Central Mexico. *International Journal of Remote Sensing*, S. 31:12, 3291-3305.
- Stow, D. A., Hope, A., McGuire, D., Verbyla, D., Gamon, J., Huemmrich, F., & . . . Tape, K. (2004). Remote sensing of vegetation and land-cover change in Arctic Tundra Ecosystems. *Remote Sens. Environ.*, S. 89, 281-308.
- Strugnell, N. C., Lucht, W., & Schaaf, C. (2001). A Global Albedo Dataset derived from AVHRR Data for use in Climate Simulations. *Geophysics Research Letters* 28 (1), S. 191-194.
- Tavares, P. A., Beltrão, N. E., Guimarães, U. S., & Teodoro, A. C. (6. March 2019). Integration of Sentinel-1 and Sentinel-2 for Classification and LULC Mapping in the Urban Area of Belém, Eastern Brazilian Amazon. *MDPI, Sensors*, S. 19, 1140; doi:10.3390/s19051140.
- Ullmann, T., Schmitt, A., Roth, A., Duffe, J., Dech, S., Huberten, H. W., & Baumhauer, R. (2014). Land Cover Characterization and Classification of Arctic Tundra Environments by Means of Polarized Synthetic Aperture X- and C-Band Radar (PolSAR) and Landsat 8 Multispectral Imagery- Richards Island, Canada. *Remote Sens.*, S. 6, 8565-8593.
- Walker, J. J., De Beurs, K. M., Wynne, R. H., & Gao, F. (2012). Evaluation of Landsat and MODIS Data Fusion Products for Analysis of Dryland Forest Phenology. *Elsevier Remote Sensing of Environment* 117, S. 381-393.

- Walker, W. S., Stickler, C. M., Kellndorfer, J. M., Kirsch, K. M., & Nepstad, D. C. (December 2010). Large-Area Classification and Mapping of Forest and Land Cover in the Brazilian Amazon: A Comparative Analysis of ALOS/PALSAR and Landsat Data Sources. *IEEE JOURNAL OF SELECTED TOPICS IN APPLIED EARTH OBSERVATIONS AND REMOTE SENSING*, VOL. 3, NO. 4, S. 594-604.
- Wang, Z., Tie, Y., & Liu, Y. (2010). Design and Implementation of Image Fusion System. *International Conference on Computer Application and System Modeling (ICCASM)*. IEEE., S. V10-140 to V10-143.
- Westphal, W. H. (1970). Physics- A textbook. 25th edition. *Springer*.
- Wu, B., & Wang, J. (2002). Winter Arctic Oscillation, Siberian High and East Asian Winter Monsoon. *Geophys. Res. Lett.*, 29, S. 1897. <https://doi.org/10.1029/2002GL015373>.
- Xu, Y., Ma, P., Ng, E., & Lin, H. (August 2015). Fusion of WorldView-2 Stereo and Multitemporal TerraSAR-X Images for Building Height Extraction in Urban Areas. *IEEE GEOSCIENCE AND REMOTE SENSING LETTERS*, S. pp. VOL. 12, NO. 8. doi: 10.1109/LGRS.2015.2427738.
- Xue, S., Zhang, Z., Meng, X., Lv, Q., & Tu, X. (2019). Point Cloud Registration Method for Pipeline Workpieces Based on RANSAC and Improved ICP Algorithms. *IOP Conf. Ser.: Mater. Sci. Eng.* 612 032190, S. doi:10.1088/1757-899X/612/3/032190.
- Zhang, Q., Cao, Z., Hu, Z., Jia, Y., & Wu, X. (March 2015). Joint Image Registration and Fusion for Panchromatic and Multispectral Images. *IEEE GEOSCIENCE AND REMOTE SENSING LETTERS*, VOL. 12, NO. 3, S. 467-471.
- Zheng, Y. (May 2011). Image Fusion And Its Applications. *Rijeka, Croatia : InTech Publication, ISBN 978-953-307-182-4*.

A List of Sentinel-1 products used for the research

A(i) Lake Illirney region (2017-2021)

- S1A_EW_GRDM_1SDH_20170720T192807_20170720T192844_017559_01D5E7_97E6
- S1A_EW_GRDM_1SDH_20170801T192808_20170801T192845_017734_01DB46_9B55
- S1A_EW_GRDM_1SDH_20180715T192813_20180715T192850_022809_027916_FAB9
- S1A_EW_GRDM_1SDH_20180727T192814_20180727T192851_022984_027E9D_0C0F
- S1A_EW_GRDM_1SDH_20190722T192820_20190722T192857_028234_033088_52D4
- S1A_EW_GRDM_1SDH_20190803T192820_20190803T192858_028409_0335DD_E9D7
- S1A_EW_GRDM_1SDH_20200716T192826_20200716T192903_033484_03E14E_36E0
- S1A_EW_GRDM_1SDH_20200728T192827_20200728T192904_033659_03E6AC_8472
- S1A_EW_GRDM_1SDH_20210804T192833_20210804T192910_039084_049CA3_CF9A

(Source: Copernicus Open Access Hub. <https://scihub.copernicus.eu/dhus/#/home>)

A(ii) Lake Khamra region (2017-2021)

- S1B_IW_GRDH_1SDV_20170719T225540_20170719T225605_006563_00B8B3_E108
- S1B_IW_GRDH_1SDV_20170731T225540_20170731T225605_006738_00BDB7_020F
- S1B_IW_GRDH_1SDV_20180726T225547_20180726T225612_011988_01611B_A5AB
- S1B_IW_GRDH_1SDV_20190721T225553_20190721T225618_017238_0206C3_8B0B
- S1B_IW_GRDH_1SDV_20190802T225553_20190802T225618_017413_020C00_EC8E
- S1B_IW_GRDH_1SDV_20200715T225559_20200715T225624_022488_02AAF2_55D9
- S1B_IW_GRDH_1SDV_20200727T225559_20200727T225624_022663_02B047_F26D
- S1B_IW_GRDH_1SDV_20210722T225605_20210722T225630_027913_0354AE_58CC

(Source: Copernicus Open Access Hub. <https://scihub.copernicus.eu/dhus/#/home>)

B List of Sentinel-2 products used for the research

B(i) Lake Illirney region (2017-2021)

- S2A_MSIL1C_20170804T004651_N0205_R045_T58WFV_20170804T004646
- S2B_MSIL1C_20180712T003609_N0206_R002_T58WFV_20180712T022040
- S2B_MSIL1C_20190727T003619_N0208_R002_T58WFV_20190727T021824
- S2B_MSIL1C_20200721T003609_N0209_R002_T58WFV_20200727T090756
- S2B_MSIL2A_20200721T003609_N0214_R002_T58WFV_20200727T111523
- S2B_MSIL2A_20210812T002609_N0301_R102_T58WFV_20210812T005656

(Source: Copernicus Open Access Hub. <https://scihub.copernicus.eu/dhus/#/home>)

B(ii) Lake Khamra region (2017-2021)

- S2B_MSIL1C_20170806T035539_N0205_R004_T49VFG_20170806T035535
- S2B_MSIL1C_20170813T034529_N0205_R104_T49VFG_20170813T034717
- S2B_MSIL1C_20180719T034529_N0206_R104_T49VFG_20180719T062950

- S2B_MSIL1C_20190717T035549_N0208_R004_T49VFG_20190717T082820
 - S2B_MSIL2A_20190717T035549_N0213_R004_T49VFG_20190717T090754
 - S2A_MSIL1C_20200812T034541_N0209_R104_T49VFG_20200812T064958
 - S2B_MSIL1C_20210815T035539_N0301_R004_T49VFG_20210815T060249
 - S2B_MSIL2A_20210815T035539_N0301_R004_T49VFG_20210815T065328
- (**Source:** Copernicus Open Access Hub. <https://scihub.copernicus.eu/dhus/#/home>)

C List of reference data used

- TDM1_DEM_04_N67E168_DEM (**Source:** TanDEM-X DEM (3 arcsec), DLR, global product)
- Vegetation Plots (2018) [**Source:** (Shevtsova, L. *et al.*, 2020; Kruse, S. *et al.*, 2021)].
- Sentinel-2 10m land cover time series of the world from 2017-2021 (**Source:** Impact Observatory, Microsoft, and Esri).
- Climate data using the station named Ostrovnoe, RS RSM00025138 located in Chukotka Autonomous Okrug, Russia [**Source:** National Oceanic and Atmospheric Administration (NOAA)]

TABLE C.1: Vegetation plots (2018) used as reference data

NAME	LON	LAT	LABEL
<i>pin_1</i>	168.3466	67.3927	EN18001
<i>pin_2</i>	168.3367	67.3868	EN18002
<i>pin_3</i>	168.3470	67.3969	EN18003
<i>pin_4</i>	168.3512	67.3974	EN18004
<i>pin_5</i>	168.3875	67.4196	EN18005
<i>pin_6</i>	168.4029	67.4150	EN18006
<i>pin_7</i>	168.3720	67.4033	EN18007
<i>pin_8</i>	168.3753	67.4021	EN18008
<i>pin_9</i>	168.3797	67.4007	EN18009
<i>pin_10</i>	168.3662	67.4024	EN18010
<i>pin_11</i>	168.3643	67.4040	EN18011
<i>pin_12</i>	168.3781	67.4021	EN18012
<i>pin_13</i>	168.3553	67.4052	EN18013
<i>pin_14</i>	168.3491	67.3953	EN18014
<i>pin_15</i>	168.3306	67.4204	EN18015
<i>pin_16</i>	168.3900	67.4267	EN18016
<i>pin_17</i>	168.3834	67.4323	EN18017
<i>pin_18</i>	168.4060	67.4563	EN18018
<i>pin_19</i>	168.4090	67.4571	EN18019
<i>pin_20</i>	168.4119	67.4592	EN18020
<i>pin_21</i>	168.3288	67.3921	EN18021
<i>pin_22</i>	168.3480	67.4010	EN18022
<i>pin_23</i>	168.3513	67.3992	EN18023
<i>pin_24</i>	168.4264	67.3710	EN18024
<i>pin_25</i>	168.4238	67.3670	EN18025
<i>pin_26</i>	168.3543	67.3961	EN18026
<i>pin_27</i>	168.3591	67.3934	EN18027
<i>pin_28</i>	112.9590	59.9749	EN18079
<i>pin_29</i>	112.9614	59.9771	EN18080

TABLE C.2: Climate data showing average temperature (F) and average precipitation (in)

<i>Year</i>	<i>Temperature (F)</i>	<i>Precipitation (in)</i>
2017	54.80	0.74
2018	55.90	2.43
2019	55.00	2.04
2020	60.00	1.74
2021	55.60	1.01

Selbstständigkeitserklärung

Hiermit versichere ich, dass ich die vorliegende wissenschaftliche Arbeit selbstständig und ohne Hilfe Dritter verfasst habe. Andere als die angegebenen Quellen und Hilfsmittel wurden nicht verwendet. Die den benutzten Quellen wörtlich oder inhaltlich entnommenen Abschnitte sind als solche kenntlich gemacht. Diese wissenschaftliche Arbeit hat in gleicher oder ähnlicher Form noch keiner Prüfungsbehörde vorgelegen und wurde auch nicht veröffentlicht.

Autor	Adeola Olanrewaju Obidiya
Matrikelnummer	799 946
Universität	Universität Potsdam
Studiengang	Remote Sensing, geoInformation and Visualization
Titel	Land-cover classification and time series analyses of Sentinel-1 and Sentinel-2 images at two contrasting sites (Northern treeline vs. taiga) with integration of additional ground and satellite validation data

Potsdam, 15. Juli 2022

Adeola Olanrewaju Obidiya